AD-A066 754 TEXAS A AND M UNIV COLLEGE STATION MECHANICS AND MAT--ETC F/G 11/4
COMPOSITE MATERIALS FOR STRUCTURAL DESIGN.(U)
MAR 79 R SCHAPERY F49620-78-C-0034

UNCLASSIFIED MM-3724-79-2 AFOSR-TR-79-0347 NL

1 OF 2
ADA
066754

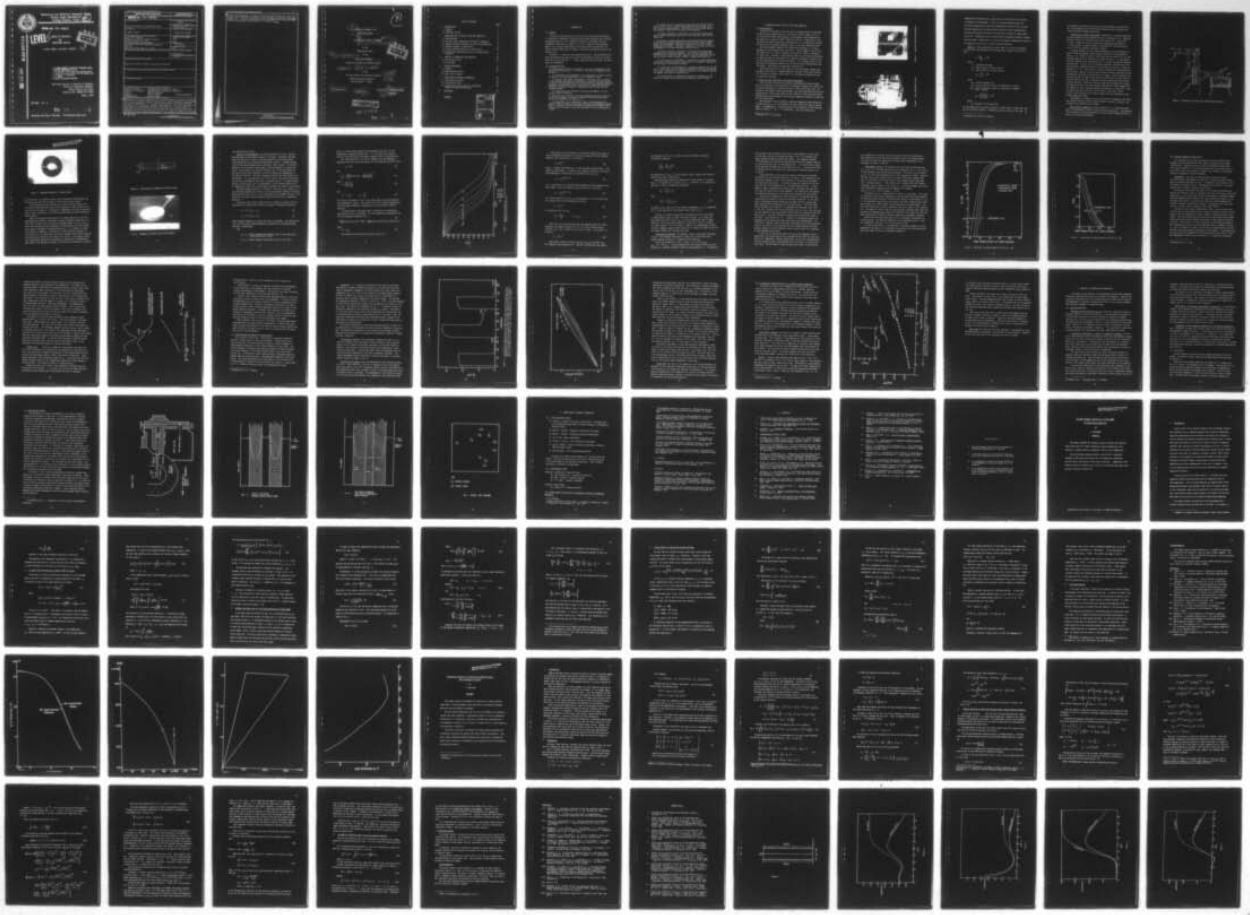

Mechanics and Materials Research Center
TEXAS A&M UNIVERSITY
College Station, Texas

(4)

AFOSR-TR- 79-0347

LEVEL II COMPOSITE MATERIALS FOR STRUCTURAL DESIGN

(FIRST ANNUAL TECHNICAL REPORT)

AIR FORCE OFFICE OF SCIENTIFIC RESEARCH
OFFICE OF AEROSPACE RESEARCH
UNITED STATES AIR FORCE
CONTRACT No. F49620-78-C-0034

MARCH 1979

MM 3724 - 79 - 2

SECURITY CLASSIFICATION OF THIS PAGE *(When Data Entered)*

REPORT DOCUMENTATION PAGE		READ INSTRUCTIONS BEFORE COMPLETING FORM
1. REPORT NUMBER AFOSR-TR- 79-0347	2. GOVT ACCESSION NO.	3. RECIPIENT'S CATALOG NUMBER
4. TITLE *(and Subtitle)* COMPOSITE MATERIALS FOR STRUCTURAL DESIGN		5. TYPE OF REPORT & PERIOD COVERED INTERIM 15 Jan 78 - 14 Jan 79
		6. PERFORMING ORG. REPORT NUMBER MM 3724-79-2
7. AUTHOR(s) RICHARD SCHAPERY		8. CONTRACT OR GRANT NUMBER(s) F49620-78-C-0034
9. PERFORMING ORGANIZATION NAME AND ADDRESS TEXAS A&M UNIVERSITY MECHANICS & MATERIALS RESEARCH CENTER COLLEGE STATION, TX 77843		10. PROGRAM ELEMENT, PROJECT, TASK AREA & WORK UNIT NUMBERS 2307B1 61102F
11. CONTROLLING OFFICE NAME AND ADDRESS AIR FORCE OFFICE OF SCIENTIFIC RESEARCH/NA BLDG 410 BOLLING AIR FORCE BASE, D C 20332		12. REPORT DATE March 1979
		13. NUMBER OF PAGES 150
14. MONITORING AGENCY NAME & ADDRESS *(if different from Controlling Office)*		15. SECURITY CLASS. *(of this report)* UNCLASSIFIED
		15a. DECLASSIFICATION/DOWNGRADING SCHEDULE

16. DISTRIBUTION STATEMENT *(of this Report)*

Approved for public release; distribution unlimited.

17. DISTRIBUTION STATEMENT *(of the abstract entered in Block 20, if different from Report)*

18. SUPPLEMENTARY NOTES

19. KEY WORDS *(Continue on reverse side if necessary and identify by block number)*

COMPOSITE MATERIALS	THERMOMECHANICAL BEHAVIOR OF RESINS	
PROCESSING OF LAMINATES	THERMOMECHANICAL BEHAVIOR OF COMPOSITES	
RESINS	FRACTURE MECHANICS	
ADHESIVES	FINITE ELEMENTS	NEUTRON RADIOGRAPHY
VISCOELASTICITY	AGING OF RESINS	

20. ABSTRACT *(Continue on reverse side if necessary and identify by block number)*

Summarized are research activities in the areas of composite materials processing and testing, elevated temperature and moisture effects on composites and adhesives, and neutron radiography. Also included are four papers which were completed during the reporting period. Primary accomplishments in the first area were the development of a processing laboratory, development of a testing method for obtaining the complex modulus of resin during the curing process, and partial characterization of thermo mechanical behavior of resins and composites close to and below the glass transition temperature. Some methods for predicting residua

DD FORM 1 JAN 73 1473

UNCLASSIFIED

SECURITY CLASSIFICATION OF THIS PAGE *(When Data Entered)*

stresses and crack growth in composites were developed, and special cases were studied. Also, nonlinear constitutive equations were incorporated into a finite element code. A neutron radiography facility was developed and applied to the inspection of moisture content and flows in composites.

4

6

COMPOSITE MATERIALS FOR STRUCTURAL DESIGN.

9

(First Annual Technical Report)
no. 1, 15 Jan 78 - 14 Jan 79

by the

Professional Staff

10 Richard Schapery of the

TEXAS A&M UNIVERSITY College Station.

Mechanics and Materials Research Center.

18 AFOSR 19 TR-79-0347

to the

16 2307

Air Force Office of Scientific Research

17 B1

Office of Aerospace Research
United States Air Force

14 MM-3724-79-2

12 152p.

15 Contract No. F49620-78-C-0034

11 March 1979

407501

TABLE OF CONTENTS

1. INTRODUCTION

1.1 Summary

Primary activities during the first year of the project consisted of: (i) developing a composites processing and testing laboratory and a neutron radiography facility, (ii) conducting research in accordance with the Statement of Work given in Section 1.2, (iii) preparing four technical papers, (iv) various interactions of the faculty with the technical community through presentation of papers, chairing of conference sessions, consulting, etc.

Sections 2 - 4 describe the research activities. The professional personnel associated with the project and the individual activities at conferences are given in Section 5. Papers completed during the year are reproduced in the Appendix.

1.2 Statement of Work

"a. Investigate the effects of composite cure cycle parameters on the mechanical characteristics of structural specimens and components (see Section 2.):

(1) Investigate the development of new innovative in-process monitoring devices and study improvements in the "Duomorph" sensor.

(2) Conduct experimental measurements on both neat resin, unidirectional laminates and cross-ply laminates to establish the relationships at various elevated temperature and relative humidities between processing parameters and mechanical strain rate behavior, linear and identified nonlinear viscoelastic behavior, dimensional stability,and fracture characterization.

(3) Investigate the influence of processing parameters on Tg at various relative humidities.

b. Investigate the influence of elevated temperature and high relative humidity environments on composite laminates and adhesively bonded structural components (see Section 3.):

(1) Investigate, on a theoretical level, the formulations of a coupled diffusion theory to accurately predict the environmental degradation of composite laminates and adhesive mechanical performance which considers the influence of cure cycle parameters being investigated in a above.

(2) Predict moisture concentration profiles and internal stress/strain fields within a laminate and bonded structure as well as in the vicinity of exposed edges. These profiles will consider generic environmental conditions of absorption and desorption.

(3) Compare theoretical predictions with available experimental data or define experiments which would yield necessary data for this comparison.

c. Investigate suitable experimental techniques which can be used to nondestructively examine composite laminate initial defects, damage growth and environmental degradation characteristics which affect mechanical performance. Initially, emphasis will be given to neutron radiography as a suitable technique (see Section 4.):

(1) Conduct necessary experiments to characterize neutron beam parameters and associated parameters' sensitivities applicable for nondestructively examining major composite laminate mechanical characteristics which affect strength, dynamic response and durability.

(2) Investigate the development of experimental neutron radiography techniques to measure moisture concentrations in composite laminates as well as spatial concentration profiles.

(3) Investigate the development of automated procedures for the analysis of data from neutron radiography experiments which accurately and efficiently characterize and identify laminate initial defects, mechanical damage, and moisture concentrations.

(4) Investigation of automated data analysis procedures in c(3) above will consider both planar and stereographic data displays."

2. PROCESSING AND TESTING OF RESIN AND COMPOSITES

2.1 New Equipment

A press for fabricating flat and curved laminated plates was designed and built at Texas A&M University. This press, which is shown in Fig. 1, is electrically heated, water cooled, and designed to apply temperatures and pressures in excess of 400°F (204°C) and 100 psi, respectively. Glass laminates have been successfully fabricated and, it is planned to initiate the processing of graphite composites early in the next reporting period.

Nine environmental chambers for conditioning specimens at various temperatures and humidities were also built. These chambers, two of which are shown in Fig. 2, have an internal glass cavity 6 inches in diameter x 15 inches long. Humidity is maintained by means of salt and acid solutions. An immersion bath was constructed for submersing specimens in water at controlled temperatures up to the boiling point. It is planned to build five additional environmental chambers for use with existing constant-load testing frames; their design is described in Section 2.2.

Also acquired during the first year are (i) Perkin-Elmer thermal test equipment consisting of a thermo-mechanical analyzer (TMS-2) and differential scanning calorimeter (DSC-2) and (ii) a Micromech microwafering saw for machining laminates.

2.2 Constant Load, Temperature and Humidity Apparatus*

Five existing lever-arm type constant load mechanical testing frames are to be modified by the addition of environmental chambers for controlling a constant temperature and humidity during a creep and recovery test. The design of the chambers, humidity generator, and load frame modifications have been detailed. The current effort on this project is being directed toward manufacturing and procurement of the various components necessary to make the facility operational.

The design goals are to maintain a constant temperature and humidity environment during a creep and recovery test over a period as long as several weeks. The temperature range of interest is 23°C (ambient) to 100°C and the humidity range is 7 - 98% relative humidity. Long term stability of

*Prepared by Dr. K. L. Jerina

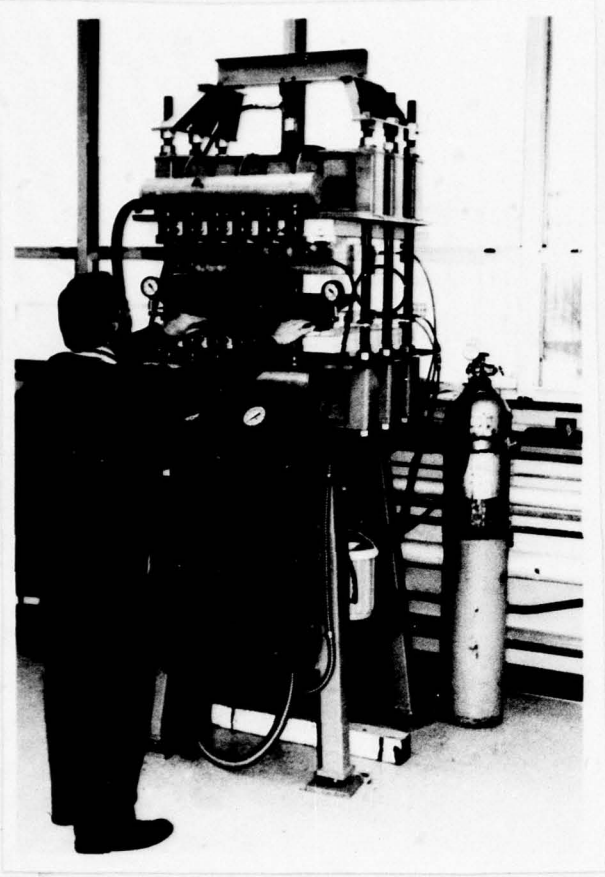

Figure 1. High Temperature Press

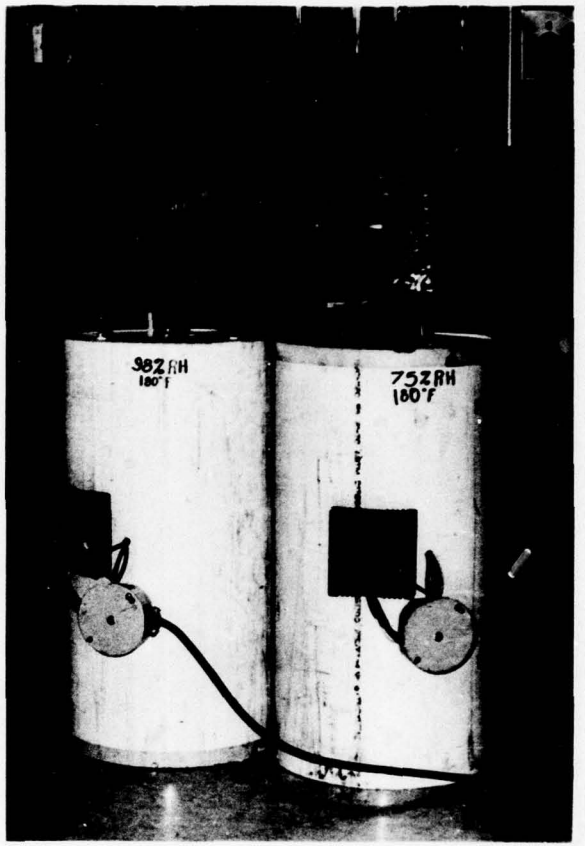

Figure 2. Specimen Conditioning Chambers

temperature and humidity was a major factor in the choice of the system to generate the environment. Electric resistance heating tapes controlled by proportional closed loop temperature controllers will be used. Constant humidity will be maintained by exposing certain saturated and non-saturated aqueous solutions to an enclosed air space at known temperature [1]*. Temperature will be controlled by placement of heaters throughout the system. Humidified air is to be circulated by mechanical convection throughout the system from a central humidity generator.

Humidity: The concentration of water vapor in air can be expressed as parts per million, percent relative humidity, or percent of saturation [2]:

$$C = \frac{p_w}{P-p_w} \times 10^6$$

where

$C \equiv$ concentration (ppm)

$p_w \equiv$ vapor pressure of water (mm Hg)

$P \equiv$ total pressure of system (mm Hg)

$$H_R = \frac{p_w}{p_{ws}} \times 10^2$$

where

$H_R \equiv$ relative humidity (%)

$p_w \equiv$ partial pressure of water at temperature T (mm Hg)

$p_{ws} \equiv$ partial pressure of water at saturation at temperature T (mm Hg)

$$H_p = \frac{p_w(P-p_{ws})}{p_{ws}(P-p_w)} \times 10^2$$

where

$H_p \equiv$ humidity (% of saturation)

At room temperature the partial pressure of water vapor is small with respect to the total pressure. Therefore H_R and H_p are nearly the same. As

---

† References are listed in Section 6.

the temperature increases the partial pressure becomes more significant for a given humidity and the difference between percent saturation and relative humidity becomes significant.

Generating a humidity environment: Production of standard atmospheres of known humidity can be achieved by several techniques [1, 2]. Numerous humidity chambers are available within the ranges of 20 - 95% H_R and 3 - 90°C. However,a special system can be designed to operated in a 2 - 98% H_R range. A passive system is desirable for long term testing since it will be inherently the most reliable.

Constant humidity air at a known temperature can be maintained in a static system by exposing certain aqueous solutions to an enclosed air space [1, 2], Tables of some of these solutions are given in [3, 4], and selected saturated salt solutions are listed in Table 1. In this manner relative humidity can be maintained from 7 to 98% by varying the saturated solution used. Sulfuric acid or glycerine and water solutions will also equilibrate to a constant humidity in an enclosed air space at a known temperature [1, 3, 4]. The H_R can be varied by changing the concentration of the solution. However, if water vapor escapes from the system the solution concentration and equilibrium humidity will change. With a saturated salt solution any loss of vapor would result in precipitation of salt from the solution thus maintaining a constant solution concentration and constant relative humidity. Glycerine solutions cannot be used above 70°C because the vapor pressure of glycerine becomes significant at these temperatures. For example, at 100°C the vapor pressure of glycerine is 140 mm Hg. Since the vapor pressure of sulfuric acid at 100°C is less than 1 mm Hg, sulfuric acid solutions can be used to obtain very dry conditions in the higher temperature range.

Consequently, in order to cover a wide range of temperature (23-100°C) and relative humidity (7-98%), glycerine water, sulfuric acid water, and saturated salt solutions will be used.

Description of apparatus: A system drawing, Fig. 3, shows the components of the mechanical testing frame and humidity generator. The generator will be capable of supplying humidity to 5 test frames although only one is shown for illustration purposes.

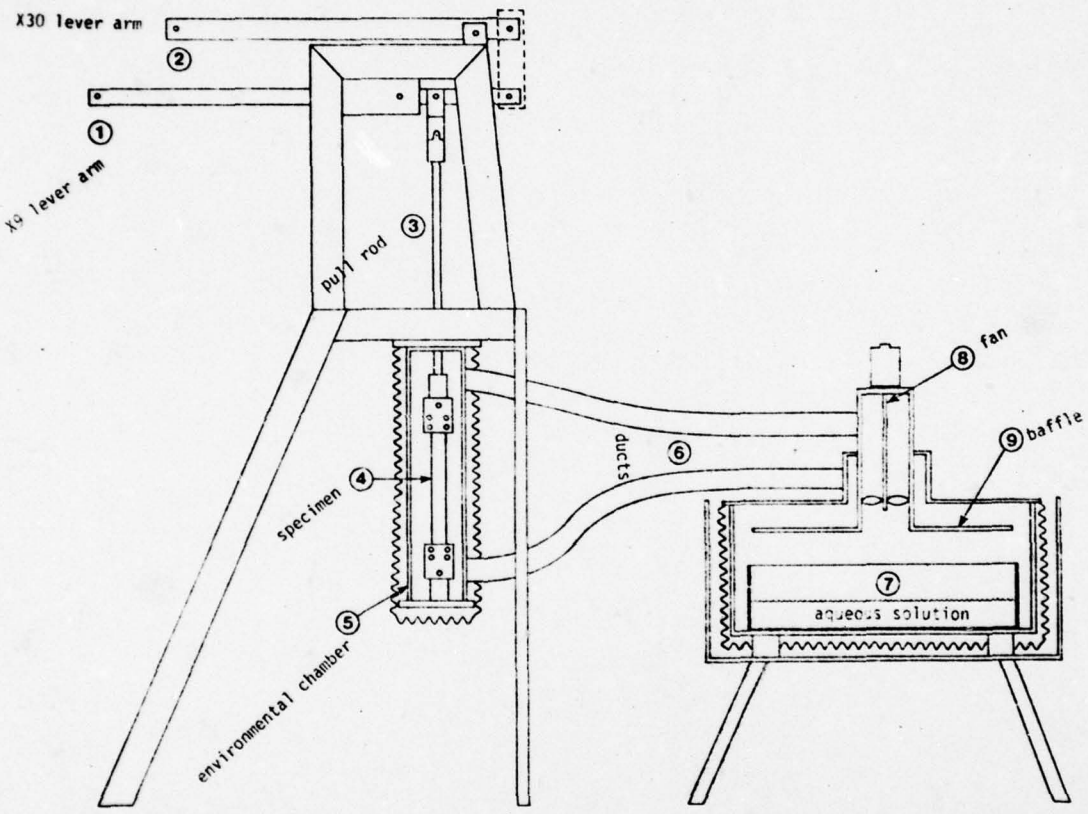

Figure 3. Mechanical Testing Frame and Humidity Generator

The constant load test frame has a single and compound lever arrangement. These levers provide a mechanical advantage of approximately 9 for the single lever and 30 for the compound lever. The maximum load capacity of the frame is 6,000 pounds on the specimen. A pull rod extends through the base of the machine and is attached to the specimen within the environmental chamber. Specimens are placed in the chamber by removing the bottom cover. Humid air is circulated through the chamber by a fan in the humidity generator. Insulation surrounds the chamber which is kept at constant temperature by electric resistance heating elements.

The humidity generator consists of a shallow container for the aqueous solution. This container is surrounded by an electrically heated and insulated shell. A small fan circulates air through a baffle in the generator to promote evaporation. The humid air is then circulated to the test chambers through heated ducts.

TABLE 1

Solutions for Maintaining Constant Humidity

H_R(%)	T(°C)	Saturated Solution
98	20	$Pb(NO_3)_2$
96.6	100	NaF
79.2	20	$NH_4C\ell$
78.3	90	$KC\ell$
47	20	KCNS
50.4	100	NaI
20	20	$KC_2H_3O_2$
22.6	80	KF
7	25	$NaOH \cdot H_2O$

2.3 Dynamic Mechanical Response of Resins and Composites*

This portion of the study on the effect of cure cycle parameters is concerned with the direct monitoring of the viscoelastic complex modulus of resins and composites during and immediately following the cure cycle. We have adapted a piezoelectric device called the "duomorph" for such use. Described in this section is the duomorph, its analysis, and the first application in which room-temperature curing epoxy was monitored. It should be noted that a torsional pendulum [5, 6] and cone and plate devices [7] have been used to follow curing of polymers; but these techniques do not lend themselves to in situ monitoring of laminates.

Description of the gage: The duomorph consists of two crystalline piezoelectric plates which are bonded together; a central metallic plate is sometimes used to alter the response characteristics of the assembly. The duomorph is electrically excited and, through a study of its bending response when in contact with a material of interest, the viscoelastic properties of this material are obtained. The gage was originally developed for the purpose of measuring in situ complex modulus when embedded in the fuel in a solid propellant rocket [8]; for this application, which involved telemetry to trigger and measure the gage response, one piezoelectric plate was employed as a driver and the voltage response of the other was used to obtain the strain response.

For precise measurement of viscoelastic properties in the laboratory it was found that it was best to use both piezoelectric plates as drivers and employ standard electrical-resistance strain gages to monitor the bending of the assembly [9]; see Fig. 4. The two plates are of opposite polarity so that when they are excited by a voltage one plate expands while the other contracts. Without external constraint this deforms a duomorph into exactly the same shape as would a uniform bending moment; i.e., a spherical surface. If an alternating voltage is applied the curvature oscillates from one direction to the other.

Two pairs of strain gages are bonded onto the two outside surfaces of the duomorph, and are used in a Wheatstone bridge to measure the extent of bending. This measurement is made with the sensor by itself and then

*Prepared by Dr. R. A. Schapery and Mr. B. C. Harbert

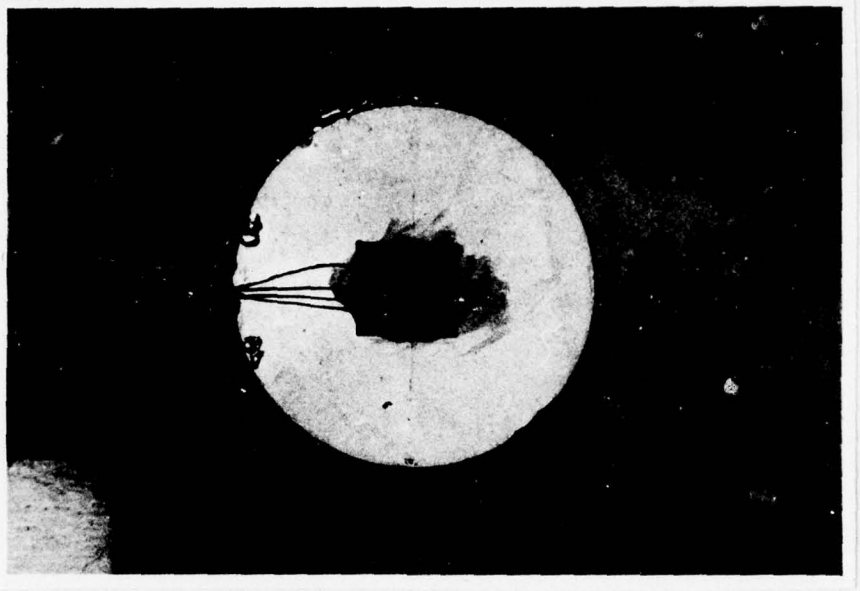

Figure 4. Duomorph Mounted on a Rubber Block

with the sensor in intimate contact with the material being tested; the difference reflects the stiffness of the material being tested.

In most laboratory applications made to-date circular plates with in-plane isotropy have been used, and the gage was either placed in contact with the surface of a large mass or embedded in the mass of material. Rubber, solid propellant, soils [8] and asphalt [10] have been studied on other projects.

Work on the present AFOSR contract has been concerned so far with developing and applying a technique to obtain mechanical properties of a thin layer of epoxy resin using the arrangement shown in Figs. 5 and 6. After the technique has been developed and demonstrated for high-temperature epoxies employed in advanced composites, it is planned to extend the concept to laminates, starting with a unidirectional laminate; in the latter case, an orthotropic rectangular duomorph which bends primarily in the direction normal to the fibers will be used. The bonding systems and strain gages now used with duomorph are applicable to temperatures above 400°F, and therefore no major difficulties are expected in standard

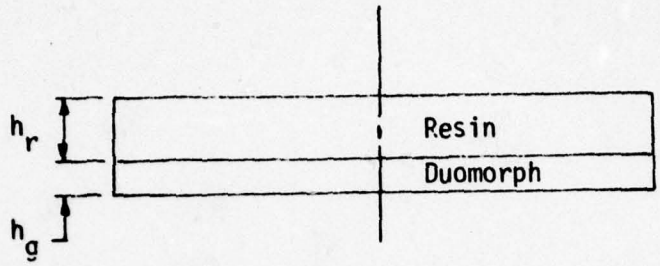

Figure 5. Cross-Section of Duomorph with Resin Layer

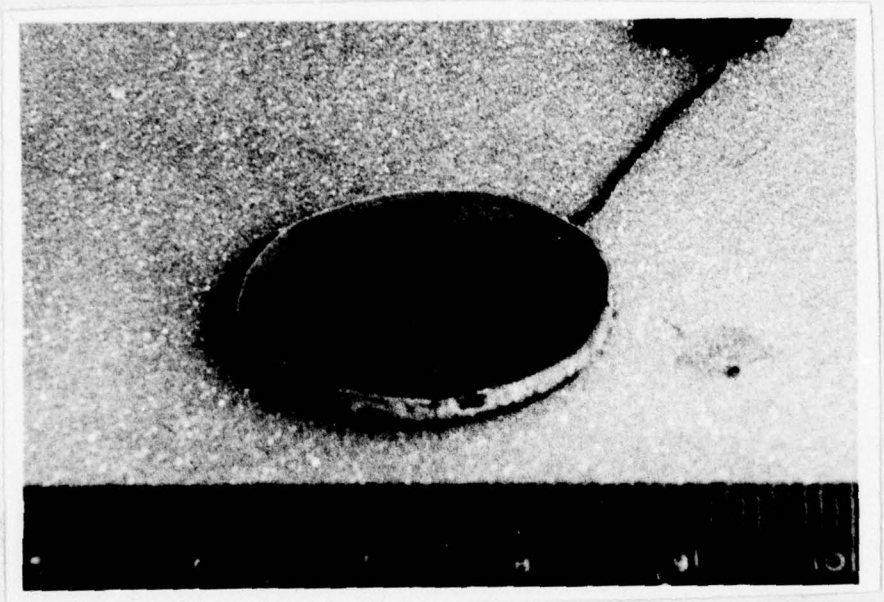

Fig. 6. Duomorph with Resin Layer on One Surface

cure and post-cure cycles.

Analysis of the Duomorph: The plate configuration in Fig. 5 had not been analyzed in the previous studies of the gage. Therefore, this geometry was analyzed in order to provide equations for selecting proper plate dimensions and interpreting experimental results. Standard assumptions of thin-plate bending theory were made. These include 1) lines perpendicular to the neutral plane remain so during bending, 2) strains are small, 3) the plate is of uniform thickness, and 4) the two materials, the sensing disk and the polymer, are each isotropic and homogeneous in the plane of the disk. The first assumption implies that edge effects are negligible; it is assumed that this will be true if the ratio of the diameter to total thickness of the plate is greater than 10. (If there are any designs for which this ratio is approached, a finite element analysis will be conducted to check thin plate theory and modify the results if necessary.)

The gage response quantity of interest is the ratio $\hat{\varepsilon}_r/\varepsilon_o$, where $\hat{\varepsilon}_r$ is the difference between the strains on the top and bottom surfaces of the duomorph with the resin, and ε_o is the same quantity but without the resin. This ratio will be given first for elastic materials and then for viscoelastic materials.

The normal stress-strain equations for an element of elastic resin or gage material in plane stress using a cylindrical coordinate system are

$$\varepsilon_r = \alpha V + \frac{1}{E}(\sigma_r - \nu\sigma_\theta) \tag{1}$$

$$\varepsilon_\theta = \alpha V + \frac{1}{E}(\sigma_\theta - \nu\sigma_r) \tag{2}$$

where standard notation for stress and strain is employed. The subscripts g and r will be used to denote mechanical properties of the duomorph gage and resin, respectively.

Thus

E_g, ν_g = Young's modulus and Poisson's ratio of the gage (with a closed electrical circuit)

E_r, ν_r = Young's modulus and Poisson's ratio of the resin.

Also, V is the voltage applied to the duomorph faces and α is the piezoelectric expansion coefficient; α = o for the resin, and the sign of α for one plate of the gage is opposite that of the other one.

The constitutive Eqs. (1) and (2) together with the remaining equations from classical plate theory for an unsupported disk,[11] yield

$$\varepsilon_o = 3\alpha V \tag{3}$$

and

$$\frac{\hat{\varepsilon}_r}{\varepsilon_o} = \frac{1}{3}\left\{\frac{4}{3}[1+(h^3-1)S] - \frac{1+(h^2-1)S}{1+(h-1)S}\right\}^{-1} \tag{4}$$

where

$$S \equiv \frac{E_r/(1-\nu_r)}{E_g/(1-\nu_g)} \tag{5}$$

and

$$h \equiv 1 + h_R \quad , \qquad h_R \equiv \frac{h_r}{h_g} \tag{6}$$

This result is plotted in Fig. 7 for a wide range of the two dimensionless parameters, S and h; the graph will aid in selecting appropriate resin and gage thicknesses, depending on the resin modulus range of interest.

In applications of the gage, one is interested in calculating S, given values of $\hat{\varepsilon}_r/\varepsilon_o$ from tests. For this purpose we rearrange Eq. (4) to find a quadratic equation for S:

$$S^2\left\{R[4(h-1)(h^3-1)-3(h^2-1)^2]\right\} + S\left\{R[4(h^3+h-2)-6(h^2-1)]-(h-1)\right\} + R-1=0 \tag{7}$$

where

$$R \equiv \hat{\varepsilon}_r/\varepsilon_o \tag{8}$$

The largest root provides the physical value of S.

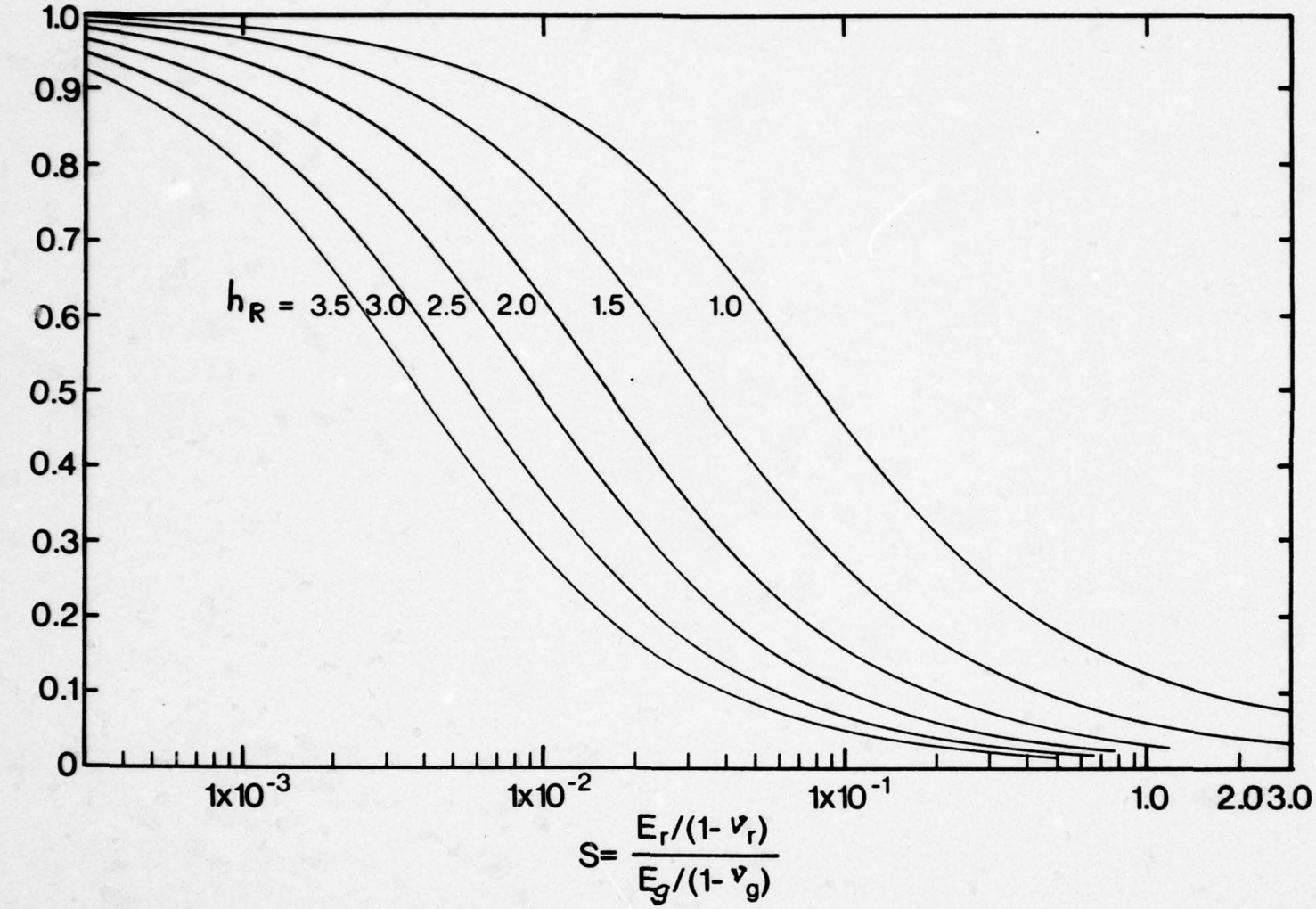

Figure 7. Duomorph Strain Ratio vs. Stiffness Ratio for Several Resin Layer Thicknesses (Elastic Analysis)

These results may be extended to viscoelastic behavior by means of the correspondence principle for vibrating systems [12]. Using complex notation, the voltage input is written as

$$V = |V| e^{i\omega t} \tag{9}$$

where $|\ |$ denotes amplitude and ω is the frequency (radians/time). The expansion coefficient α is found to be a complex function as a result of electromechanical interactions, and therefore from Eq. (3),

$$\varepsilon_o = |\varepsilon_o| e^{i(\omega t - \phi_g)} \tag{10}$$

$|\varepsilon_o| = 3|\alpha||V|$ and ϕ_g is the phase angle between free gage expansion and the voltage. Also, the bending strain with resin is written as

$$\hat{\varepsilon}_r = |\hat{\varepsilon}_r| e^{i(\omega t - \theta_r)} \tag{11}$$

It is found that both ϕ_g and θ_r are non-negative (i.e. the strain lags the voltage input) and consequently we obtain

$$R = |R| e^{-i\theta} \tag{12}$$

R is defined in Eq. (8) and

$$|R| = \frac{|\hat{\varepsilon}_r|}{|\varepsilon_o|} , \qquad \theta = \theta_r - \phi_g \tag{13}$$

After $|R|$ and θ have been obtained from duomorph tests at a given frequency, the complex version of S, Eq. (5),can be found from the solution of Eq. (7), in which R in Eq. (12) is input. The solution is written as

$$S = |S| e^{i\phi} \tag{14}$$

Experimental studies indicate that E_g and ν_g are constant over the frequency range employed (0.1 - 100 HZ), and therefore the complex

resin modulus $E_r^*/(1-\nu_r^*)$ is (where an asterisk denotes a complex, viscoelastic property)

$$\frac{E_r^*}{1-\nu_r^*} = \frac{E_g}{1-\nu_g} |S| e^{i\phi} \tag{15}$$

The quantities E_r^* and ν_r^* are the complex Young's modulus and Poisson's ratio of the resin, respectively.

Below the glass-transition temperature of cured epoxy it is found that ν_r^* is essentially a constant, say ν_r. Therefore, it is helpful to rewrite Eq. (15) by introducing the modulus

$$\hat{E}_r^* \equiv \frac{1-\nu_r}{1-\nu_r^*} E_r^* \tag{16}$$

Thus,

$$|\hat{E}_r^*| = \frac{1-\nu_r}{1-\nu_g} E_g |S| \tag{17}$$

According to Eq. (16), and if the frequency dependence of ν_r^* is neglected, $|\hat{E}_r^*|$ is the amplitude of the complex Young's modulus, E_r^*.

Finally, it should be noted that the maximum value of S for epoxy is approximately 0.05, as shown in the next section. As a result, we have found that the S^2 term in Eq. (7) can be neglected; thus a complex solution is easily found analytically in terms of $R = |R|e^{-i\theta}$ by means of a small amount of complex algebra. However, for completeness, we have written a computer program which solves Eq. (7) exactly in order to provide the complex modulus $\hat{E}_r^*$ from gage test data.

Experimental technique: The duomorph used to study epoxy consisted of two 1 inch diameter piezoelectric ceramic disks 0.010 inch thick, bonded together by means of a conductive epoxy adhesive.

Using the information in Fig. 7 and $E_r \simeq 0.5 \times 10^6$ psi and $E_g \simeq 11.8 \times 10^6$ psi, it was estimated that the thickness ratio h_R (resin thickness to duomorph thickness) should be approximately 3:1. In preparing

for casting a layer of epoxy on one side of the duomorph a circular dam of thin paper was built up around the edge of the 1 inch diameter duomorph extending 0.060 inch above the surface. The frequency response of the duomorph with the dam was then determined with the assembly resting on a one inch thick layer of polyurethane foam. The position and support to be used when the epoxy was to be placed for cure. Excitation was from a sine wave source at 18 volts p-p, and covered a frequency range of 0.1 to 100 Hz.

Since the effort at this point was mostly concerned with checking the feasibility of following the cure of an epoxy, a room temperature cure system was selected so that it would be easy to evacuate any entrapped air from the mixing process. A suitable system was found by mixing Shell Epon 815 with 5 parts/hundred D.E.P. (Diethylaminoproylamine). A small amount of these ingredients was mixed by hand, evacuated, and then cast into the thin space on top of the duomorph. The response of the duomorph was obtained periodically as the epoxy passed through the cure process.

Following the completion of the cure process the duomorph with the cured epoxy was examined to check for thickness variation. It was found that a slight meniscus had formed near the edge with the circular edge being approximately 0.005 above the flat section part. The total thickness (including the thickness of the duomorph) was measured to be 0.087 ± .005 inch, yielding the total h_R thickness ratio of 3.35:1. The meniscus was next removed to the point where a flat surface was obtained across the epoxy layers. The total thickness following this operation was found to be 0.082 ± .002 yielding $h_R \simeq 3.1$. Figure 6 is a photograph showing the duomorph with the epoxy layer after the surface was smoothed down. The "effective" thickness ratio of the epoxy with meniscus was then determined from Eq. (4) to be 3.15 by requiring the resin modulus before and after meniscus removal to be the same;this value of h_R was used in all analyses of data obtained during cure.

At the time of casting the layer of epoxy on the duomorph, similar shapes were cut from the epoxy mix to provide material with the same cure history for independent property determination on the fully cured material. The test apparatus used in making these tests consisted of a simple cantilever beam. The thin beam cut from the epoxy was loaded at the free end

by a weight having a hook to precisely locate the point of application. Beam deflection at the free end was monitored using a microscope mounted on a precise traversing stage which provided linear measurement of displacement to within ± 0.001 mm.

Experimental results: The bending strain amplitude $|\hat{\varepsilon}_r|$ and phase angle θ_r (cf. Eq. (11)) were obtained at four frequencies (0.1, 1, 10, 100 Hz) at ten different times during the cure process; the strain $|\varepsilon_o|$ and angle ϕ_g (cf. Eq. (10)) were obtained prior to the initiation of curing. Equation (13) was then used to derive R and θ at these times which, together with Eqs. (7), (12) and (17) provided values of the complex modulus amplitude $|\hat{E}_r^*|$ and phase angle ϕ. The results cover a greater than 100:1 change in modulus, and are shown in Figs. 8 and 9. It should be added that earlier direct mechanical calibration of the duomorph [9] yielded $E_g/(1-\nu_g) \simeq 16.8 \times 10^6$ psi (where $\nu_g \simeq 0.3$).

All moduli in Fig. 8 approach 0.45×10^6 psi at long times. This value is identical to that found independently from the early-time creep response of a beam in flexure tested at 70 hours after mixing of the polymer (cf. Fig. 8). An additional beam flexure test made at 360 hours revealed almost negligible creep out to 1000 seconds, and provided again the same modulus. The fact that the 70 hour old resin exhibited significant creep is very interesting. This behavior implies that the aging actually continued well beyond the age where the duomorph data leveled off; therefore, the longer the resin was under load,the more influence long-term aging has on mechanical response.

Notice that the phase angle data in Fig. 9 decreases continuously as curing proceeds. The behavior exhibited is very reasonable since $\phi = 90°$ for a Newtonian fluid and $\phi = 0°$ for an elastic solid.

In view of the success of the duomorph in following changes in a room temperature cure epoxy, it is planned to next evaluate it with the Hercules 3502 resin, which is used in an advanced composite.

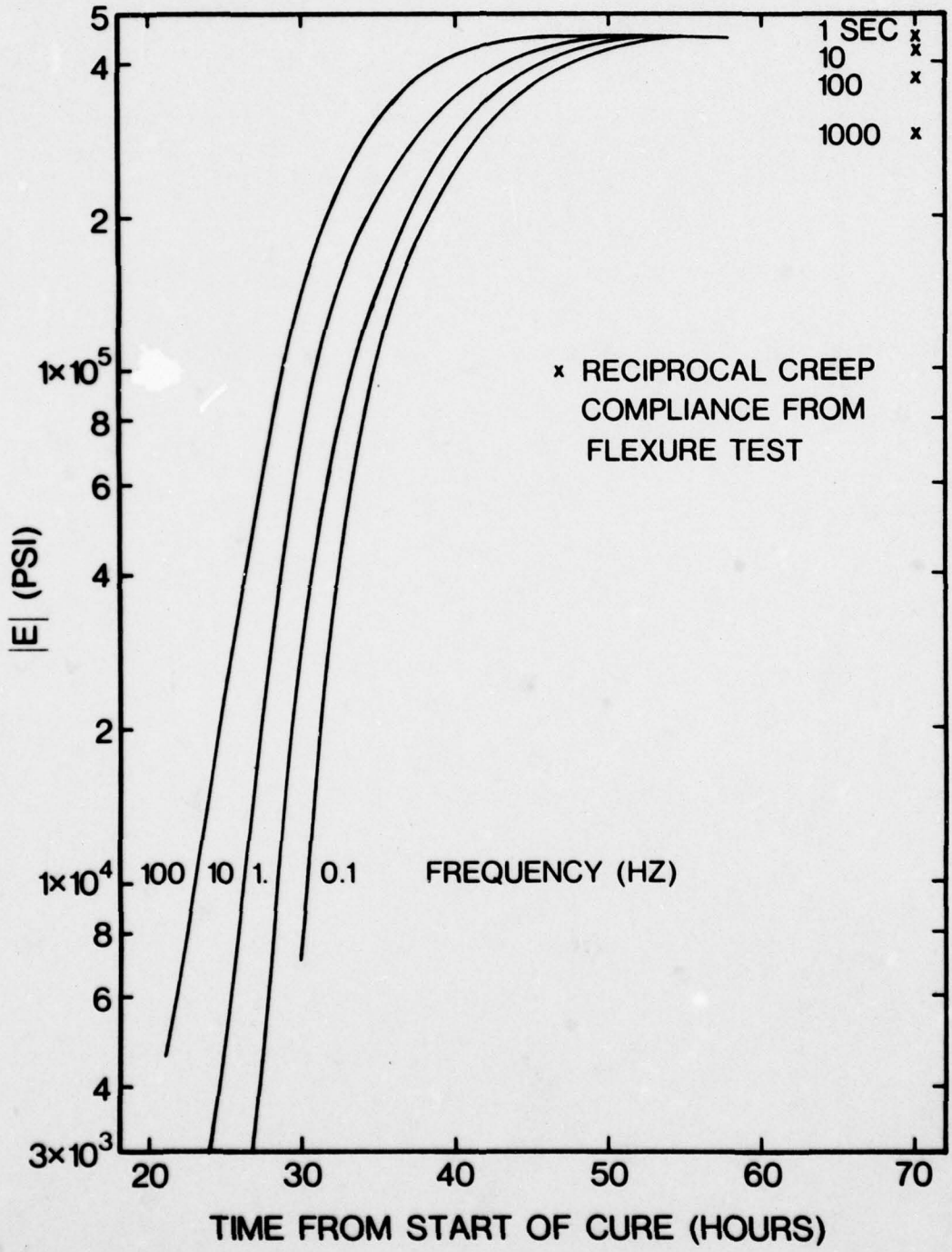

Figure 8. Amplitude of Complex Modulus of Resin vs. Age

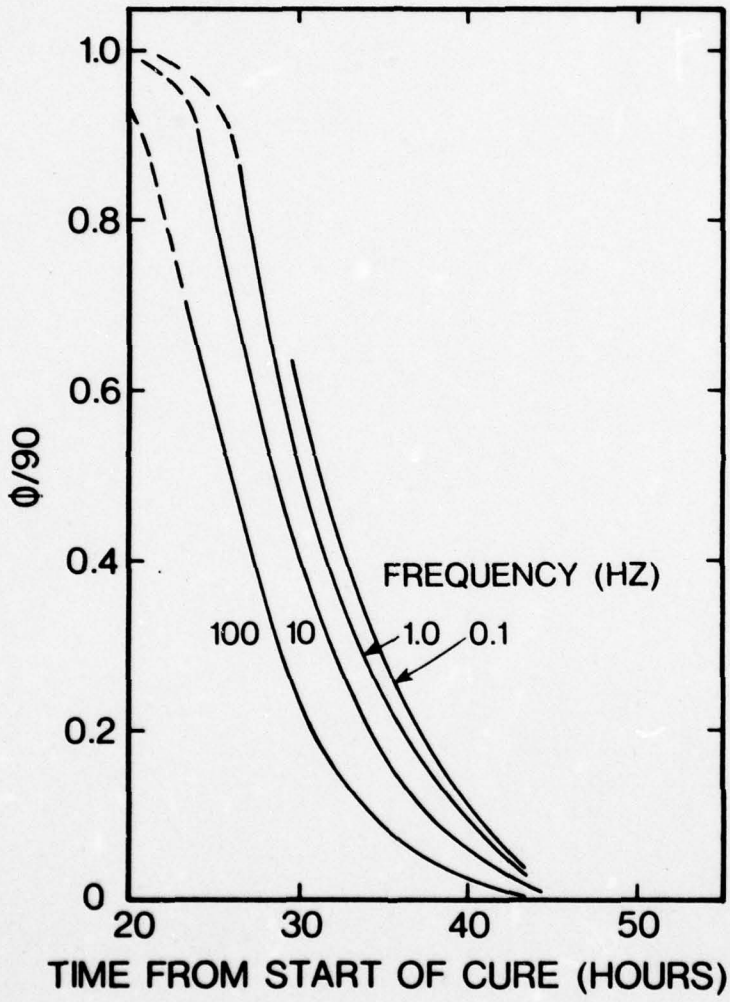

Figure 9. Phase Angle of Complex Modulus of Resin vs. Age

2.4 Enthalpy Changes in Epoxy Resin *

The influence of cure cycle parameters and age following cure on enthalpy and associated specific heat changes in epoxy resin is under investigation. Emphasis to-date has been on developing maximum sensitivity and reproducibility in the measurements with the scanning calorimeter (DSC) since we are seeking to measure small changes in the thermal properties produced by various treatments.

Background: This type of study has been carried out on other materials but the measurements are difficult in that the thermal history must be carefully specified [13 - 20]. An additional complication is that the effect of thermal history is confounded with the effects of moisture content which is known to produce large effects.

The materials now used as the matrix for the advanced graphite composites are selected to have an extremely high value of the glass transition temperature, T_g, to insure good structural performance at elevated temperatures and humidities;since moisture and other plasticizers reduce T_g, the extremely high value of T_g permits more reduction before degradation of properties becomes a more serious problem. Consequently, the glass transition in the dry state is often well above 200°C (392°F).

The rate of cure slows at temperatures below T_g, and the glass transition raises with the extent of cure; therefore T_g often rises only to the range of the cure temperature leaving a number of unreacted groups in the sample. This undercured sample will then cure further whenever the temperature and moisture content become high enough for some molecular mobility to result. This results in a glass transition of the undercured material which changes with time at any high temperature which is needed to measure it. One is limited in the upper limit of the cure temperature by the temperature that causes chemical degradation of the sample. It may happen that the glass transition temperature can be elevated into this region of thermal degradation so that, even in principle, T_g is impossible to measure.

---

*Prepared by Dr. J. S. Ham

Hercules Inc. has provided us with one gallon each of 3502 and 3501-6 uncured epoxy resins for study on this project. However, these resins are proprietary and no molecular structure is given. We will make comparison with our studies of these resins with similar studies on a series of epoxies whose structure and composition is known and where reactions can be completed. These latter resins are the series based upon DGEBA cured with MDA. DGEBA is the common commercial epoxy and comes in a variety of molecular weights which can be used to control the molecular weight between crosslinks. The MDA (methylenedianiline) is a common curing agent that is similar to the diaminodiphenysulfone probably used as a curing agent in the proprietary resins. These are high temperature epoxy resins with glass transitions ranging from 95° to 180°C depending upon the molecular weight of the epoxy component. Such materials have been studied in the literature and have a regular sequence of properties varying as the crosslink density varies over a range of values [21]. Since the crosslink density is one of the important parameters used in the proprietary aerospace resins to achieve a very high value of Tg, we hope to be able to extrapolate from the standard epoxy materials to the properties of the proprietary resins.

Experimental procedures for casting resins: The samples are cast with some differences in technique depending upon the properties of the starting materials. We have been casting 1/8 inch thick slabs using the standard techniques of using two glass plates held apart by spacers with a soft rubber tube as a gasket. We use either mold release agent on the glass or two mylar sheets to protect the glass surface from the resin. The mold release agent may contaminate the surface of the resin but one obtains smooth flat surfaces. The mylar sheets sometimes wrinkle making the sample thickness uneven. For our thermal measurements, either technique is possible, but avoiding the possible contamination of the mold release agent makes the mylar sheet preferable. We will need smaller variations in sample thickness than we find using the mylar sheet when mechanical measurements are to be made on the same samples and so need to refine the casting technique.

The low molecular weight epoxy components are liquids and the higher molecular weight components are solids. The MDA is a high melting solid but will dissolve slowly at temperatures below its true melting temperature.

The low molecular weight materials are mixed with the MDA to form a slurry which is then poured into the molds. The higher molecular weight epoxies are ground and mixed with the MDA as two powders and this is then put into the mold.

The mold is held in a vacuum oven where we can watch the melting through a window. The samples are heated to between 90 and 100°C while under vacuum. At these temperatures there is a component given off (possibly dissolved water, but the volume released seems to be too large for this to be the case) producing a foam. The pressure is increased whenever the foam threatens to overflow the cell so that, by varying the pressure, we expand and contract the bubbles and they gradually work their way to the surface of the material. The low molecular weight resins and the proprietary materials become quite fluid at these temperatures so the bubbles can be worked out quickly. The higher molecular weight epoxy components are viscous and so considerable patience is required to get the bubbles from these materials.

While higher temperatures would make the material more fluid it can also start the curing reaction which is to be avoided until the bubbles are completely removed. Once the bubbles are removed, the samples are cured at 180°C for two hours.

The proprietary resins have a curing reaction triggered at high temperatures by the decomposition of an amine complex of BF_3. Thus, these resins have a broad temperature range in which they are liquid before they start curing. We have cured samples up to 1/8 inch thick and have had no difficulty with thermal runaway which can happen in the resin samples according to reports. Thermal runaway is a phenomenon where the reaction produces heat faster than it can be conducted away and so the reaction accelerates in the middle of the sample to scorch the material there. This can be avoided when it is a problem by initially curing at a low curing temperature until enough of the reaction is complete so that the remainder will not get out of control.

Enthalpy measurements: Our first study is an attempt to measure the relaxation of enthalpy with time at a temperature below the glass transition temperature [19, 20]. To do this, the samples are cured in the

scanning calorimeter so that no further reactions can be detected with repeated heating to some determined high temperature. The sample in its aluminum holder is then held for a determined amount of time at some fixed lower temperature where relaxations in the glassy material take place. This time is up to one month. The DSC scan is run at a high sensitivity and the sample is held above the glass transition for 5 or 10 minutes and then rerun. The difference in these two runs is the effect of aging at the lower temperature since the sample is restored to its original condition by heating above the glass transition temperature. The observed effects are small and some typical traces are shown in Fig.10 but we have not been able to make a sufficient number of runs to get systematic data since the DSC must be set very precisely to permit the slope and intercept to be set appropriately without a trial run.

The sample in Fig.10 was aged one month at room temperature after holding above T_g to erase prior history. The trace obtained is the uppermost curve. After holding this sample above T_g for 5 minutes, the next curve was obtained. This curve has the normal step shaped curve typical of a glass transition. The difference between these two curves is due to aging or enthalpy relaxations. (The slope of the background has been selected so that the trace stays on the scale even with the change of specific heat around the glass transition; subtract this slope from the data to obtain the true variation of specific heat. A vertical shift was made so that the traces would not cross each other; the true value of the specific heat is the same above the transition region for the two runs shown.

Future work: There are a number of correlations to be made once we are able to measure the relaxation of the enthalpy with high precision. First, we would like to compare the behavior of the standard materials with that of the proprietary materials used in the advanced composites. These should have quite similar behavior except for T_g. Struik says that this enthalpy relaxation occurs at all temperatures above that of the secondary transition [18]. This should be similar in these materials.

Second, we would like to look at the influence of moisture upon the relaxation of the enthalpy. It is known that moisture can lower the glass transition by many degrees and it may enhance the rates of enthalpy

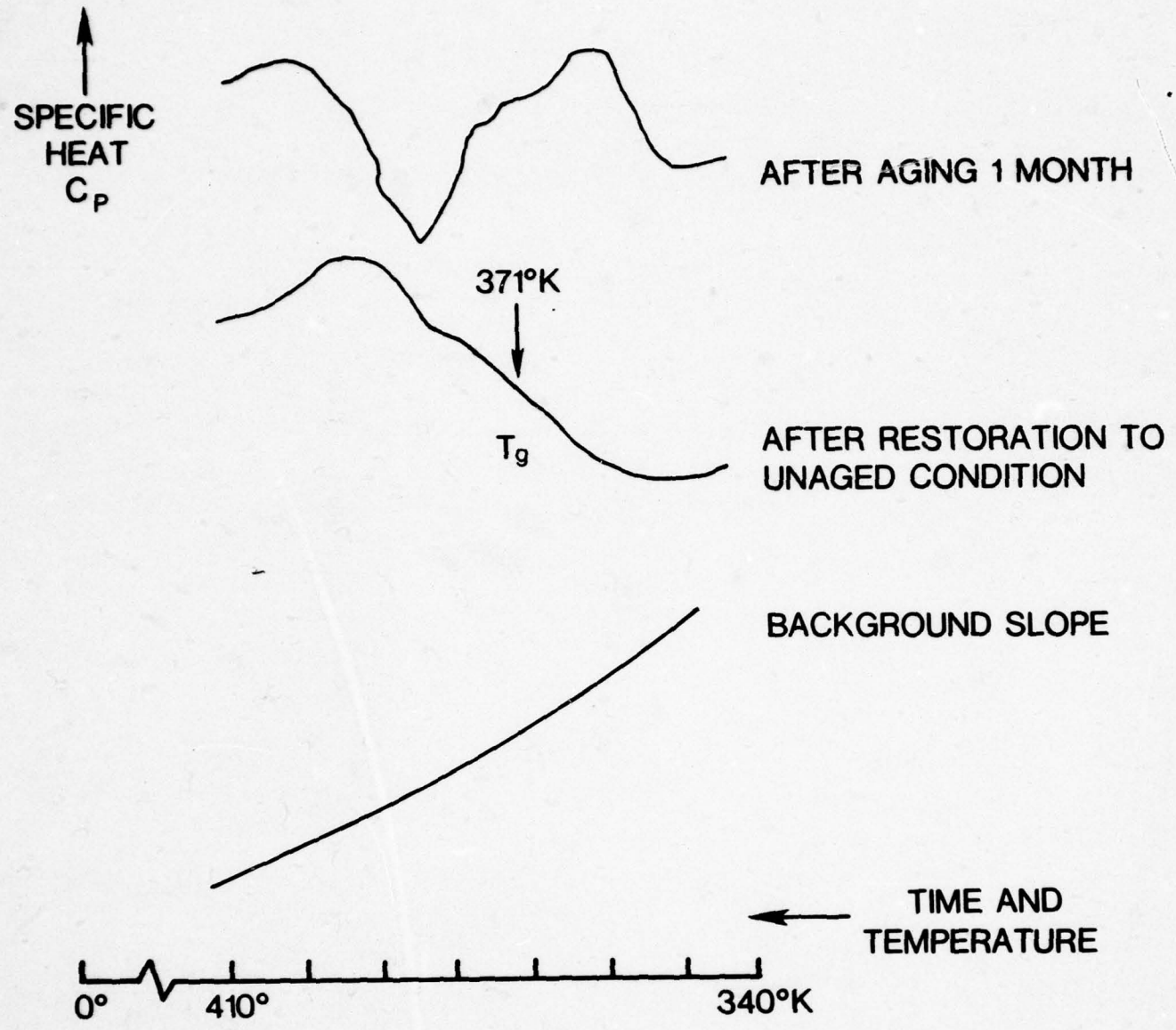

Figure 10. DSC Scan of Epoxy Resin System

relaxation also. There is little information on this question in the literature.

Third, there is a cluster of questions concerning the relationship of the relaxation in the enthalpy with the relaxation in residual stresses and mechanical measurements. There seems to be some correlation but also some differences in the published data [18, 19].

Finally, after looking at the various phenomena related to the glass transition, we plan to study curing cycle phenomena. This would involve the determination of the extent of reaction at various temperatures from the heat produced [22]. Possibly the enthalpy relaxations will affect further curing so that different temperature profiles will result in different material properties. Although a more complete cure might be obtained by a temperature profile which increases as the cure progresses, this may not be desirable in that the stresses frozen in during the cool down may produce cracking in the more completely cured sample.

These problems involve the use of the DSC as the major experimental technique along with some mechanical measurements. None are easy questions to answer experimentally since they all require precise control and specification of the sample history as well as high precision and reproducibility of the measurements.

2.5 Thermal Expansion Behavior of Epoxy Resin*

The influence of post-cure cooling path on subsequent mechanical behavior of epoxy resins is under investigation. Optimizing the post-cure cooling path to minimize residual stresses or other parameters in graphite/epoxy composites is the ultimate objective in this study. The initial approach to characterizing physical behavior has been to measure the relative amount of free volume retained below T_g as a function of cooling rate. According to current understanding,a subsequent aging phenomenon would be associated with a time dependent reduction of this free volume. The volume measurements are being made on a Perkin-Elmer TMS-2 ("Thermo-Mechanical Analyzer"),which provides the change in a linear dimension of a virtually unstressed sample with temperature and time.

---

* Prepared by Dr. W. L. Bradley

Background: It is generally observed that most epoxies experience some degree of change in mechanical properties with time (the so-called "aging" phenomenon) subsequent to cooling through their glass transition temperature (T_g). As a test of this behavior the creep/recovery response at 300°F of Hercules Inc. epoxy resin 3502 was first determined for a specimen "aged" at ambient temperature for several months. The specimen was subsequently heated at 10°F/min. to 425°F ($T_g \simeq 375$°F), and then quenched to 300°F where creep/recovery behavior was determined in two succesive one-hour tests. The results are presented in Fig. 11. A dramatic increase in compliance immediately after quenching through T_g is noted. The material is still much softer than in the original aged condition even one hour after quenching when the second creep/recovery test is initiated. Thus, the transients associated with aging after quenching through T_g appear to be sufficiently sluggish to be significant in their influence on selecting optimum post-cure cooling paths.

The simplest explanation for the observed aging behavior is that it is associated with a time-dependent densification due to reduction of free volume. An alternative explanation is that possibly high residual stresses produced during quenching are influencing the mechanical properties through nonlinear mechanisms.

Experimental approach: Our experimental approach has been to run a series of thermal cycles from 348K to 490K (167-422°F) using a constant heating rate of 10K/min and cooling rates which varied from 10K/min to 80K/min. The variation of specimen thickness with temperature is monitored using the TMS-2. Loads on the quartz tube are maintained very low to avoid surface indentation of the small rectangular specimens. The linear measurements may be converted to volume as the epoxy is isotropic. Typical results are shown in Fig. 12.

Discussion of results: The cure temperature of the as-received epoxy was 375°F. A well defined T_g of 375°F is observed on the first thermal cycle (not shown in Fig. 12). Subsequent thermal cycles to the same maximum temperature show no well-defined T_g unless the maximum temperature used in previous cycles is exceeded. This phenomenon of the effective T_g equalling the previous maximum thermal cycle temperature (and effectively the

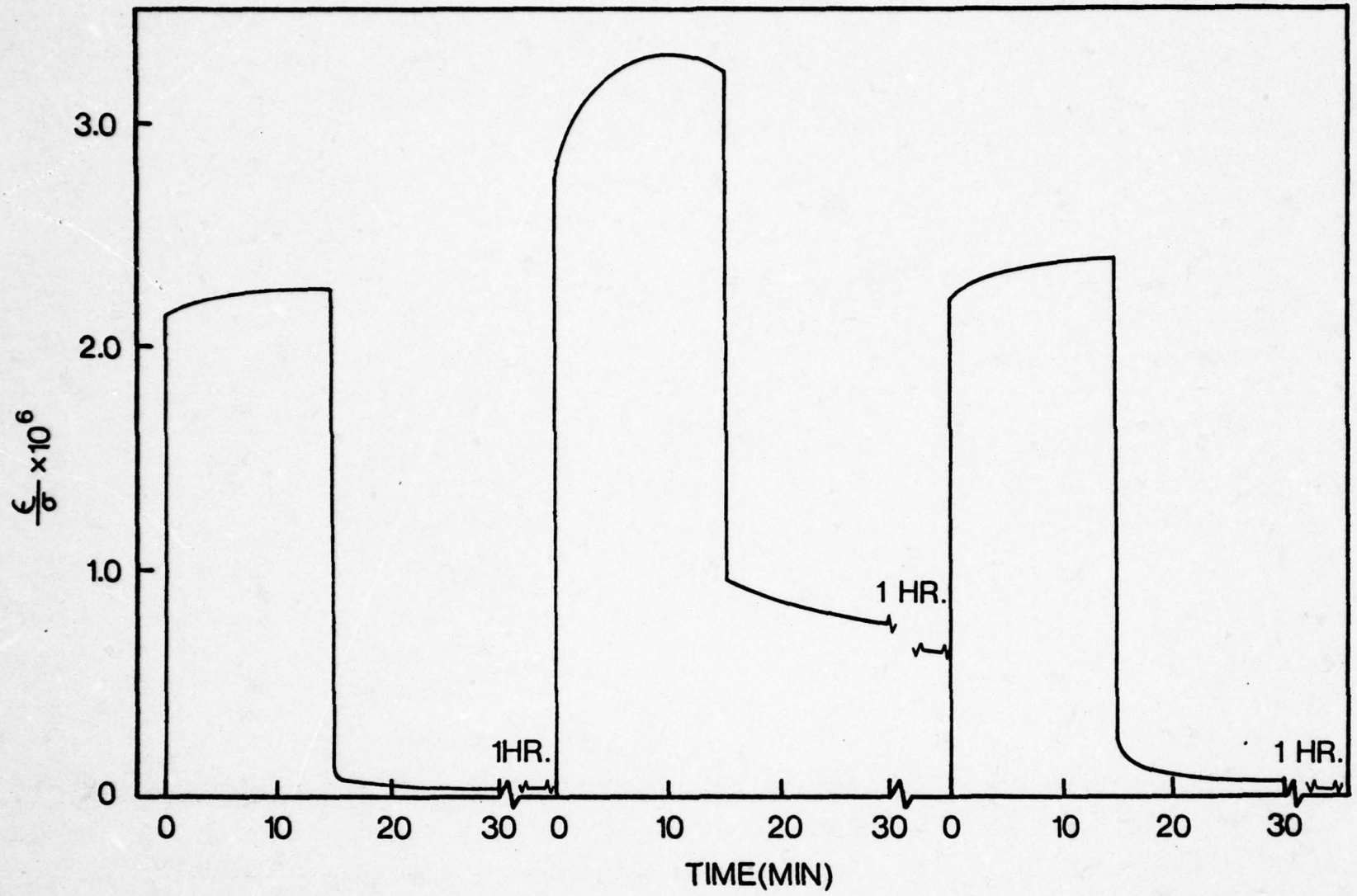

Figure 11. Time Dependent Compliance of Hercules Epoxy 3502 (using Creep/recovery Test) Measured on a Specimen Previously Aged for Several Months at Room Temperature, with Two Subsequent Creep/recovery Tests Performed Immediately after Heating above T_g and Quenching to 300°F in 90s. All compliance data is for T=300°F.

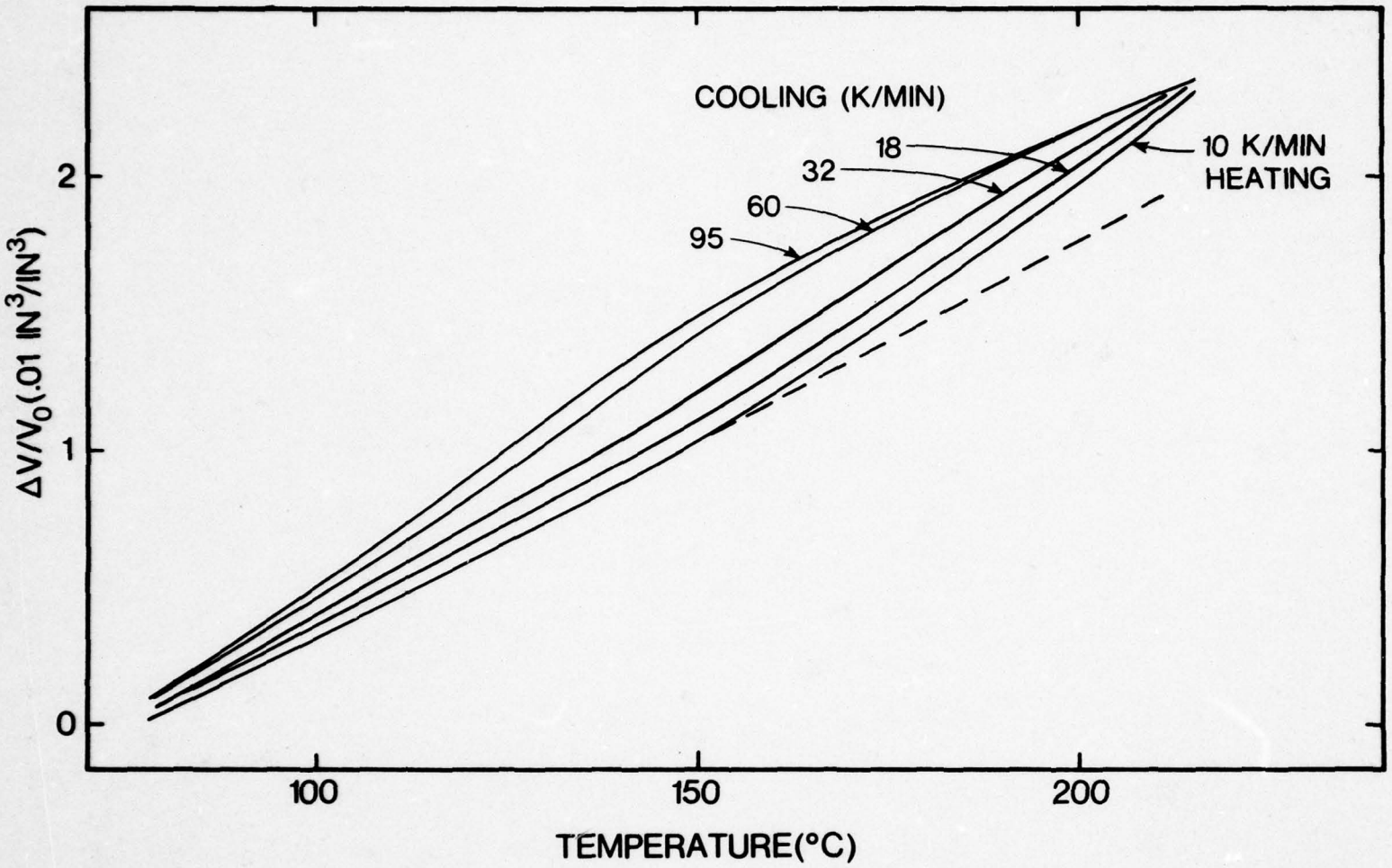

Figure 12. Thermo-mechanical hysteresis of Hercules Epoxy 3502, as Measured on the TMS-2. Note the Measured Fractional Change in Thickness has been converted to a Fraction Volume Change.

maximum curing temperature) continues up to 590K (600°F), where the epoxy experiences significant degradation. The differential scanning calorimeter was used to determine that each time the T_g is exceeded additional curing occurs, thus raising the T_g to this new temperature. The mobility of the molecules above T_g is short-lived, as this new mobility appears to allow further curing to occur.

While a true (fixed) T_g is not observed below the highest cure temperature, the thermal expansion curves do show considerable nonlinearity, beginning at about 300°F. If one assumes a two phase solid begins to develop at 300°F, say a rubbery phase precipitating in the glassy phase, the change in slope and a rule-of-mixtures calculation suggest a 0.1 - 0.2 volume fraction of rubber. Dr. Kibler at General Dynamics has recently observed changes in the viscoelastic behavior of[$\pm$ 45]graphite/epoxy at about 300°F which may also be explained by such a hypothesis.

Because T_g cannot be exceeded except on the first thermal cycle in epoxy (unless each successive cycle goes to a higher maximum temperature), the magnitude of free volume available to be "trapped" on quenching is rather small. When the effects of thermal lag due to temperature gradients through the specimen are taken into account, the change in free volume fraction after quenching at 50K/min. is estimated to be no greater than 0.1%. This was done by measuring the width of the thermomechanical hysteresis loop (cf. Fig. 12) for specimens of thickness 0.125", 0.062", and 0.037" and then extrapolating thermal lag ΔT vs $(\text{thickness})^2$ to zero thickness.

Additional experiments in which the quench was interrupted at 300°F to allow for aging have indicated that the difference in free volume (between the lowest and highest cooling rates) is no greater than .03%; this value is only 1/100 of the free volume at T_g [23]. The small value for free volume change leads us to believe that residual stresses, which also occur on quenching but give no net free volume, may be the more important cause of the observed aging phenomenon for 3502 epoxy.

Future work: Our work in the coming year will include additional experiments to more completely characterize the effect of various post-cure cooling paths on the viscoelastic behavior of the material. It is anticipated that modelling of this behavior will allow us to better establish whether annealing residual stresses or collapse of free volume is principally responsible for the observed behavior.

2.6 Viscoelastic Characterization of a Graphite/Epoxy Composite*

The effect of stress level, temperature and moisture on the viscoelastic behavior of graphite/epoxy Hercules Inc. AS/3502 composite material $[\pm 45]_{2S}$ and $[90]_{15}$ is being investigated. Current tests are on specimens produced by a standard cure cycle. The results will provide baseline data for later studies on the effects of cure cycle parameters and post curing.

It is known that moisture absorption causes resin to soften, behaving as if it were effectively closer to its glass transition temperature (T_g). We want to characterize this behavior to better understand the mechanistic basis for the interaction of absorbed moisture and mechanical behavior; for example, the influence of moisture on creep and on residual stress relaxation is of particular interest. Our results to-date include characterization of the dry composite as a standard to which the wet specimen may be compared, construction of environmental chambers to condition wet specimens (cf. Section 2.1) and construction of environmental chambers in which the specimens may be tested without any significant change in moisture content (cf. Section 2.2).

Experimental approach: The initial viscoelastic characterization work has been done on dry specimens using creep/recovery tests. Strain gages have been used. More recently, a high temperature, high sensitivity linear variable differential transformer (LVDT) system was purchased and special grips were built. This gives us the capability of testing at high temperatures (450°F maximum) and in hot, wet environments where strain gages are not suitable. The last part of the dry specimen characterization was done using the new LVDT system. The results agreed nicely with the earlier strain gage measurements, proving the reliability of both techniques.

Results: Typical creep compliance data taken at 75°F, 175°F, 231°F and 261°F is presented in Fig. 13 for the $[\pm 45]_{2S}$ composite. The compliance data were found to obey a power law in time; the exponent is approximately independent of temperature up to 231°F. The data at different temperatures can be superimposed on a single curve by choosing appropriate horizontal translations, $\log a_T$ values. These are also presented in Fig. 13. All

---

*Prepared by Dr. W. L. Bradley

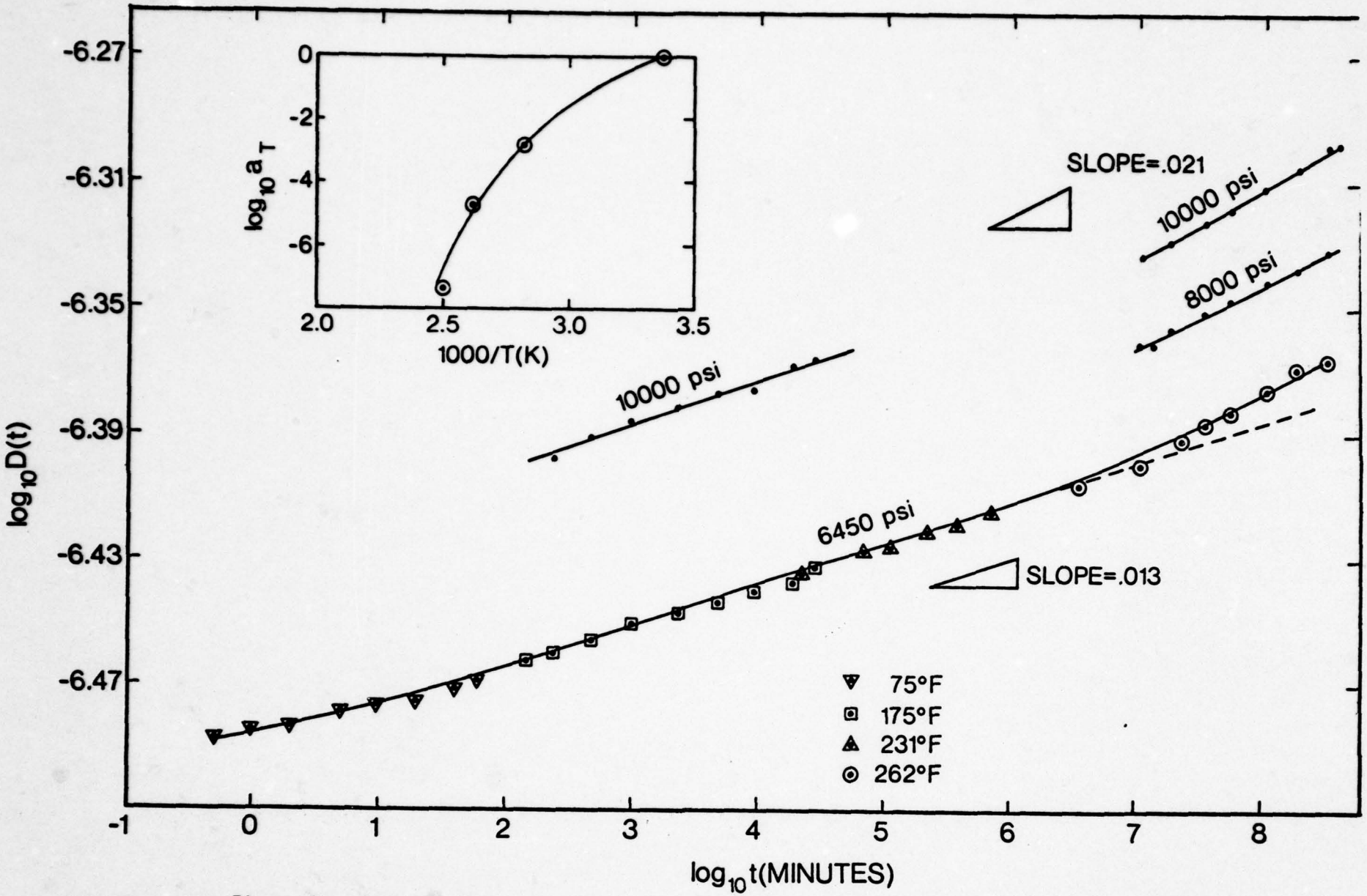

Figure 13. Time Dependent Compliance of a Graphite/Epoxy Composite as Measured for Several Stress Levels and Temperatures. Matrix Material is Hercules 3502 Epoxy with ± 45° Fiber Orientation.

of the data on the continuous curve were taken at a stress level of 6450 psi; these results turn out to be very close to low-stress level data recently obtained by General Dynamics on the T300/5208 $[\pm 45]_{2S}$ composite [24].

Several additional tests were run at higher stresses at 175°F and 261°F. The material is seen in Fig. 13 to be nonlinear at these higher stress levels. The high temperature data (261°F) seem to have a slightly higher slope at all three stress levels. A subsequent test of the specimen at 6450 psi after it was tested at 10,000 psi gave a curve that extrapolated the lower temperature data, maintaining the same slope (dotted line in Fig. 13).

These results may imply that at sufficiently high temperatures and stresses, residual stresses are relaxed so that the subsequent behavior at lower stress levels is modified. Tests have also been conducted on dry unidirectional specimens $[90]_{15}$. Analysis of the results is expected to aid in the understanding of residual stress effects since they are a minimum in a unidirectional composite.

Future work: The testing of the wet specimens is now beginning, using specimens soaked to saturation in 75% and 98% relative humidity. Additional very long time tests on dry specimens are also to be made.

3. ANALYSIS OF COMPOSITES AND ADHESIVES*

Four papers on the analysis of time-dependent behavior were completed during the reporting period and are included in the Appendix. They help to provide an analytical basis for predicting effects of post-cure cooling and the dependence of mechanical response and failure on hot, wet environments. Work currently underway is summarized below.

3.1 Current Activities

Moisture-stress interaction analysis: One major theoretical study on moisture effects in resins and composites is now concerned with theories of diffusion and interaction of moisture content and mechanical response. Specifically, a critical study of publications on continuum and equilibrium and nonequilibrium thermodynamic theories is being conducted for multi-phase media. The aim is to incorporate realistic effects of moisture on the behavior of polymers and polymeric composites. This investigation should also provide guidelines for experimental work and interpretation of data.

Viscoelastic hygrothermal stresses in composite laminates: An analytical investigation has been initiated to evaluate the hygrothermal stresses which arise in a multi-directional laminate accounting for the viscoelastic behavior of the material. The purpose of the investigaion is to quantify the stress levels which arise within the individual plies and determine their relation to the conditioning regimes that are employed in various experimental studies on moisture effects on composites.

All major factors which affect the linear viscoelastic behavior of composite materials have been identified and quantified on the basis of the best available data. These include the swelling strains due to moisture diffusion, and the temperature and moisture dependence of the viscoelastic "shift factor" which governs the creep compliances of the composite.

The analytical formulation of the problem has been completed for the elastic case, and the viscoelastic formulation for a balanced 0°/90° laminate is being finalized. The moisture diffusion, which is temperature dependent,affects the material compliances differently at each location across the

*Prepared by Drs. Y. Weitsman and R. A. Schapery

thickness, since each such position is subjected to a different moisture history. The formulations account for the transient, non-uniform moisture profiles which prevail within the laminate for long times.

The solution of the viscoelastic problem will require discretization of the analytical expressions in the time domain and in the spatial coordinate across the thickness. The stresses will then be evaluated by means of an incremental, time-marching, numerical computation (cf. paper by D. R. Sanders and Dr. W. E. Haisler in the Appendix).

Optimization of cool-down temperatures in composites: An optimization scheme is being developed to optimize the cool-down temperatures in order to reduce the residual stresses in multi-directional laminates with specific attention to 0°/90° balanced laminates. The scheme considers the thermo-rheologically complex viscoelastic response of composites and strives to develop an optimal cool-down path that will increase the residual strength of the predominant plies at termination of cooling.

Fundamental fracture toughness parameters for viscoelastic materials: Work is underway to extend the J-integral theory for fracture initiation to time-dependent composite materials. A preliminary version of the extension is given in the Appendix (cf. paper by R. A. Schapery). It is shown that for a class of realistic loading histories and nonlinear constitutive equations one can use a time-dependent J-integral to characterize fracture initiation. It is believed that such a criterion will prove useful in characterizing fracture behavior of resins and composites at elevated temperatures and humidities.

3.2 Future Work

Current analytical studies which are summarized above will be continued. The effort includes supporting the experimental work described in Section 2.

Also, the finite element modelling (cf. paper by D. R. Sanders and Dr. W. E. Haisler in the Appendix) will be extended. Current plans are to allow the relevant material parameters to be functions of temperature, stress, moisture content and perhaps other parameters. We will assume this functional dependence is given in either analytical form or tabular form. The model will be utilized to predict viscoelastic behavior of

specimens subjected to various loading and environmental conditions in experiments to be conducted during the course of the present research.

4. NEUTRON RADIOGRAPHY*

4.1 Summary

Through the past year the Nuclear Science Center has developed an extremely high quality neutron radiography facility. The operational parameters such as geometric resolution, beam uniformity, film density, and neutron flux have been optimized to a point where variation in material density of less than 0.5% may be measured. A variety of laminate sections with known moisture contents has been radiographed in an attempt to establish a relationship between film density changes for increased moisture in the samples. A laminate with known defects was also studied.

4.2 Beam Characterization

The initial effort was directed towards producing neutron radiographs and inspection techniques adequate for identifying minute defects or moisture content in laminate sections. For this purpose the existing radiographic facility was modified with a series of collimators, scrapers and filters designed to produce a parallel beam of neutrons of uniform intensity (Fig.14). The initial and final beam parameters are as follows:

	Initial	Final
Thermal neutron flux	1.5×10^6 n/cm^2/sec	$>10^7$ n/cm^2/sec
Scattered and fast neutron content	15%	10%
Gamma intensity	4.0×10^6 $\frac{n/cm^2}{mr}$	4.0×10^6 $\frac{n/cm^2}{mr}$
Beam uniformity	$\pm$17%	$\pm$3.5%
Beam divergence	1.5°	1.5°

Also, optimum film developing, handling and inspection procedures necessary for reproducible data collections have been established.

* Prepared by Mr. J. P. Taft and Dr. J. D. Randall

4.3 Sensitivity Studies

The application of neutron radiography to the study of composite materials was directed in two areas: (1) the determination of the sensitivity in measuring absorbed water concentration and (2) the determination of the sensitivity in detecting voids, cracks and delaminations. Neat resin and graphite and glass fiber-reinforced epoxy samples were used to investigate sensitivity to absorbed water. Dry samples were radiographed initially in pairs (2 neat,2 glass,etc), and the samples were radiographed again after one sample of each material was saturated with moisture at 98%RH. Evaluation of these radiographs revealed unanticipated geometry effects and interactions between the samples which hampered proper interpretation of the data collected (see Fig.15). These effects are caused by neutrons scattering from the sample and adding to the background film density near the sample. To alleviate this problem, samples were surrounded by material with similar scattering characteristics so the effect due to the scattered neutrons is uniform in and around the sample (see Fig. 16.) Also, due to the large lag time between initial radiography of the samples and radiography of the samples after saturation it was decided to simulate the presence of moisture in dry samples with a hydrocarbon in the form of polyethylene sheeting. This procedure has met with success, with the equivalent of 1 w% H_2O being easily detected in a glass laminate section. Future work will pick up at this point and establish a relationship between the film density and percent water absorbed.

In the area of void, crack and delamination detection, studies have begun of a test plate* in which known defects have been introduced. Figure 17 presents a view of the defects which have been identified at this point. The defects are referred to only as additions or removals (i.e., an addition being a positive change in the effective sample thickness and removal being a negative change); introduction of a material which does not interact with the neutron beam would constitute a removal. A more complete analysis depends upon further knowledge of the relationship between sample thickness and film density.

---

*Furnished by Dr. G. P. Sendeckyj of the Air Force Flight Dynamics Laboratory.

SCALE: 1" = 4'-0"

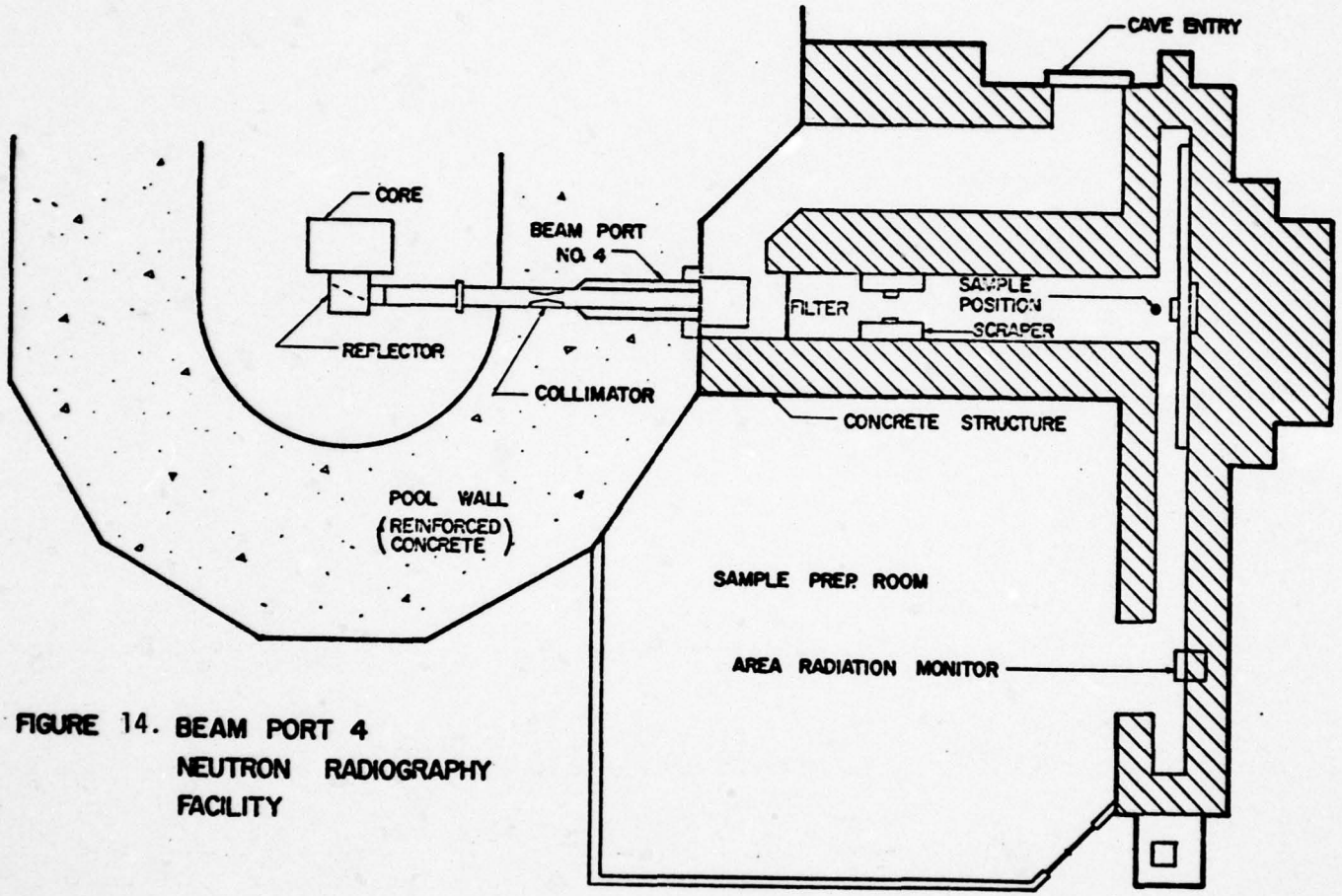

FIGURE 14. BEAM PORT 4
NEUTRON RADIOGRAPHY
FACILITY

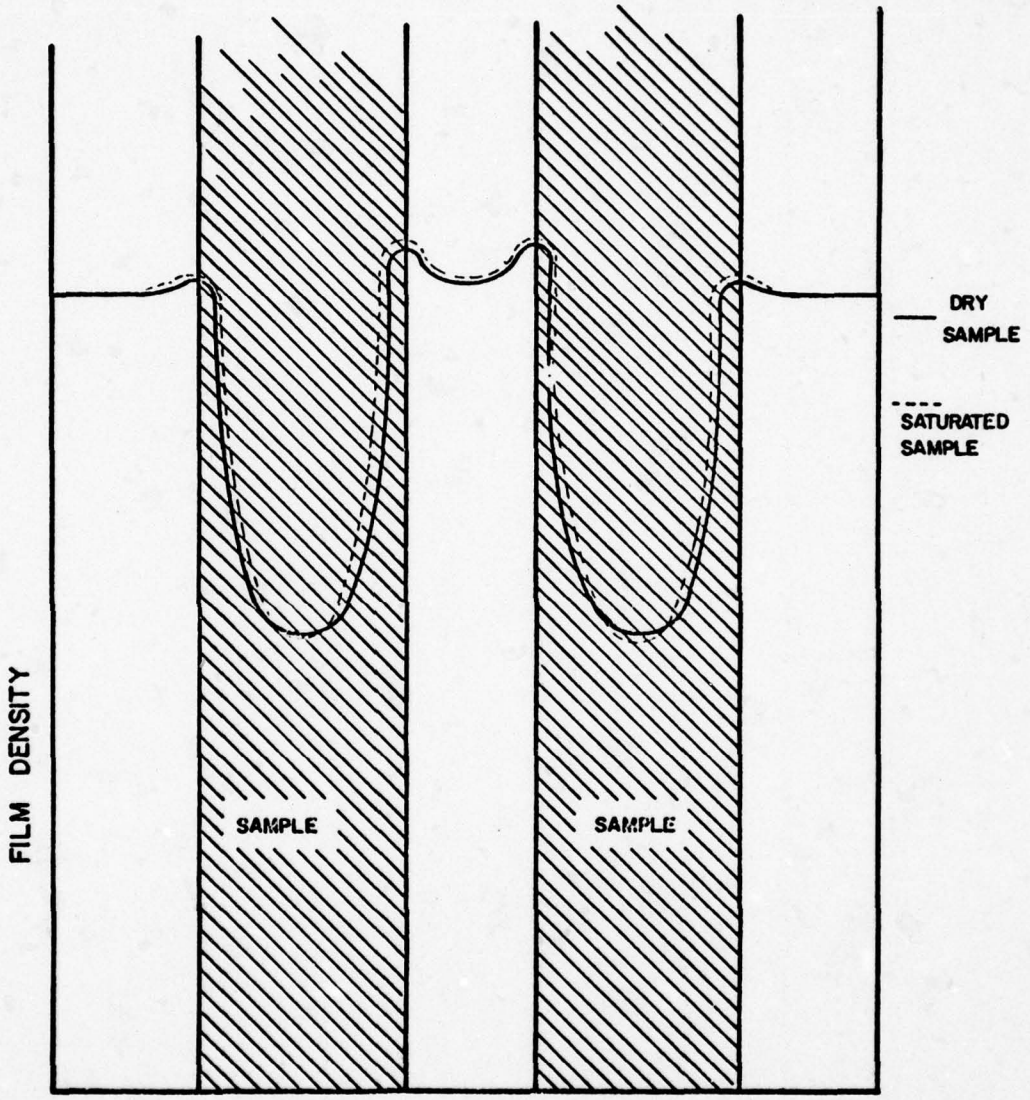

FIG. 15. TYPICAL FILM DENSITY VARIATION ACROSS SAMPLE IMAGE

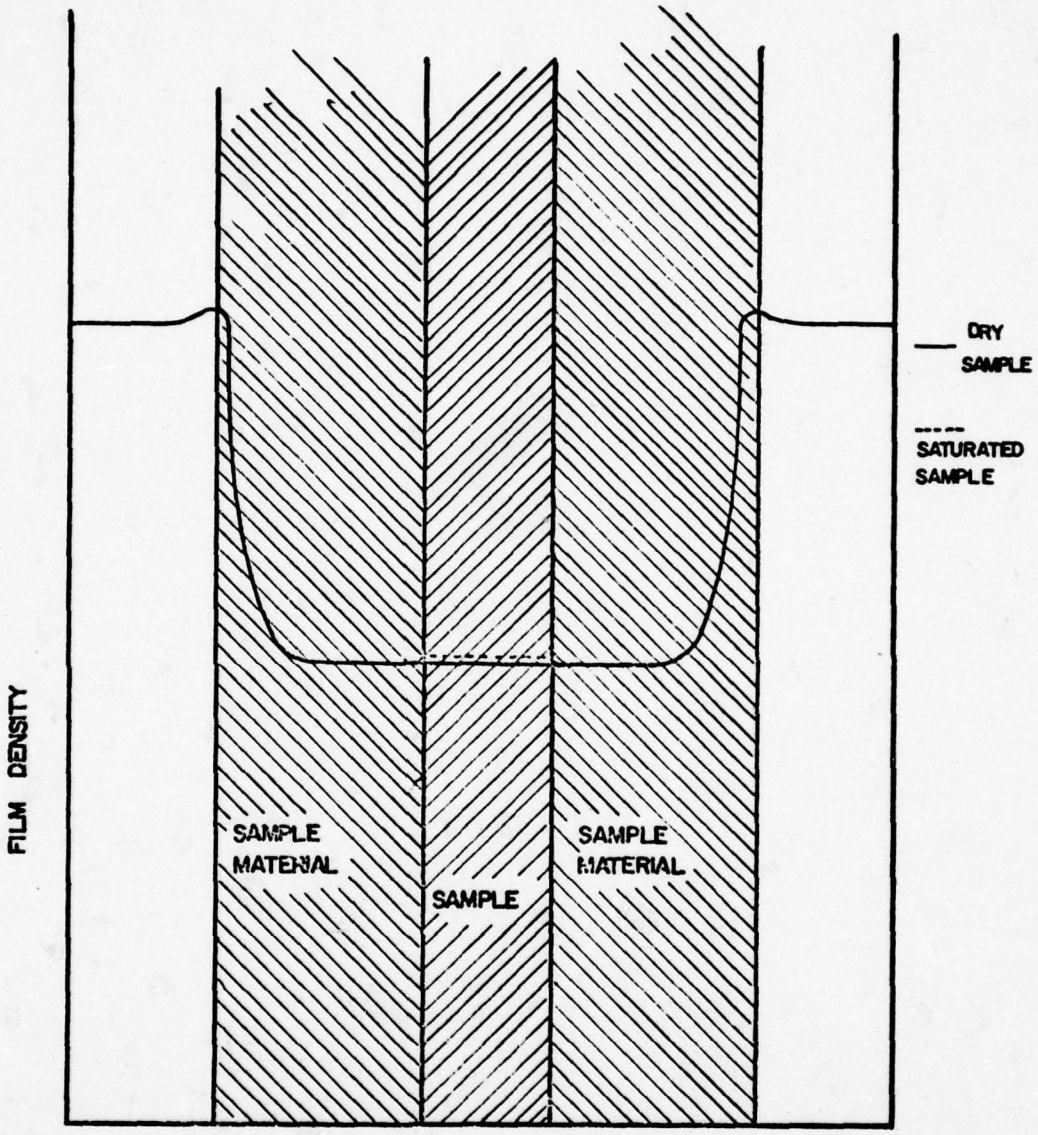

FIG. 16. FILM DENSITY DISTRIBUTION WITH SAMPLE SURROUNDED BY SIMILAR MATERIAL

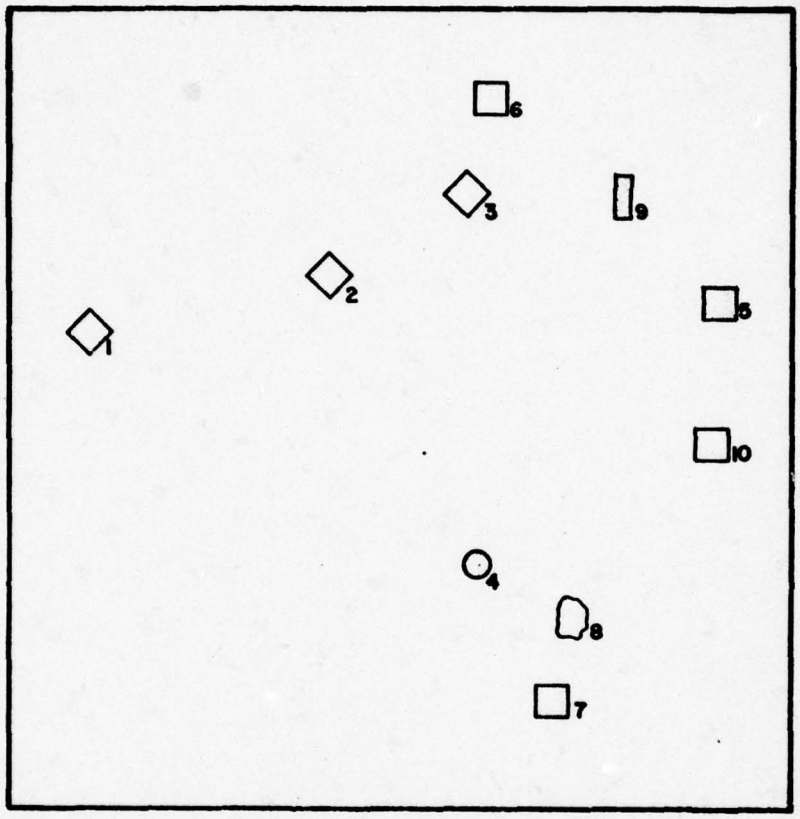

KEY

MATERIAL REMOVED

MATERIAL ADDED

FIG. 17. DEFECT TEST SPECIMEN

5. PROFESSIONAL PERSONNEL INFORMATION

5.1 Participating Faculty

Dr. Richard A. Schapery (Principal Investigator) - Aerospace and Civil Engineering Departments, Director, Mechanics and Materials Research Center

Dr. Walter L. Bradley - Mechanical Engineering Department

Dr. Walter E. Haisler - Aerospace Engineering Department

Dr. Joe S. Ham - Physics Department

Dr. Kenneth L. Jerina - Civil Engineering Department

Dr. John D. Randall - Nuclear Engineering Department, Director, Nuclear Science Center

Dr. Jack Weitsman - Civil Engineering Department

In addition to these faculty members, Drs. Donald Saylak and James S. Noel assisted during the first half of the project period in the development of the processing laboratory. Their valuable assistance is gratefully acknowledged.

5.2 Professional Staff

Mechanics and Materials Research Center:

Mr. Carl Fredericksen - Electronics Technician

Mr. Bob C. Harbert - Research Engineer

Dr. S. B. Raju - Computer Programmer

Nuclear Science Center:

Mr. Joseph Taft - Research Engineer

5.3 Spoken Papers and Lectures at Conferences Related to Composite Materials:

R. A. Schapery:

"Effect of Moisture on Flaw Growth in Viscoelastic Composites," Gordon on Composites, Santa Barbara, Ca., Jan. 1978.

"Time-Dependent Behavior of Composites," ASTM Symposium on Composite Materials: Testing and Design, New Orleans, La., March, 1978.

"On the Analysis of Crack Growth in Non-homogeneous Viscoelastic Media," American Mathematical Society Symposium on Fracture Mechanics, New York, March 1978.

"The Graduate Academic Program in Composites at Texas A&M University," ASTM Symposium on Composite Materials, New Orleans, La., March, 1978 and the International Conference on Composite Materials, Toronto, Canada, April, 1978.

"Designing with Composite Materials," Annual Meeting of the Society of Plastics Engineers, Washington, D. C., April 1978.

"Fracture Mechanics of Solid Propellants," ONR International Symposium on Fracture Mechanics, Washington, D. C., September 1978.

"Review of the Composite Materials Research Program at Texas A&M," Air Force Mechanics of Composite Review Meeting, Dayton, Ohio, November, 1978.

"High Speed Crack Propagation in Solid Propellant," ONR Workshop on the Detonation-to-Deflagration Transition in Solid Propellant, Akron, Ohio, December 1978.

J. D. Randall:

"Neutron Radiographic Facility at Texas A&M", Air Force Mechanics of Composite Review Meeting, Dayton, Ohio, November, 1978.

Y. Weitsman:

"A Review on Moisture Effects in Composites," Army Materials and Mechanics Research Center, Boston, Mass., July, 1978.

"Mechanical Behavior of Polymeric Composite Materials Under the Influence of Temperature and Moisture Fluctuations," NSF Workshop on General Constitutive Relationships for Wood and Wood Based Materials. Syracuse University, NY, July, 1978.

"Stresses in Adhesive Layers due to Sorption of Moisture," Fourth Conference on Fibrous Composites in Structural Design, San Diego, Cal. November, 1978.

6. REFERENCES

1. "Maintaining Constant Relative Humidity by means of Aqueous Solutions," 1974, Manual Book of ASTM Standards, part 41, E-104.

2. Nelson, G.O., Controlled Test Atmosphere Principles and Techniques, Science Publishers, Inc., Ann Arbor, 1971.

3. Langue, N. L., Handbook of Chemistry, revised tenth edition, McGraw-Hill, 1967.

4. International Critical Tables

5. Gillham, J. K., Glandt, C. A., and McPherson, C.A., Characterization of Thermosetting Epoxy Systems using a Torsional Pendulum, Chemistry and Properties of Crosslinked Polymers, Academic Press, N. Y., 1977.

6. Davis, W. M., and Macosko, C. W., "A Forced Torsional Oscillator for Dynamic Mechanical Measurements," Society of Plastics Engineers, 34th Annual Technical Conference, Atlantic City, N.J., Spec. Tech. Papers, 22, 408 (1976).

7. Broyer, E., and Macosko, C.W., "Comparison of Cone and Plate, Bicone and Parallel Plates Geometries for Melt Rheological Measurements," Presented at the 33rd Annual Technical Conference, Society of Plastics Engineers, Atlanta, Ga. (1975), Spec. Tech. Papers 21, 343 (1975).

8. Briar, H.P., Bills, K.W. Jr., and Schapery, R. A., "Design and Test of the Operational In-Situ Gage for Solid Propellant Surveillance," Final Report, Air Force Rocket Propulsion Laboratory Report No. AFRPL-TR-76-36 (Contract No. F04611-73-C-0040) June, 1976.

9. Harbert, B. C., and Schapery, R.A., "A Piezoelectric Plate Device for Determination of Viscoelastic Properties, Texas A&M University Report No. MM-3168-79-1, January, 1979.

10. Noel, J. S., Bogess, R., and Swift, G., "Pavement Evaluation," Final Report Federal Highway Administration, Contract No. DOT-FH-11-8264, June, 1978.

11. Timoshenko, S., and Woinowsky-Krieger, S., Theory of Plates and Shells, McGraw-Hill, 1959.

12. Christensen, R.M., Theory of Viscoelasticity - An Introduction, Academic Press, NY, 1971.

13. Kovacs, A.J., "Transition Vitreuse dans les Polymeres Amorphes. Etude Phenomenologique," Fort. Hochp. Forsch. 3, 394-507 (1963).

14. Lipatov, Y., "The Iso-Free-Volume State and Glass Transitions in Amorphous Polymers," Adv. Polymer Sci., 26, 63,(1978).

15. Morgan, R. J., and O'Neal, J. E., "A Review of the Relation between the Physical Structure and Mechanical Response of Epoxies," Chemistry and Properties of Crosslinked Polymers, Ed. by S. S. Labana.

16. Boyer, R. F., "General Reflections on the Symposium on Physical Structure of the Amorphous State," in Physical Structure of the Amorphous State, Ed. by G. Allen and S.E.B. Petrie, Dekker, (1976).

17. Wong, J., and Angell, C.A., Glass-Structure by Spectroscopy, Dekker 1976.

18. Struik, L.C.E., Physical Aging in Amorphous Polymers and Other Materials, Elsevier (1977).

19. Ophir, Z. H., Emerson, J.A., and Wilkes, G.L., "Sub-T_g Annealing Studies of Rubber-modified and Unmodified Epoxy Systems," J. Appl. Physics, 49, 5032 (1978).

20. Robertson, R. E., "The Aging of Glassy Polymers as Determined by Scanning Calorimeter Measurements," J. Appl. Physics, 49, 5048 (1978).

21. Misra, S. C., Dissertation from Lehigh U., May 1978, "Effect of Network Structure on Mechanical Behavior of Epoxies."

22. Fava. R. A., "Differential Scanning Calorimetry of Epoxy Resins," from Differential Thermal Analysis, Ed. by M. I. Pope Heyden (1967).

23. Aklonis, J. J., MacKnight W.J., and Shen, M., Introduction to Polymer Viscoelasticity, Wiley Interscience, NY (1972)

24. Kibler, K., General Dynamics, Ft. Worth, TX., private communication.

APPENDIX

1. Residual Thermal Stresses due to Cool-Down of Epoxy-Resin Composites by Y. Weitsman

2. Interfacial Stresses in Viscoelastic Adhesive-Layers due to Moisture Sorption, by Y. Weitsman

3. On the Analysis of Crack Initiation and Growth in Nonhomogeneous Viscoelastic Media, by R. A. Schapery.

4. An Incremental Form of the Single-Integral Non-linear Viscoelastic Theory for Elastic-Plastic-Creep Finite Element Analysis, by D. R. Sanders and W. E. Haisler.

RESIDUAL THERMAL STRESSES DUE TO COOL-DOWN OF EPOXY-RESIN COMPOSITES

BY

Y. WEITSMAN*

Abstract

This paper concerns the residual thermal stresses that develop within the resin of a fiber-reinforced composite-laminate as the material is cooled from cure temperature down to room temperature.

The calculations presented herein consider the viscoelastic response of the resin and account for the temperature dependence and the stress sensitivity of the creep compliance. Comparisons with linear elasticity indicate that viscoelastic relaxation may reduce the residual stresses by about 20%.

Submitted for publication in The Journal of Applied Mechanics.

1. Introduction

Linear elastic stress analysis predicts that the thermal stresses, which develop within a composite material due to typical temperature excursions experienced by the structure, may exhaust the strength of various laminae even before the application of external loads. Effects which were attributed to high residual thermal stresses in composite laminates were reported by several investigators [1]* [2]. A similar prediction can be made for the micromechanical thermal stresses within the epoxy resin when its response is assumed to follow linear thermo-elasticity. The assumption of linear-elastic behavior tends to over-estimate the residual thermal stresses and, by ignoring the time, temperature and stress dependencies of the resin's response - rules out any advantage that may accrue from the consideration of special temperature histories.

A major portion of the thermal stress is introduced into the composite laminate during cooling from cure temperature down to room temperature. This cool-down stage may be viewed as part of the manufacturing process and therefore lends itself to careful control. It has already been shown that the selection of an optimal cool-down path could reduce residual termal stresses in plexiglass [3] and the same idea can be carried over to epoxy and epoxy-based composites.

This paper presents calculations of the "michromechanical" residual stresses within the epoxy due to cool-down. Our purpose is

---

* Numbers in brackets indicate references listed at end of paper.

to provide a quantitative assessment of the role of inelastic response. The calculations are based upon a thermorheologically-complex viscoelastic model, which includes some aspects of the non-linearity that is attributed to stress effects on relaxation.

The findings of this paper are preliminary since they are based upon incomplete data. Consequently it was necessary to extrapolate existing data to higher temperature ranges and to infer the non-linear stress-effects by analogy from similar materials (glass-reinforced epoxy). Perhaps most significantly, due to the complete lack of data, it was necessary to omit any aging effects, which may be very prominent during the cool-down of a newly created laminate.

Several experimental programs, currently in progress, should provide information which would enable us to reassess and refine the model which is used in the present work.

2. Formulation

Consider a fiber-reinforced, multi-directional, composite laminate - $h \leq z \leq h$, $-\infty < x,y < \infty$, traction free at the boundaries $z = \pm h$ and subjected to spatially uniform temperature fluctuations. For sufficiently slow fluctuation of the ambient temperature and sufficiently thin layers it is possible to discard the transient states and consider the quasi-static case of uniform temperature $\theta(z,t) \tilde{=} \theta(\pm h,t) = \theta(t)$.*

---

*In typical laminates, the transient effects may be ignored up to temperature fluctuations of 5°K/min.

Since the present analysis aims at investigating the thermo-viscoelastic response of the resin let us assume that the multi-directional fibers, all of which lie in planes z = const., affect the behavior of the resin through the following geometric constraint

$$\varepsilon_x = \varepsilon_y = \alpha_f \, \Delta\Theta \tag{1}$$

In (1) α_f is the coefficient of thermal expansion of the fibers, $\Delta\Theta$ is the difference between the initial and final temperatures, $\Delta\Theta = \Theta_0 - \Theta_f$, and ε_x, ε_y are the in-plane strains.

If we assume in-plane isotropy of the layer, and consider linear-elastic response, we obtain the following results [3]

$$\begin{aligned} &\sigma_x = \sigma_y = \sigma = -cG\Delta\Theta \\ &\sigma_z = 0 \text{ and all shears vanish.} \end{aligned} \tag{2}$$

where

$$c = 2\,\frac{1+\nu}{1-\nu}\,(\alpha_m - \alpha_f). \tag{2'}$$

In (2) and (2') G, ν are the shear modulus and Poisson's ratio of the resin, and α_m is its coefficient of thermal expansion,

If the resin responds viscoelastically equation (2) takes the form

$$\sigma(t_f) = -c\int_0^{t_f} G\left[\xi(t_f)-\xi(t')\right]\dot{\theta}(t')dt' \tag{3}$$

where ξ is a "reduced time", given by

$$\xi(u) = \int_0^u \frac{ds}{\alpha_T(s)} \tag{4}$$

and G(t) is the shear-relaxation function for the resin.

The purpose of the subsequent investigation is to consider and evaluate the significance of various factors which affect the function α_T, and investigate the influence of the history $\Theta(t)$ on $\sigma(t_f)$.

3. A Linear Thermorheologically Complex Model for Epoxy

On the basis of uniaxial tension data obtained for "shell 58-68R" epoxy resin [4], for temperatures ranging between 20°F and 160°F, it is possible to express the creep compliance as follows

$$D(\Theta,t) = D_0(\Theta) + D_1\left[\frac{t}{\alpha_T(\Theta)}\right]^q \tag{5}$$

where

$$D_0(\Theta) = [0.2731 + 0.000574\ (\Theta - 297)]\ 10^{-6}$$

$$D_1 = 0.01 \times 10^{-6},\ \alpha_T(\Theta) = \exp\left(\frac{6480}{\Theta} - 21.82\right), q = 0.19$$

In (5), D is in $(kPa)^{-1}$, the time t is in minutes, and the temperature Θ is in degrees Kelvin. Furthermore, the Poisson's ratio for epoxy is approximately constant at $\nu = 0.35$. For temperatures below glass transition the coefficients of thermal expansion are such that $\alpha = \alpha_m - \alpha_f = 5 \times 10^{-5}$ m/m/1°K.

Consider a composite cooled-down between a cure-temperature $\Theta_0 = 438$°K and room-temperature $\Theta_f = 298$°K. For lack of more complete

data assume that (5) can be extrapolated up to the elevated cure-temperature. In terms of the imposed thermal strain $(\alpha_m - \alpha_f)(\theta_o - \theta(t))$ and the creep compliance (5) we obtain the following integral equation for the stress σ:

$$\frac{\alpha}{1-\nu}\left[\theta_o-\theta(t)\right] = D_o(\theta)\sigma(t) + D_1\int_0^t\left[\xi(t)-\xi(t')\right]^q \dot{\sigma}(t')dt' \qquad (6)$$

where $\alpha = \alpha_m - \alpha_f$.

If the temperature drops linearly between θ_o and θ_f over a time interval t_f then

$$\theta(t) = \theta_o+Rt \text{ with } R = (\theta_f-\theta_o)/t_f$$

and equation (6) reads

$$-\frac{\alpha}{1-\nu}Rt = D_o(\theta_o + Rt)\sigma(t)$$
$$+ D_1\int_0^t\left[\int_0^t \frac{ds}{\alpha_T(\theta(s))} - \int_0^{t'} \frac{ds}{\alpha_T(\theta(s))}\right]^q \dot{\sigma}(t')dt' \qquad (7)$$

where in (7) $\alpha_T(\theta(s)) = \exp\left(\frac{6480}{\theta_o+Rs} - 21.82\right)$

The solution of (7) was obtained numerically. Following the scheme developed in reference [3], the time interval t_f was divided into sub-intervals $\Delta t = t_f/n$ and each intermediate time was denoted by $t_j = j\Delta t$. Denoting $\theta_j = \theta(t_j) = \theta_o + Rt_j$, $\sigma_j = \sigma(t_j)$ and computing the n values of

$$\xi_j = \xi(t_j) = \int_0^{t_j} \frac{ds}{\alpha_T(\theta(s))}$$

and n values of $D_{oj} = D_o(\theta_j) = \left[0.2371 - 0.000574(\theta_j - 297)\right]10^{-6}$

the following expression was obtained for σ_j

$$\sigma_j = \frac{1}{D_{oj}+\frac{1}{2}(\xi_j-\xi_{j-1})^q}\left\{-\frac{\alpha}{1-\nu}Rt_j + \frac{1}{2}D_1(\xi_j-\xi_{j-1})^q\sigma_{j-1}\right.$$
$$\left.-\frac{1}{2}D_1H(j-2)\sum_{m-1}^{j-1}\left[(\xi_j-\xi_m)^q + (\xi_j-\xi_{m-1})^q\right](\sigma_m-\sigma_{m-1})\right\} \qquad (8)$$

In (8), H(j-2) is a unit step function which vanishes for $j < 2$. In addition, it is necessary to employ the initial conditions $\sigma_o = 0$, $\xi_o = 0$.

Calculations were performed on an Amdahl 470 computer. The residual stress at the termination of cool-down is shown in Fig. 1 as a function of the time t_f allowed for the cooling. The reduction in the residual stress with the increase in cooling-time t_f is due to viscoelastic relaxation. The value of σ = 39430 kPa at $t_f = 0$ corresponds to the linearly-elastic case.

Additional relaxation of stresses occurs, at $\Theta = \Theta_f$, at times $t > t_f$. The calculation of these stresses requires a slight modification of expressions (7) and (8), which is omitted here. The additional relaxation, which is drawn by the dashed lines in Fig. 1, further reduces the residual stresses by about 3 - 4%.

4. Optimal Cool-Down Path for the Thermorheologically Simple Model

It has been shown previously [3] that, for a prescribed time t_f for cool-down, there exists an optimal cool-down path $\Theta = \Theta(t)$ which minimizes the residual stress σ_f. A remarkable feature of this optimal path is that it contains discontinuities at times $t = 0$ and $t = t_f$. It is interesting to note that the discontinuous character of the solution is apparently quite common, since a similar result was obtained recently for optimal strain paths [5]. The sharp discontinuity represents an impractical mathematical idealization and indicates that the best results can be realized by rapid cooling during the initial and final stages.

In order to reduce the computational effort consider the approximate form of the creep compliance

$$D(t) = b(1+at^q)$$

where $b = 0.3126 \times 10^{-6}(kPa)^{-1}$, $a = 0.032$ and $q = 0.19$ (9)

Equation (9) was derived from (5), with $\Theta = 75°F$ (297°K) and when $D_o(\Theta)$ is approximated by a constant value $D_o = b$.

Furthermore, it is more convenient to employ the relaxation modulus E(t) instead of the compliance D(t). This task is accomplished with the aid of Laplace transforms. The Laplace transform of D(t) yields

$$p\,\bar{D}(p) = b\left[1+a\,\frac{\Gamma(q+1)}{p^q}\right] = \frac{1}{p\bar{E}(p)} \qquad (10)$$

where $\bar{E}(p)$ is the Laplace transform of E(t) [6]. An approximate inversion, based upon the expression [7] $E(t) \approx \frac{1}{pD(p)}\Big|_{p=\frac{1}{2t}}$ yields

$$E(t) = \frac{3.2 \times 10^6}{1+0.0336t^{0.19}} \text{ kPa} \qquad (11)$$

The validity of (11) was verified by comparison with a collocation scheme for the inversion of (10). The collocation method will be discussed in the following section on nonlinear effects. The comparison is shown in Fig. 2.

Employment of (11) in (3) yields

$$\sigma(t_f) = -c_1 S(t_f) \qquad (12)$$

where

$$S(t_f) = \int_0^{t_f} \left\{ 1 + a \left[\int_{t'}^{t_f} \frac{ds}{\alpha_T(s)} \right]^q \right\}^{-1} \cdot \dot{\theta}(t')dt' \qquad (13)$$

and $c_1 = \dfrac{3.2 \times 10^6 \alpha}{1 - \nu}$.

Also, in (13) $\alpha_T = \exp\left[\dfrac{6480}{\theta(s)} - 21.82\right]$

To determine the optimal path $\theta(t)$ subdivide t_f into n equal portions as before and consider a "stair-case" drop in θ

$$\theta(t) = A_k \qquad t_k < t < t_{k+1} \qquad 0 \le k \le n-1$$

whereby

$$\dot{\theta}(t) = (A_k - A_{k-1})\ \delta\ (t-t_k) \qquad 1 \le k \le n \qquad (14)$$

and

$$\dot{\theta}(t) = (A_0 - \theta_0)\ \delta\ (t) \qquad k=0$$

Substitution of (14) into (13) gives

$$S(t_f) = \frac{A_0 - \theta_0}{1 + a\left\{\Delta t \sum_{j=0}^{n-1} 1/\alpha_T(A_j)\right\}^q} + \sum_{k=1}^{n-1} \frac{A_k - A_{k-1}}{1 + a\left\{\Delta t \sum_{j=k}^{n-1} 1/\alpha_T(A_j)\right\}^q} - (A_{n-1} - \theta_f) \qquad (15)$$

Equations (12) and (15) express the residual stress $\sigma(t_f)$ in terms of the unknown intermediate temperatures, $A_j = A(t_j)$ $j = 0,1,\ldots n-1$.

For a stationary value it is necessary that $\partial S(t_f)/\partial A_j = 0$, $j = 0,1...n-1$. This results in n simultaneous equations in the n unknown A_j as follows

$$\frac{A_o-\Theta_o}{Z_o^2}\ \frac{\partial Z_o}{\partial A_k} + H(i-1) \sum_{i=1}^{k} \frac{A_i-A_{i-1}}{Z_i^2}\ \frac{\partial Z_i}{\partial A_k} + \frac{1}{Z_{k+1}} - \frac{1}{Z_k} = 0 \qquad (16)$$

$$k = 0,\ 1,\ldots\ n-1$$

where, in (16) $Z_n = 1$, $H(i-1)$ is the unit step-function which vanishes for negative arguments, and

$$Z_j = 1 + a\left\{\Delta t \sum_{j-i}^{n-1} 1/\alpha_T(A_j)\right\}^q$$

$$\frac{\partial Z_j}{\partial A_k} = -6480\ A_k^{-2}\left\{\Delta t \sum_{j=i}^{n-1} 1/\alpha_T(A_j)\right\}^q$$

The solution of (15) and (16) was obtained by an iteration technique.* The resulting optimal path is shown in Fig. 3 for $t_f = 100$ min. It is worth noting that the value of $\sigma(t_f)$ is insensitive to the details of the "tail-end" of the path, i.e., near t_f. Cooling along the optimal path results in a residual stress $\sigma(t_f) = 32900$ kPa. This represents an improvement of about 6% over the linear cool-down path.

---

*We refrained from using standard optimization methods, because those techniques presuppose a smooth functional which can be approximated by quadratic function (see e.g., Ref. [8]) while the present case revolves about a discontinuous function.

5. Stress Effects on Relaxation during Cool-Down

We note that the residual stresses reach levels which exceed half the ultimate stress of epoxy, σ_u = 52,200 kPa. Stresses of such magnitude were found to influence the creep-response of epoxy-based composites [9]. The stress effect can be incorporated into the "shift-factor" α_T of Eq. (4) as follows

$$\alpha_T(\sigma,\theta) = \exp\left\{\frac{A/\theta_R - (B/\theta_R)H[\sigma-\sigma_c(\theta)]\,[\sigma-\sigma_c(\theta)]/\sigma_u(\theta)}{\theta/\theta_R} - \frac{A}{\theta_R}\right\} \quad (17)$$

In (17) θ_R is a reference absolute temperature, σ_c is a "threshold stress" beyond which stress starts to affect α_T, σ_u is the ultimate stress of the resin, H( ) is a unit step-function which vanishes for negative arguments and A, B are material constants.

From the data given in Ref. [9], which were obtained at a reference temperature θ_R = 293°K, and from recent data which detailed the dependence of σ_u on θ [10], the following values were selected

$A = 6500, \quad B = 2000$

$\sigma_u(\theta) = 55200 - 190\ (\theta-\theta_R)$

$\sigma_c(\theta) = 13800 - 47.5\ (\theta-\theta_R)$.

where σ_u and σ_c are in kPa.

A significant reduction in the computational effort is achieved if the relaxation function E(t), as given in (11), is expanded in a sum of exponentials. To this purpose, the method of collocation [7] was employed and E(t) was expressed as

$$E(t) = \sum_{I=1}^{22} E_I e^{-\lambda_I t} \qquad \lambda_I = 10^{-18},\ 10^{-17},\ \ldots 10^{3} \tag{18}$$

The values of E_I, which are not listed here, were obtained from solving the simultaneous equations

$$\sum_{I=1}^{22} (1+\lambda_I/\lambda_J)^{-1} E_I = p\bar{E}(p)\Big|_{p=\lambda_J}$$

with $p\bar{E}(p)$ given in (10). The form (18) of $E(t)$ is shown in Fig. 2.

Substitution of (17) and (18) in (3) and (4) yields

$$\sigma(t) = \sum_{I=1}^{22} E_I \int_0^t \exp\left[-\lambda_I \xi(t)+\lambda_I \xi(t')\right] \frac{d\epsilon}{dt'}\, dt' \tag{19}$$

where $\xi(u) = \int_0^u \frac{ds}{\alpha_T[T(s),\sigma(s)]}$

with the form of α_T given in (17).

Consider a linear cool-down from Θ_0 to Θ_f during a time interval t_f. Denote the constant cooling rate by $R = (\Theta_0-\Theta_f)/t_f$ and let $c_2=\alpha R/(1-\nu)$. In this case (19) reduces to

$$\sigma(t) = c_2 S(t)$$

where (20)

$$S(t) = \sum_I E_I \int_0^t \exp\left[-\lambda_I \xi(t)+\lambda_I \xi(t')\right] dt'$$

Divide the time interval t_f into n equal intervals Δt and denote $t_k = k\Delta t$ as before. The initial condition is $\sigma_o = 0$ and the intermediate temperatures are $\theta_k = \theta_o - Rt_k$. If we employ the approximation that

$$\alpha_T(\sigma,\theta) \simeq \alpha_T(\sigma_k,\theta_k) \text{ for } t_k < t < t_{k+1} \tag{21}$$

then, as a consequence of expansion (18), it is possible to integrate S(t) analytically over each sub-interval $t_k < t < t_{k+1}$. This leads to a substantial reduction in computations.

Denote $V_k = \alpha_T(\sigma_k,T_k)$ and $W_k = e^{-V_k}$. From (21) it follows that

$$\xi_k = \xi(t_k) = \sum_{i=1}^{k} (t_i - t_{i-1})\, W_{i-1}$$

Denote further

$$\psi_{rk} = \sum_{m=0}^{r-1} (t_m - t_{m-1})\, W_{m-1} - \xi_k$$

and $(r=1,..k. \quad k=1,..n)$

$$\phi_{rk} = \psi_{rk} + W_{r-1}(t_r - t_{r-1})$$

Straightforward manipulations lead to

$$S_k = S(t_K) = \sum_{I=1}^{22} E_I \left\{ \sum_{r=1}^{k} (\lambda_I\, W_{r-1})^{-1} \left[\exp(\lambda_I \phi_{rk}) - \exp(\lambda_I \psi_{rk}) \right] \right\} \tag{22}$$

and

$$\sigma_k = c_2\, S_k$$

For times beyond termination of cool-down $t_k > t_f$, the temperature retains a constant value Θ_f but the stress σ_k continues to relax. The computational scheme (22) remains valid except that now

$$\alpha_T(\sigma_k,\Theta_k) = \alpha_T(\sigma_k,\Theta_f), \qquad (t_K > t_f).$$

Results for a constant cooling rate from Θ_o = 438°K down to Θ_f = 293°K are shown in Fig. 4 for t_f = 100 minutes, followed by a relaxation at 293°K, and for t_f = 300 minutes. Note that a prolongation in the cool-down time does not effectively reduce the residual stresses. Comparison with results based upon the lineal thermorheologically complex model shows that when stress effects are incorporated into α_T,(Eq. (17)),the relaxation is enhanced and the residual stresses reduce by an additional 10%.

Finally, consider the case of a "two-step cooling". In this case the temperature is dropped suddenly from Θ_o to Θ_b, held at $\Theta = \Theta_b$ for a period $t = t_f$ and dropped sharply again to $\Theta = \Theta_f$ at $t = t_f$. For such cooling-history Eq. (19) yields

$$\sigma(t_f) = c_m S(t_f) + c_f \sum_I E_I \qquad (23)$$

In (23) $c_m = \frac{\alpha}{1-\nu}(\Theta_o-\Theta_b)$, $c_f = \frac{\alpha}{1-\nu}(\Theta_b-\Theta_f)$

and

$$S_i = \sum_I E_I e^{-\lambda_I \xi_i}$$

where ξ_i is defined and evaluated as before.

Following a numerical scheme similar to (22), the dependence of

the residual stress $\sigma(t_f)$ on the intermediate temperature Θ_b has been computed for a "hold-time" t_f = 100 minutes. In the calculations we took Θ_o = 438°K and Θ_f = 293°K. The results are shown in Fig. 5.

Note that the residual stress attains a minimum at the intermediate temperature Θ_b = 333°K. A similar behavior was observed experimentally for epoxy coupons reinforced by unidirectional fibers. Those coupons were cooled-down in two-steps and a qualitative assessment of the residual stresses was obtained by means of a frozen fringe pattern. It was observed that a minimal fringe count was attained at an intermediate value of temperature Θ_b ($\Theta_f > \Theta_b > \Theta_o$).*

6. Concluding Remarks

It has been shown that a linear elastic analysis of residual stresses overestimates their magnitude by more than 20%. If account is taken of the viscoelastic response of the material it may be possible to design a cool-down path that will yield a reduced value of residual stresses. It seems that the details of the cool-down path influence the magnitude of the residual stresses more noticeably than the duration of the cooling period.

The computations conducted in the present paper are based upon incomplete data. It is intended to modify the calculations and analysis in light of new data as they become available. It should be noted that the effects of aging were not considered in the present formulation. These effects may be of prime importance because it is conceivable that the newly created epoxy may be undergoing rapid aging while it is being cooled down. An inquiry into this matter is now under way.

---

*The author is indebted to Dr. Frank Crossman, of Lockheed Missiles and Space Co., Palo Alto, California, for this information.

Acknowledgements

The author wishes to thank Professor R. A. Schapery for many helpful discussions and Professor J. Ham for several useful comments. The assistance of Dr. S. B. Raju in obtaining the numerical results presented herein is gratefully acknowledged.

This work was conducted under Contract F49620-78C-0034 from the Air Force Office for Scientific Research (AFOSR).

References

[1] Chamis, C. C., "Residual Stresses in Angleplied Laminates and their Effects on Laminate Behavior." NASA Report NASA TM-78835, (April 1978).

[2] Hahn, H.T., and Pagano, N.J., "Curing Stresses in Composite Laminates," J. Composite Materials Vol. 9. pp. 91-106 (1975).

[3] Weitsman, Y., and Ford. D., "On the Optimization of Cool-Down Temperatures in Visco-elastic Resins," Recent Advances in Engineering Science, Proc. 14 Annual Meeting of the Society of Engineering Science, G. C. Sih, Editor, pp. 323-339 (1977).

[4] Beckwith, S. W., "Viscoelastic Characterization of a Nonlinear Glass/Epoxy Composite Including the Effect of Damage," Ph.D. dissertation, Texas A&M University,(Dec. 1974).

[5] Gurtin, M. E., McCamy, R.C., and Murphy, L. F., "On Optimal Strain Paths in Linear Viscoelasticity," Forthcoming.

[6] Fung, Y. C., "Foundations of Solid Mechanics," Prentice Hall, p. 417, (1965).

[7] Schapery, R. A., "Stress Analysis of Viscoelastic Composite Materials," J. Composite Materials,Vol.1, pp. 228-266 (1967).

[8] Fox, R. L., "Optimization Methods for Engineering Design," Addison-Wesley, Chapter 2. (1973).

[9] Lou, Y. C., and Schapery, R. A., "Viscoelastic Characterization of a Nonlinear Fiber-Reinforced Plastic," J. Composite Materials Vol. 5, pp. 208-234 (1971).

[10] Kibler, K., General Dynamics Corp., Fort Worth, Texas. (Private Communication).

Figure Titles

Fig. 1. Dependence of the Residual Stress σ on Cooling Time t_f. Linear Thermorheologically Complex Model. Linear (constant-Rate) Cool-Down from Θ_o = 438°K to Θ_f = 298°K. Dashed lines indicate Further Relaxation of Residual Stressts at Θ_f = 298°K After Termination of Cool-Down.

Fig. 2. Relaxation Modulus E(t) Obtained by Approximate Inversion of D(t) as Given in Equation (11) (Dashed line) and by Exponential-Series Determined Through Collocation (solid line).

Fig. 3. Optimal Cool-Down Path for the Thermorheologically Complex Model.

Fig. 4. Variation of Residual Stress σ with Time t. Stress Effected Relaxation (Equation 17)). Linear (Constant-Rate) Cool-Down from Θ_o = 438°K to Θ_f = 293°K. Solid Line Corresponds to Cooling Time t_f = 100 min. and also Shows Relaxation Beyond Termination of Cool-Down. Dashed Line Corresponds to t_f = 300 min.

Fig. 5. Two-Step Cool-Down. Variation of the Residual Stress σ with the Intermediate-Level Temperature Θ_b. Θ_o = 438°K, Θ_f = 293°K, t_f = 100 min. Note minimal residual stress at Θ_b = 333°K.

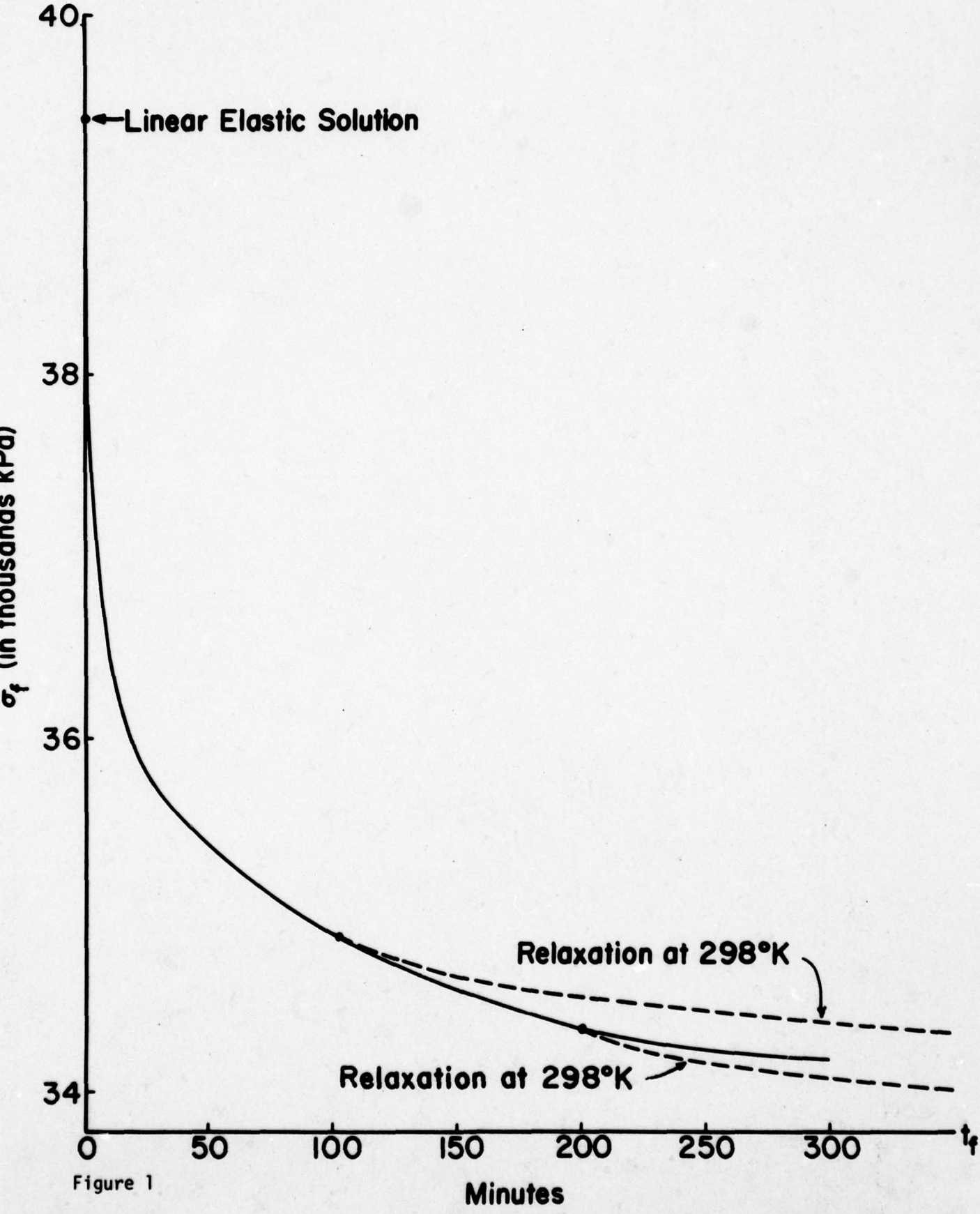
40
38
36
34
Linear Elastic Solution
σ_f (in thousands kPa)
Relaxation at 298°K
Relaxation at 298°K
0
50
100
150
200
250
300
t_f
Minutes

Figure 1

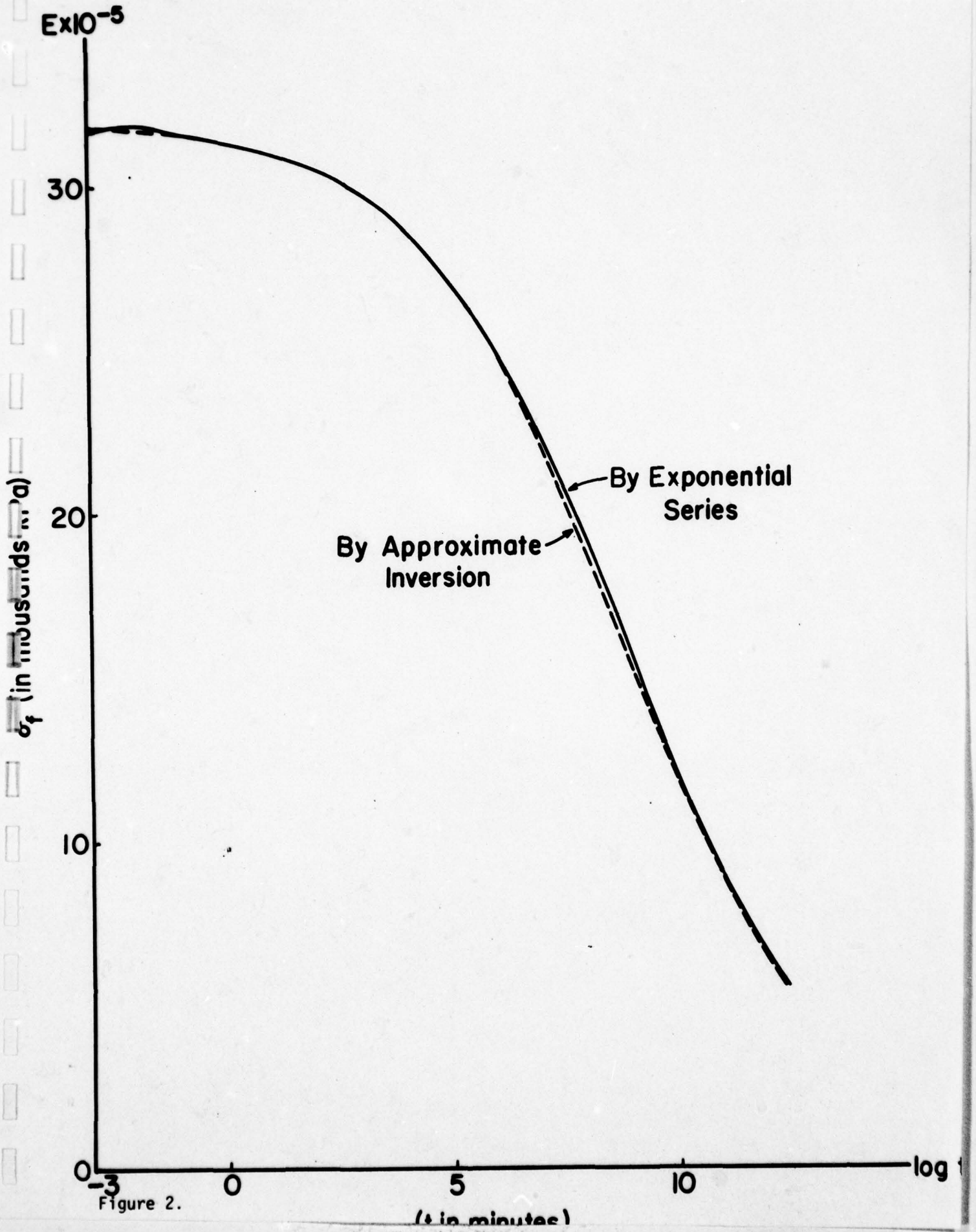
Ex10⁻⁵
30
20
10
0
-3
0
5
10
log t
(t in minutes)
By Exponential Series
By Approximate Inversion

Figure 2.

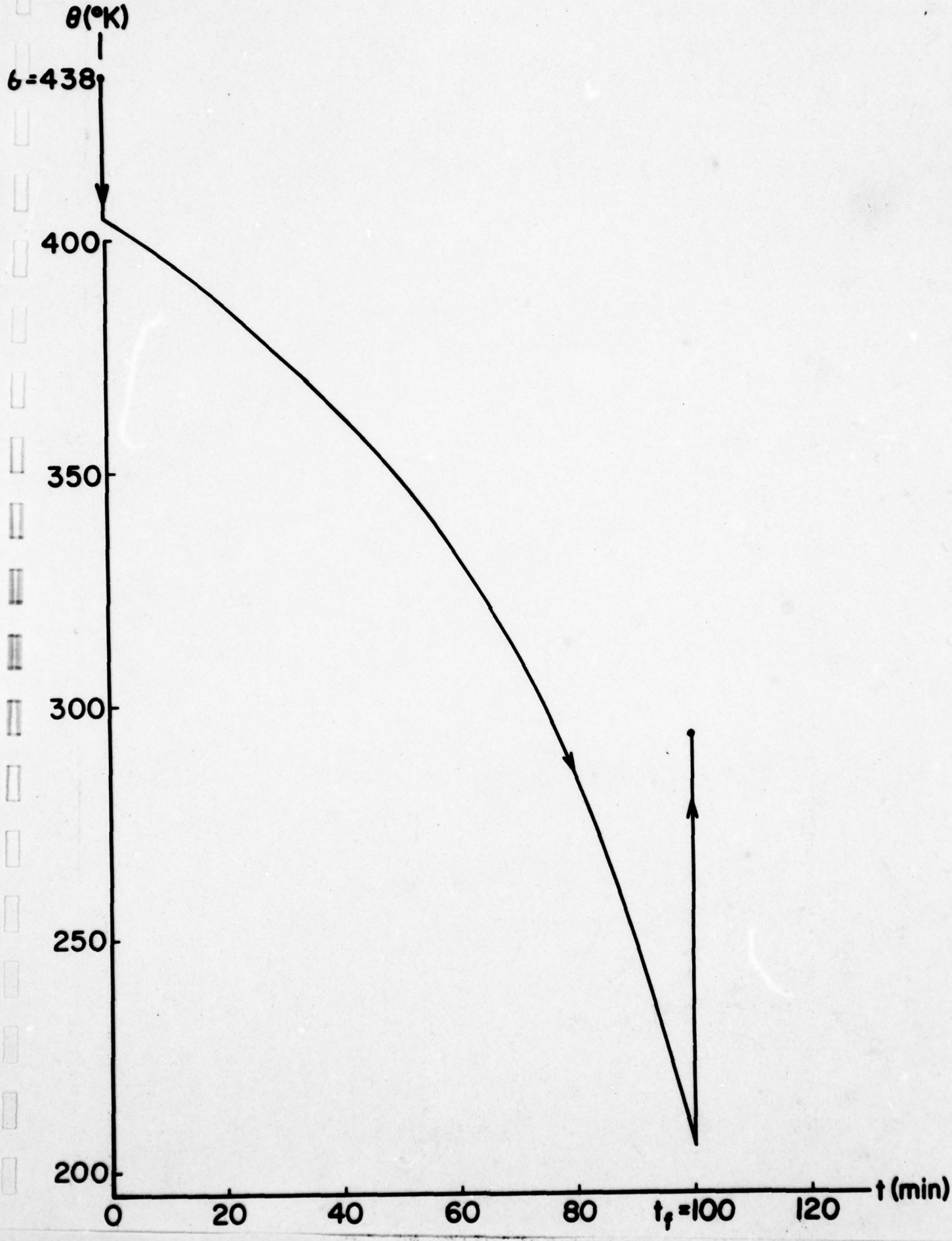
θ(°K)
6=438
400
350
300
250
200
0
20
40
60
80
t_f=100
120
t (min)

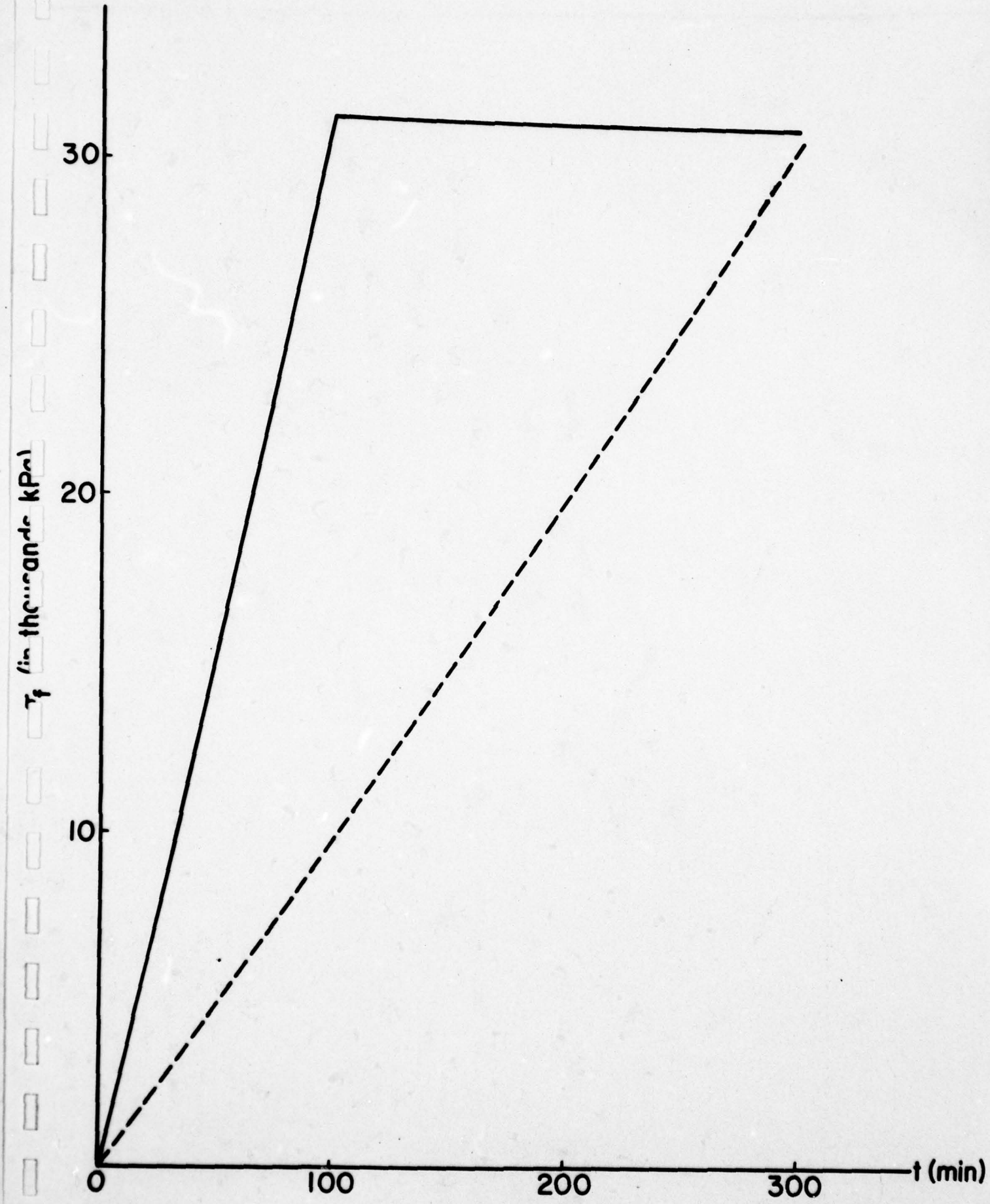

Figure 4

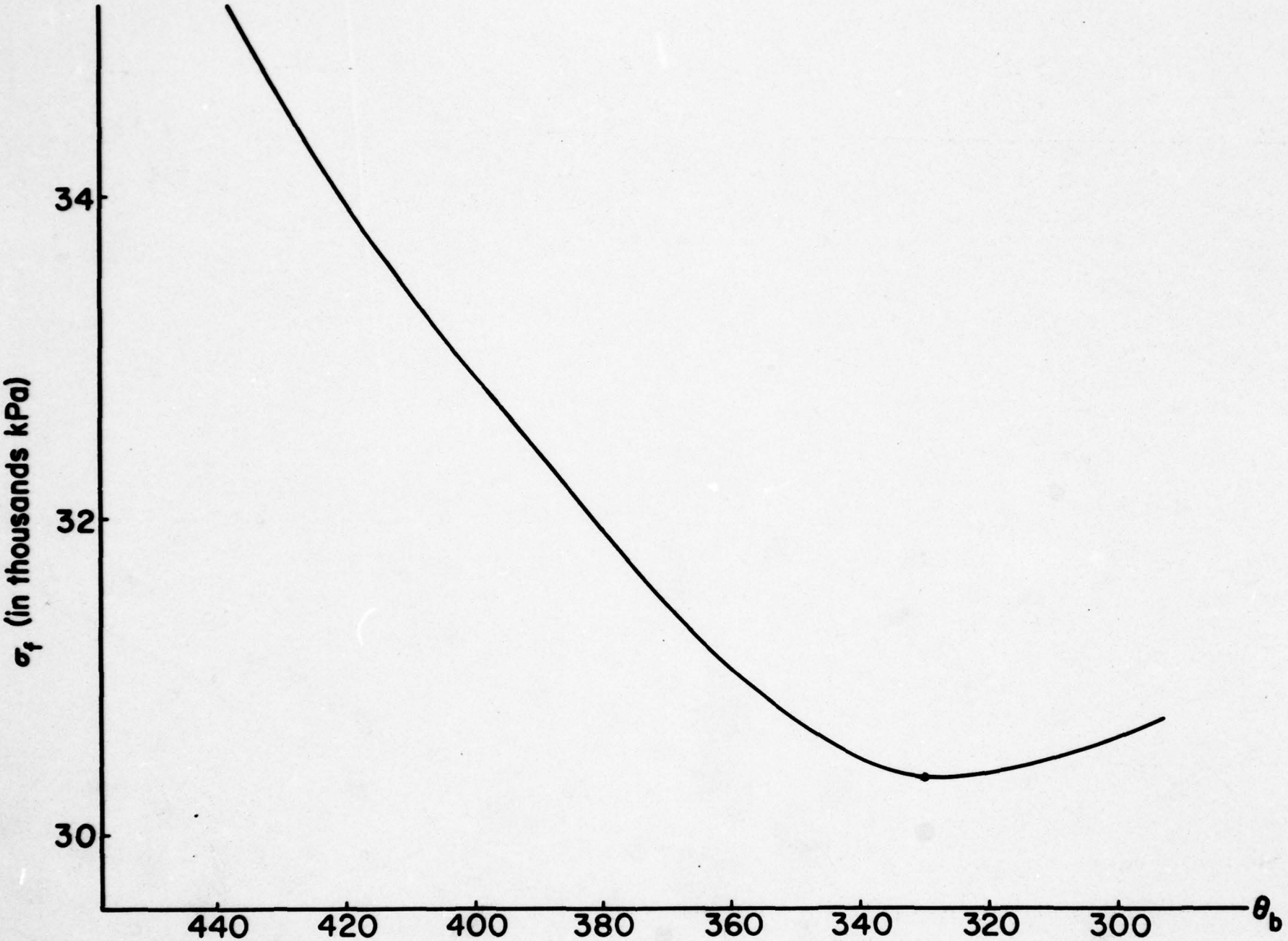
34
32
30
σ_t (in thousands kPa)
440
420
400
380
360
340
320
300
θ_b

Figure 5.

Interfacial Stresses in Viscoelastic Adhesive-Layers due to Moisture Sorption

by

Y. Weitsman*

ABSTRACT

This paper concerns the mechanical behavior of an epoxy adhesive layer that is located between stiff adherends as the adhesive absorbs moisture from the ambient environment.

As the moisture penetrates the layer by an extremely slow diffusion-process the epoxy undergoes a simultaneous process of stress-relaxation. Calculations of viscoelastic interfacial stresses were performed for a time-dependent response which is typical of epoxy and for a layer geometry as encountered in practice.

The results show that for exposure to steady ambient humidity the viscoelastic stresses are smaller than their elastic counterparts. However, under fluctuating ambient humidity the viscoelastic response may cause stress reversals, and thereby failure modes, which are not predicted by elasticity theory.

Accepted for publication in The International Journal of Solids and Structures

1. Introduction

Adhesive bonding forms an attractive method of joining structural members. In analyzing the stresses which develop within the bond it is necessary to account for the fact that the adhesive materials respond in a viscoelastic manner under loads and their time-dependent behavior is greatly affected by moisture and temperature.

When two adherends are joined together by a thin adhesive layer the adhesive absorbs moisture from the ambient environment, at its exposed edges, which induces swelling strains into the layer. Since the adherends are much stiffer than the adhesive they constrain the adhesive-layer against its tendency to swell, thus causing the formation of extremely high stresses within the layer. In this paper attention is focused on the interfacial-stresses which arise at the interfaces between the adherends and the adhesive.

Since the moisture penetrates the layer by an extremely slow diffusion-process, the epoxy may undergo noticeable creep and relaxation while the diffusion process is in progress. The main purpose of this paper is to relate the interaction, which occurs concurrently, between the two time-dependent phenomena - moisture-diffusion and stress-relaxation.

The analysis employes a variational method and is inherently approximate in nature. It is due to this approximation that the edge singularity in the stress field is replaced here by finite,though large, values. However, for the exceedingly thin layers that are utilized in practice, the selected expressions for the displacement fields should provide a good approximation. Furthermore, the approximation should not detract from the basic purpose of this work which is to provide information about the relative influence of the diffusion and relaxation times.

2. Formulation

Consider a semi-infinite, isotropic and elastic adhesive layer, of thickness 2a, between two semi-infinite adherend plates as shown in Fig. 1.

Let X, Y denote Cartesian coordinates and t time. Let $\epsilon(X,t)$ represent the unconstrained swelling induced by moisture and μ, ν be the elastic shear-modulus and Poisson's ratio, respectively. Assume a state of plane strain.

Introduce the following non-dimensional quantities

$$x = X/a, \quad y = Y/a, \quad e(x,t) = \epsilon(X/a, t)$$
$$s_x = \sigma_x/\mu, \quad s_y = \sigma_y/\mu, \quad s_{xy} = \tau_{xy}/\mu \tag{1}$$

Also, denote

$$f_1 = 2\nu/(1-2\nu)\ ,\quad f_2 = 2(1-\nu)/(1-2\nu),\quad f_3 = 2(1+\nu)/(1-2\nu)$$

Consider now the following approximate form for the displacement fields within the adhesive-layer

$$\begin{aligned} U(X,Y) &= a u_0(x) + \tfrac{1}{2}\, a\, u_2(x) y^2 \\ V(X,Y) &= a\, v_1(x) y + \tfrac{1}{3}\, a\, v_3(x) y^3 \end{aligned} \tag{2}$$

In (2) U and V are components of displacement in the X and Y directions, respectively, and u_0, u_2, v_1, v_3 are dimensionless, yet to be determined functions of the dimensionless coordinate x. Note that for an induced swelling-strain of the form e(x,t) the displacements U and V possess the required symmetries in Y.

Form (2) is the lowest-order approximation which provides information on the interfacial stresses, at the boundary between adhesive and adherend, in a self-contained manner. For exceedingly thin layers the approximation provides sufficient accuracy.

Expressions (2) are essentially the same as used in reference [1]*.

Employing Hooke's law we obtain the following non-dimensional form for stress-strain relations:

$$\begin{bmatrix} s_x \\ s_y \\ s_{xy} \end{bmatrix} = \begin{bmatrix} f_2 & f_1 & f_3 & 0 \\ f_1 & f_2 & f_3 & 0 \\ 0 & 0 & 0 & 1 \end{bmatrix} \begin{bmatrix} u_0' + \tfrac{1}{2} u_2'\, y^2 \\ v_1 + v_3\, y^2 \\ -e \\ u_2 y + v_1'\, y + \tfrac{1}{3} v_3' y^3 \end{bmatrix} \tag{3}$$

where primes designate derivatives with respect to x.

The rigid adherends force the boundary conditions:

---

*Numbers in brackets indicate references listed at the end of this paper.

$$u(x, 1, t) = 0$$
$$v(x, 1, t) = 0 \qquad (4)$$

The boundary conditions (4) imply that the unknown functions u_o, u_2, v_1, and v_3 in (2) are not independent. As noted in [1] the four above mentioned functions can be treated independently by introducing suitable Lagrange multipliers s_n and s_t. The s_n and s_t are the dimensionless force-conjugates of $v(x, 1, t)$ and $u(x, 1, t)$ respectively, and represent the interfacial normal and shear stresses.

Using the Lagrange multipliers defined above in the principle of virtual work as in [1][§] yields the following expression for the variation of the internal energy δE

$$\delta E = \mu a^2 \int_0^\infty \left\{ \int_0^1 \left[s_x(\delta u_o' + \tfrac{1}{2} y^2 \delta u_2') + s_y(\delta v_1 + y^2 \delta v_3) + s_{xy}(y\delta u_2 + y\delta v_1' + \tfrac{1}{3} y^3 \delta v_3') \right] dy - s_t (\delta u_o + \tfrac{1}{2} \delta u_2) - \delta s_t(u_o + \tfrac{1}{2} u_2) - s_n (\delta v_1 + \tfrac{1}{3} \delta v_3) - \delta s_n(v_1 + \tfrac{1}{3} v_3) \right\} dx \qquad (5)$$

Similarly, the variation of the external work, δW, is given by

$$\delta W = \mu a^2 \int_0^1 \left[s_x^*(o,y) (\delta u_o + \tfrac{1}{2} y^2 \delta u_2) + s_{xy}^*(o,y)(y\delta v_1 + \tfrac{1}{3} y^3 \delta v_3) \right] dy \qquad (6)$$

Integration-by-parts of (5) and employment of (3) yield, upon factoring-out the now independent variations δu_o, δu_2, δv_1 and δv_3:

$$\begin{aligned}
&\tfrac{2}{3} f_2 u_o'' - f_3 e' + s_t = 0 \\
&\tfrac{1}{15} f_2 u_o'' - \tfrac{2}{15} (f_1 + 1) v_1' + \tfrac{2}{3} u_o - \tfrac{1}{6} f_3 e' + \tfrac{1}{2} s_t = 0 \\
&\tfrac{2}{3}(f_1 + 1) u_o' - \tfrac{2}{15} v_1'' - f_3 e - s_n = 0 \\
&\tfrac{2}{5}(f_1 + 1) u_o' - \tfrac{2}{35} v_1'' - \tfrac{4}{5} f_2 v_1 - f_3 e - s_n = 0
\end{aligned} \qquad (7)$$

§See particularly the section "Variational Formulation of the Totally Constrained Case ($v_o = 0$)".

To these are adjoined the constraint conditions

$$u_o + \frac{1}{2} u_2 = 0$$
$$v_1 + \frac{1}{3} v_3 = 0 \qquad (8)$$

Equations (7) and (8) express the field equations of the problem. The concomitant from the integration-by-parts of (5) combines with (6) to determine the boundary conditions at x = 0. This combination, together with (3), yields

$$-7\, u_o + 2\, v_1' = 0$$
$$2\, u_o' + \frac{f_1}{f_2} v_1 = \frac{5}{2} \frac{f_3}{f_2} e(o, t) \qquad (9)$$

Note that the boundary conditions (9) were obtained after employment of (8), which hold also at x = 0.

In order to solve for u_o and v_1 we first eliminate s_t between the first pair of (7) and s_n between the last pair. Next, we employ (8) to eliminate u_2 and v_3. This procedure yields:

$$2 f_2 u_o'' + (f_1 + 1) v_1' - 5 u_o = \frac{5}{2} f_3 e'$$
$$\frac{2}{7} v_1'' - (f_1 + 1) v_o' - 3 f_2 v_1 = 0 \qquad (10)$$

The solution of (10) is expressed with the aid of the following second-order equation

$$\frac{4}{7} f_2 Z^2 + \left[(f_1 + 1)^2 - 6 f_2^2 - \frac{10}{7}\right] Z + 15 f_2 = 0 \qquad (11)$$

Denote the roots of (11) by Z_1 and Z_2 and define

$$\alpha_1 = \sqrt{Z_1}, \quad \alpha_2 = \sqrt{Z_2}$$
$$X_m = \frac{(f_1 + 1)\, \alpha_m}{\frac{2}{7} Z_m - 3 f_2}, \ (m = 1, 2) \quad D = \frac{5}{4} \frac{f_3}{f_2} \frac{1}{\alpha_1 X_2 - \alpha_2 X_1}$$

The solution of (10), which vanishes as $x \to \infty$, is

$$u_0 = D\left[\chi_1 \int_x^\infty \sinh \alpha_2(x - s)e'(s)ds - \chi_2 \int_x^\infty \sinh \alpha_1(x-s)e'(s)ds\right]$$
$$+ A_1 e^{-\alpha_1 x} + A_2 e^{-\alpha_2 x}$$
$$v_1 = D\chi_1\chi_2 \int_x^\infty \left[\cosh \alpha_2(x - s) - \cosh \alpha_1(x - s)\right] e'(s)ds \qquad (12)$$
$$- \chi_1 A_1 e^{-\alpha_1 x} - \chi_2 A_2 e^{-\alpha_2 x}$$

In (12) A_1 and A_2 are arbitrary constants determined by boundary conditions (9).

3. Elastic Solution for Moisture-Diffusion Under Constant Ambient Humidity

It has been observed [2], [3]* that the saturation-moisture level in "neat" epoxy, as well as in epoxy-based composites, depends on the relative humidity of the ambient environment. The dilatational strains that accompany moisture sorption are about 2/3 of the swelling that would be anticipated by straightforward"volume additivity".

The penetration of moisture into several epoxy resins was shown to follow the classical diffusion equations [2] [3] [4].

For the one-dimensional diffusion process considered herein, it follows that under constant ambient humidity the moisture-induced swelling is given by

$$\varepsilon(X,t) = A\,\mathrm{erfc}\left(\frac{X}{2\sqrt{kt}}\right) \qquad (13)$$

In (13) A is a constant which converts moisture content to dilatational strain and k is the coefficient of moisture diffusion.

In terms of the non-dimensional time $\beta = kt/a^2$, the non-dimensional form of (13) reads

$$e(x,\beta) = A\,\mathrm{erfc}(x/2\sqrt{\beta}) \qquad (14)$$

---

*For most of this information, the author is greatly indebted to Messrs. J. E. Halkias and E. L. McKague of General Dynamics Corporation, Fort Worth Division.

Substitution of (14) into (12) leads to closed form expressions [5],[6], e.g.

$$\int_x^\infty \sinh\alpha(x-s)e'(s)ds = -\frac{A}{2}e^{\beta\alpha^2}\left\{\sinh\alpha x\left[1-\frac{1}{2}\left(\operatorname{erf}\left(\frac{x}{2\sqrt{\beta}}+\alpha\sqrt{\beta}\right)\right.\right.\right.$$

$$\left.\left.\left.-\operatorname{erf}\left(\frac{x}{2\sqrt{\beta}}-\alpha\sqrt{\beta}\right)\right)\right]-\frac{1}{2}\cosh\alpha x\left[\operatorname{erf}\left(\frac{x}{2\sqrt{\beta}}+\alpha\sqrt{\beta}\right)-\operatorname{erf}\left(\frac{x}{2\sqrt{\beta}}-\alpha\sqrt{\beta}\right)\right]\right\}$$

and a similar expression for $\int_x^\infty \cosh\alpha\,(x-s)\,e'(s)ds$.

With the simpler, closed-form version of u_o and v_1 that replaces all the integrals in (12) it is possible to evaluate analytically the unknowns A_1 and A_2 therein.

Employing the boundary conditions (9), with $e(o,t) = A$, the values of A_1 and A_2 are determined from the following two-by-two algebraic system:

$$\begin{bmatrix} L_1 & L_2 \\ M_1 & M_2 \end{bmatrix}\begin{bmatrix} A_1 \\ A_2 \end{bmatrix} = \begin{bmatrix} D(-L_2\chi_1 J_2 + L_1\chi_2 J_1) \\ -\frac{5}{2}\frac{f_3}{f_2}A + D(-M_1\chi_2 K_1 + M_2\chi_1 K_2) \end{bmatrix} \qquad (15)$$

where, in (15)

$$L_m = 7-(2\alpha\chi)_m \qquad M_m = 2\alpha_m + \frac{f_1}{f_2}\chi_m$$

$$K_m = -Ae^{\beta\alpha_m^2} \qquad J_m = -K_m \operatorname{erf}(\alpha_m\sqrt{\beta}) \qquad (m = 1, 2)$$

Solving for A_1 and A_2 from (15) we obtain the complete solution for u_o and v_1 in (12), which enables us to evaluate the interfacial tractions s_n and s_t by using the first and third of Eqs. (7).

After straightforward, though tedious, manipulations we obtain

$$s_n(x,\beta) = \frac{2}{3} D \left[\alpha_2 \chi_1 P_2 K_2(x,\beta) - \alpha_1 \chi_2 P_1 K_1(x,\beta)\right]$$

$$- \frac{2}{3} \alpha_1 P_1 A_1 e^{-\alpha_1 x} - \frac{2}{3} \alpha_2 P_2 A_2 e^{-\alpha_2 x} - f_3\, e(x,\beta)$$

$$s_t(x,\beta) = - \frac{2}{3} f_2 D \left[\alpha_2^2\, \chi_1 J_2(x,\beta) - \alpha_1^2 \chi_2 J_1(x,\beta)\right] \qquad (16)$$

$$- \frac{2}{3} f_2 \left(\alpha_1^2 A_1 e^{-\alpha_1 x} + \alpha_2^2 A_2 e^{-\alpha_2 x}\right) - \frac{A f_3}{6\sqrt{\pi\beta}} e^{-\frac{x^2}{4\beta}}$$

In (16)

$$J_{1,2}(x,\beta) = - \frac{A}{2} e^{\beta\alpha_{1,2}^2} \left(\psi_{1,2}^{+} - \psi_{1,2}^{-}\right)$$

$$K_{1,2}(x,\beta) = - \frac{A}{2} e^{\beta\alpha_{1,2}^2} \left(\psi_{1,2}^{+} + \psi_{1,2}^{-}\right)$$

where $\psi_{1,2}^{+} = e^{\alpha_{1,2} x} \operatorname{erfc}\left(\alpha_{1,2}\sqrt{\beta} + x/2\sqrt{\beta}\right)$

$$\psi_{1,2}^{-} = e^{-\alpha_{1,2} x} \operatorname{erfc}\left(-\alpha_{1,2}\sqrt{\beta} + x/2\sqrt{\beta}\right)$$

Also, $P_{1,2} = f_1 + 1 - \frac{1}{5}(\alpha x)_{1,2}$

Form (16) is the elastic solution to the present problem. While this form provides a necessary step toward the generation of the viscoelastic solution, because its Laplace transform is readily available, it cannot be evaluated numerically for a wide range of x and t because $J_1(x,\beta)$, $K_1(x,\beta)$, A_1 and A_2 become numerically unstable.* Difficulties of this sort stem from the peculiar geometry of the adhesive layer, namely, the extremely small ratio of thickness to length.

---

* For $x = 3$ and $t = 1000$, with typical values for k, a, and ν, J_1 and K_1 involve products of numbers of $O(10^{22})$ with numbers of $O(10^{-22})$, thus exceeding the accuracy provided even by "double precision".

The difficulty is overcome by the employment of an approximate form for erfc (z), as follows [7]:

$$\text{erfc } z = Q(t(z))e^{-z^2}$$

where (17)

$$Q(t) = \sum_{j=1}^{5} a_j t^j \quad \text{and} \quad t(z) = (1 + pz)^{-1} \ *$$

Appropriate substitution of (17) into (16) yields an alternative, numerically stable, form for the interfacial stresses. We obtain

$$\frac{1}{A} s_n(x,\beta) = \frac{5}{3}\frac{f_3}{f_2}\frac{\alpha_2 P_2 L_1 e^{-\alpha_2 x} - \alpha_1 P_1 L_2 e^{-\alpha_1 x}}{\Delta} - f_3 \operatorname{erfc}(x/2\sqrt{\beta})$$

$$+ \frac{2}{3} D \Bigg\{ -\alpha_2 \chi_1 P_2 \Bigg[\frac{1}{2} e^{-\frac{x^2}{4\beta}} \left(Q\left(\alpha_2\sqrt{\beta} + \frac{x}{2\sqrt{\beta}}\right) + h(x-2\alpha_2\beta) Q\left(\left|\alpha_2\sqrt{\beta} - \frac{x}{2\sqrt{\beta}}\right|\right)\right)$$

$$- H(x-2\alpha_2\beta)\, e^{\beta\alpha_2^2 - \alpha_2 x} \Bigg] + \alpha_1 \chi_2 P_1 \Bigg[\frac{1}{2} e^{-\frac{x^2}{4\beta}} \Bigg(Q\left(\alpha_1\sqrt{\beta} + \frac{x}{2\sqrt{\beta}}\right)$$

$$+ h(x - 2\alpha_1\beta) Q\left(\left|\alpha_1\sqrt{\beta} - \frac{x}{2\sqrt{\beta}}\right|\right)\Bigg) - H(x - 2\alpha_1\beta) e^{\beta\alpha_1^2 - \alpha_1 x} \Bigg] +$$

$$+ \frac{B}{\Delta}\left(\alpha_1 P_1 M_2 e^{-\alpha_1 x} - \alpha_2 P_2 M_1 e^{-\alpha_2 x}\right) \Bigg\}$$

$$\frac{1}{A} s_t(x,\beta) = \frac{5}{3}\frac{f_3}{\Delta}\left(\alpha_2^2 L_1 e^{-\alpha_2 x} - \alpha_1^2 L_2 e^{-\alpha_1 x}\right) - \frac{1}{6}\frac{f_3}{\sqrt{\pi\beta}} e^{-\frac{x^2}{4\beta}} \qquad (18)$$

$$+ \frac{2}{3} f_2 D \Bigg\{ \alpha_2^2 \chi_1 \Bigg[\frac{1}{2} e^{-\frac{x^2}{4\beta}} \left(Q\left(\alpha_2\sqrt{\beta} + \frac{x}{2\sqrt{\beta}}\right) - h(x-2\alpha_2\beta) Q\left(\left|\alpha_2\sqrt{\beta} - \frac{x}{2\sqrt{\beta}}\right|\right)\right)$$

$$+ H(x-2\alpha_2\beta) e^{\beta\alpha_2^2 - \alpha_2 x} \Bigg] - \alpha_1^2 \chi_2 \Bigg[\frac{1}{2} e^{-\frac{x^2}{4\beta}} \left(Q\left(\alpha_1\sqrt{\beta} + \frac{x}{2\sqrt{\beta}}\right)\right.$$

$$\left. - h(x-2\alpha_1\beta)\, Q\left(\left|\alpha_1\sqrt{\beta} - \frac{x}{2\sqrt{\beta}}\right|\right)\right) + H(x-2\alpha_1\beta) e^{\beta\alpha_1^2 - \alpha_1 x} \Bigg]$$

$$+ \frac{B}{\Delta}\left(\alpha_1^2 M_2 e^{-\alpha_1 x} - \alpha_2^2 M_1 e^{-\alpha_2 x}\right) \Bigg\}$$

* The numerical value of a_j (j = 1, 2, ...5) and p are given in section 7.1.26, on page 299 of ref. [7]. This approximation is valid for all z.

In (18)

$$H(\xi) = \begin{cases} 0 & \xi<0 \\ 1 & \xi\geq 0 \end{cases} \qquad h(\xi) = \begin{cases} -1 & \xi<0 \\ 1 & \xi>0 \end{cases}$$

and

$$A = L_1M_2 - L_2M_1 \ , \qquad B = \chi_2 L_1 Q(\alpha_1\sqrt{\beta}) - \chi_1 L_2 Q(\alpha_2\sqrt{\beta})$$

In the limit $t \to \infty$ the "fully saturated" elastic solution is

$$\begin{aligned} \frac{1}{A}\, s_n(x,\infty) &= -f_3\left[1 + \frac{5}{3}\,\frac{1}{f_2\Delta}\,(\alpha_1 P_1 L_2 e^{-\alpha_1 x} - \alpha_2 P_2 L_1 e^{-\alpha_2 x})\right] \\ \frac{1}{A}\, s_t(x,\infty) &= -\frac{5}{3}\,\frac{f_3}{\Delta}\,(\alpha_1^2 L_2 e^{-\alpha_1 x} - \alpha_2^2 L_1 e^{-\alpha_2 x}) \end{aligned} \tag{19}$$

4. Viscoelastic Solution for Moisture-Diffusion Under Constant Ambient Humidity.

Uniaxial-tension experiments [8] on epoxy indicate that its creep-response can be described by a "power law" form as follows:

$$D(t;T) = D_o(T) + D_1\left[\frac{t}{a(T)}\right]^q \tag{20}$$

In (20) T denotes temperature and a(T) is the "shift-factor" function. Additional data on polyester [9] and epoxy [10] indicate that the creep-response depends also on the moisture content m, namely D = D (t; T, m). However, this dependence is omitted in the present analysis. Furthermore, we shall consider the case of uniform temperature for the entire adhesive.

In most adhesives the Poisson's ratio ν remains constant under a wide range of conditions. Consequently we shall consider a viscoelastic shear-compliance of the form

$$\mu(t) = d_o(1 + d_1 t^q) \tag{21}$$

where $d_o = 2(1 + \nu)\, D_o$ *

---

*The non-dimensional viscoelastic stresses are given by $s_{ij} = \sigma_{ij}/d_o$

Denote $\tau = a^2/k$ and $\tau_r = d_1^{-1/q}$. Let p be the variable of the Laplace transform in the time domain and $\eta = p\tau$. Finally, let the ratio between the characteristic diffusion-time τ and the characteristic creep time τ_r be $\theta = \tau_r/\tau$.

Then, the Laplace-transform of (21) is

$$\frac{1}{d_o}\, p\bar{D}(p) = 1 + \frac{\Gamma(q+1)}{(\theta\eta)^q} \tag{22}$$

The reciprocity relations between the transforms of the creep and relaxation functions [11] yield

$$d_o p\bar{E}(p) = 1/[\,1 + \Gamma\,(q+1)/(\theta\eta)^q] = R(\theta\eta) \tag{23}$$

Upon insertion of the explicit expressions for A_1 *and* A_2 *into* (16), the Laplace transforms of the elastic stresses (denoted by $\hat{s}$) become

$$\begin{aligned}\frac{1}{A}p\hat{s}_n(x,p) = \frac{2}{3}D\Bigg[&\eta\left(\frac{\alpha_1 x_2 P_1}{\sqrt{\eta}+\alpha_1}\cdot\frac{e^{-\sqrt{\eta}\,x}-e^{-\alpha_1 x}}{\sqrt{\eta}-\alpha_1} - \frac{\alpha_2 x_1 P_2}{\sqrt{\eta}+\alpha_2}\cdot\frac{e^{-\sqrt{\eta}\,x}-e^{-\alpha_2 x}}{\sqrt{\eta}-\alpha_2}\right)\\ &+\sqrt{\eta}\left(\frac{x_2 L_1}{\sqrt{\eta}+\alpha_1} - \frac{x_1 L_2}{\sqrt{\eta}+\alpha_2}\right)\frac{\alpha_1 P_1 M_2 e^{-\alpha_1 x} - \alpha_2 P_2 M_1 e^{-\alpha_2 x}}{\Delta}\Bigg]\\ &- f_3 e^{-\sqrt{\eta}\,x} + \frac{5}{3}\frac{f_3}{f_2}\,\frac{\alpha_2 P_2 L_1 e^{-\alpha_2 x} - \alpha_1 P_1 L_2 e^{-\alpha_1 x}}{\Delta}\end{aligned} \tag{24}$$

$$\begin{aligned}\frac{1}{A}p\hat{s}_t(x,p) = &-\frac{f_3}{6}\sqrt{\eta}e^{-\sqrt{\eta}\,x} - \frac{5}{3}f_3\,\frac{L_2\alpha_1^2 e^{-\alpha_1 x} - L_1\alpha_2^2 e^{-\alpha_2 x}}{\Delta}\\ &-\frac{2}{3}f_2 D\sqrt{\eta}\Bigg[\frac{\alpha_1^2 x_2}{\sqrt{\eta}+\alpha_1}\,\frac{\sqrt{\eta}e^{-\alpha_1 x} - \alpha_1 e^{-\sqrt{\eta}x}}{\sqrt{\eta}-\alpha_1} - \frac{\alpha_2^2 x_1}{\sqrt{\eta}+\alpha_2}\,\frac{\sqrt{\eta}e^{-\alpha_2 x} - \alpha_2 e^{-\sqrt{\eta}x}}{\sqrt{\eta}-\alpha_2}\\ &\left(\frac{x_2 L_1}{\sqrt{\eta}+\alpha_1} - \frac{x_1 L_2}{\sqrt{\eta}+\alpha_2}\right)\frac{\alpha_2^2 M_1 e^{-\alpha_2 x} - \alpha_1^2 M_2 e^{-\alpha_1 x}}{\Delta}\Bigg]\end{aligned}$$

Note that the singularities at $\sqrt{\eta} = \alpha_1$ and $\sqrt{\eta} = \alpha_2$ are removable.

From the fundamental equations of linear viscoelasticity [12] it follows that the Laplace-transforms of the viscoelastic solution to our problem(denoted by overbars) are

$$\frac{d_o}{A}\, p\, \bar{s}_n(x,p) = R(\theta\eta)\ \cdot \frac{1}{A}\, p\hat{s}_n(x,p)$$

$$\frac{d_o}{A}\, p\, \bar{s}_t(x,p) = R(\theta\eta)\ \cdot \frac{1}{A}\, p\hat{s}_t(x,p) \qquad (25)$$

In order to obtain the viscoelastic solution in the real-time domain it is necessary to invert (25). The inversion was obtained by the method of collocation [13]. Typically, expressions (25) were plotted vs. log η and a set on N points $\eta_i (i = 1, \ldots N)$ was selected to cover the ranges where those plots show noticeable curvatures. It was found that the shapes of the above-mentioned plots, as well as the locations of high curvature regions, depended on x. Therefore, it was impossible to employ any specific set of points η_i in the inversion and an appropriate selection had to be made for each value of x.

The calculations followed the scheme of ref. [13]. Note, however, that for "power-law" creep as given in (20) we have $\lim_{t\to\infty} D(t,T)\to\infty$, hence the equilibrium stress vanishes. Furthermore, in the present case the transform variable is $\eta = p\tau$, whereby the inversion is obtained in terms of dimensionless time t/τ, rather than real time t.

Calculations were performed for an adhesive-layer with the following selected properties:

Thickness a = 0.003", moisture diffusivity $k = 0.2 \times 10^{-8}$ in^2/sec, Poisson's ratio $\nu = 0.45$, 100% R. H.- to - swelling conversion-factor A = 0.03, creep compliances $D_o = 2 \times 10^{-6}$ in^2/lb, $D_1 = 0.2 \times 10^{-6}$ in^2/lb with q = 0.19. The corresponding value of the shift-factor function was a(T) = 1.

With the above numerical values we obtain $\tau = 4500\ \text{sec}^{-1}$ and the value of θ in (22) is $\theta = 2450$.

Numerical evaluations were performed on an Amdahl 470 digital computer. The results are shown in Figs. 2 - 9. The heavy solid lines in Figs. 2 - 7 show the dependence of the non-dimensional viscoelastic normal and tangential interlaminar stresses s_n and s_t on time t at three fixed stations within the

layer, x = X/a = 0.01, 1 and 3, when the free edge (x = 0) is exposed to a constant R.H. = 100% at t = 0. Note that the time scale is logarithmic.

For comparison purposes, the elastic stresses - as given in (18) - are shown in thin solid lines in Figs. 2 - 7. Note that any station within the layer senses the build-up and approach of the moisture in a gradual manner and that a steep increase in stress occurs after the passage of a time-span, which depends on the characteristic diffusion time and the location of the station. Beyond that time the station notices a "fully saturated" state, which explains the leveling-off of the elastic stresses for longer times.

The viscoelastic values, which are affected by relaxation, diminish to zero with time.

Thus far all viscoelastic results were obtained from inversion of (25) by means of collocation.

Consider now an approximate expression for the relaxation modulus [14]

$$E(t) = \frac{1}{D(t)} \frac{\sin \pi n}{\pi n} \tag{26}$$

where $n = n(t) = \frac{d}{d \log t} D(t)$.

Employing (26), the "quasi-elastic" (viscoelastic) solution is given by [13]

$$s_n^{v.e.}(x,t) = F(t) s_n(x,t)$$
$$s_t^{v.e.}(x,t) = F(t) s_t(x,t) \tag{27}$$

where, in (27), $s_n(x,t)$ and $s_t(x,t)$ and the elastic expressions given in (18) and

$$F(t) = \frac{1}{1 + bt^q} \frac{\sin \pi n(t)}{\pi n(t)}$$

$$n(t) = qbt^q/(1 + bt^q)$$

with b = 0.046 and q = 0.19.

It is interesting to note that for the particular geometric and physical values for the adhesive-layer employed in the present problem the quasi-

elastic approach yielded results which were almost indistinguishable from the collocated inversion. This fortuitous circumstance could not be anticipated a-priori because the transformed expressions,(24) and (25), do exhibit large curvatures in the η domain. In general, the usefulness of a quasi-elastic method must be verified in such circumstances. In the present case expression (27) are certainly easier to evaluate than (25).

Employing (27), values of $s_n^{v.e.}(x,t)$ and $s_t^{v.e.}(x,t)$ were calculated for fixed values of time, t = 1000 secs. and 10000 secs, along the interface between the adhesive and adherent. These results are shown in Figs. 8 and 9 for $0 \leq x \leq 1.6$. (For comparison purposes, the elastic values are also shown in dashed lines).

5. Viscoelastic Solution under Fluctuating Ambient Humidity.

Thus far the adhesive layer was considered to be subjected to a sudden exposure to ambient-humidity at time t = 0, with a swelling conversion factor A.

For fluctuating ambient-humidity A = A(t) the interlaminar stresses are given by a superposition integral as follows

$$\underset{\sim}{s}_m^{v.e.}(x,t) = \int_0^t s_m^{v.e.}(x,t-t') \frac{d\,A(t')}{dt'}\, dt' \qquad (28)$$

where m = n or t.

In (28) the kernel-functions, under the integral sign, are given by (27).

A sample computation was performed for a sudden exposure to 100% R.H. followed by drying at a later time $t = t_1$. In this case

$$A(t) = A[H(t) - H(t-t_1)] \qquad (29)$$

whereby

$$\underset{\sim}{s}_m^{v.e.}(x,t) = s_m^{v.e.}(x,t) - s_m^{v.e.}(x,t-t_1) \quad (m = n \text{ or } t) \qquad (30)$$

Results for t_1 = 10,000 sec. at x = 0.01, x = 1.0 and x = 3.0 are shown by the dashed lines in Figs. 2 - 7. Note that the superposition of wetting and subsequent drying is algebraically additive in the elastic case. Therefore,

all the elastic stresses,represented by thin dashed lines in Fig. 2 - 7, tend to zero as $t \to \infty$ without any further sign changes.* However, in the viscoelastic case, the drying effects are superimposed on a relaxed wet state and this causes an overcompensation - thereby introducing sign-reversals in the stresses. Eventually, as $t \to \infty$, the viscoelastic stresses too tend to zero.

It is observed that viscoelasticity predicts detrimental effects that are caused by fluctuations in relative humidity - such as low cycle fatigue and interfacial tension - that are absent in an elastic analysis.

6. Concluding remarks

The present analysis is based on several idealizations which restrict the validity of the results. The exceedingly large stresses which are predicted by linear theories near the corners $X = 0$, $Y = \pm a$ cannot be borne by real adhesives and the response in those regions must be represented by a suitable non-linear model.

In addition, the actual viscoelastic response of resins depends on the moisture content, which introduces yet another non-linearity into the analysis of adhesive layers.

The evaluation of those non-linear effects still awaits an appropriate characterization at the present time. Once available it would require solution by means of numerical methods.

Acknowledgements

The author wishes to thank Professor R. A. Schapery for many valuable discussions and Dr. S. B. Raju for his assistance in obtaining the numerical results presented herein. The author is greatly indebted to Messrs. J. E.Halkias and E.L. McKague of General Dynamics Corporation, Fort Worth, Texas for much of the information concerning the response of resins to moisture.

This work was conducted under Contract F-49620-78C-0034 from the Air Force Office of Scientific Research (AFOSR).

---

*There is nevertheless an exception in Fig. 3.

References

[1] Weitsman, Y.: "Stresses in Adhesive Joints due to Moisture and Temperature," J. Composite Materials, Vol. 11. pp. 378-394 (Oct. 1977).

[2] Shirrell, C. D.: "Diffusion of Water Vapor in Graphite/Epoxy Composites." A privately communicated Air Force Materials Laboratory manuscript.

[3] Shen, C-H., and Springer, G.S.,: "Moisture Absorption and Desorption of Composite Materials." J. Composite Materials Vol. 10 pp. 2-20 (Jan. 1976).

[4] McKague, E. L. Jr., Halkias, J. E., and Reynolds, I. D.: "Moisture in Composites: The Effect of Supersonic Service on Diffusion." J. Composite Materials, Vol. 9, pp. 1-9 (Jan. 1975).

[5] Gradshteyn, I. S., and Ryzhik, I. W.: "Table of Integrals, Series and Products." Academic Press, 1965. See page 307, section 3.322.

[6] Erdelyi, A., Magnus, W., Oberhettinger, F., and Tricomi, F. G.: "Tables of Integral Transforms." (Bateman Manuscript Project) Vol. I, McGraw-Hill, 1954. See page 146, Eq. (21).

[7] "Handbook of Mathematical Functions", Abramowitz, M., and Stegun, I. A., Editors. National Bureau of Standards, June 1964.

[8] Beckwith, S. W.: "Viscoelastic Characterization of a Nonlinear Glass/Epoxy Composite, Including the Effect of Damage." Ph. D. Dissertation, Texas A&M University, Dec. 1974.

[9] Maximov, R. D., Sokolov, Ye. A., and Mochalov, V. P.: "Effect of Temperature and Humidity on Creep of Polymeric Materials." (In Russian) Mechanica Polimerov, 1975, Vol. 3, pp. 393-399.

[10] Crossman, F. W., Mauri, R. E., and Warren, W. J.: "Moisture Altered Viscoelastic Response of Graphite-Epoxy Composites." Lockheed Palo Alto Research Laboratory Report. Presented at the Symposium on Environmental Effects on Advanced Composite Materials, sponsored by ASTM D30 Committee, Dayton Ohio 29-30 September 1977.

[11] Fung, Y. C. : "Foundations of Solid Mechanics." Prentice-Hall, 1965. See page 417.

[12] Ibid, p. 414.

[13] Schapery, R. A.: "Stress Analysis of Viscoelastic Materials". J. Composite Materials, Vol. 1,, pp. 228-266 (1967). Especially section titled "Collocation Method" pp. 246-247.

[14] Ferry, J. D., "Viscoelastic Properties of Polymers" Wiley, 1961. See page 77.

FIGURE TITLES

1. The Adhesive Layer Between Rigid Adherends Exposed to Moisture at X = 0.

2. Elastic and Viscoelastic Values of the Non-Dimensional Normal Interlaminar Traction s_n at x = X/a = 0.01 vs. log t (t in seconds). Heavy Lines - Viscoelastic, Thin Lines - Elastic. Solid Lines - Exposure to a Constant Ambient R.H., Dashed Lines - Exposure to Fluctuating Ambient R.H. (according to Eq. (29)).

3. Elastic and Viscoelastic Values of the Non-Dimensional Tangential Interlaminar Traction s_t at x = X/a = 0.01 vs. log t (t in seconds). Heavy Lines - Viscoelastic, Thin Lines - Elastic. Solid Lines - Exposure to a Constant Ambient R. H., Dashed Lines - Exposure to Fluctuating Ambient R.H. (according to Eq. (29)).

4. Elastic and Viscoelastic Values of the Non-Dimensional Normal Interlaminar Traction s_n at x = X/a = 1 vs.log t (t in seconds). Heavy Lines - Viscoelastic, Thin Lines - Elastic. Solid Lines - Exposure to a Constant Ambient R. H., Dashed Lines - Exposure to Fluctuating Ambient R.H. (according to Eq. (29)).

5. Elastic and Viscoelastic Values of the Non-Dimensional Tangential Interlaminar Traction s_t at x = X/a = 1 vs. log t (t in seconds). Heavy Lines - Viscoelastic, Thin Lines - Elastic. Solid Lines - Exposure to a Constant Ambient R. H., Dashed Lines - Exposure to Fluctuating Ambient R. H. (according to Eq. (29)).

6. Elastic and Viscoelastic Values of the Non-Dimensional Normal Interlaminar Traction s_n at x = X/a = 3 vs. log t (t in seconds). Heavy Lines- Viscoelastic, Thin Lines - Elastic. Solid Lines - Exposure to a Constant Ambient R.H., Dashed Lines - Exposure to Fluctuating Ambient R. H. (according to Eq. (29)).

7. Elastic and Viscoelastic Values of the Non-Dimensional Tangential Interlaminar Traction s_t at x = X/a = 3 vs. log t (t in seconds). Heavy Lines - Viscoelastic, Thin Lines - Elastic. Solid Lines - Exposure to a Constant Ambient R.H., Dashed Lines - Exposure to Fluctuating Ambient R. H. (according to Eq. (29)).

8. Elastic and Viscoelastic Values of the Non-Dimensional Normal Interlaminar Traction s_n at Times t = 1000 sec. and t = 10000 sec. vs. x. Dashed lines - Elastic, Solid Lines - Viscoelastic.

9. Elastic and Viscoelastic Values of the Non-Dimensional Tangential Interlaminar Traction s_t at Times t = 1000 sec. and t = 10000 sec. vs. x. Dashed lines - Elastic, Solid Lines - Viscoelastic.

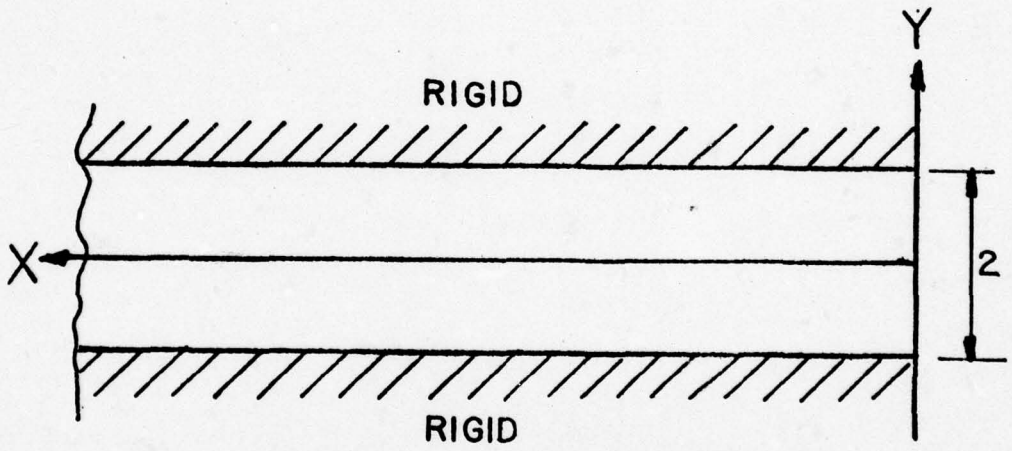

Figure 1.

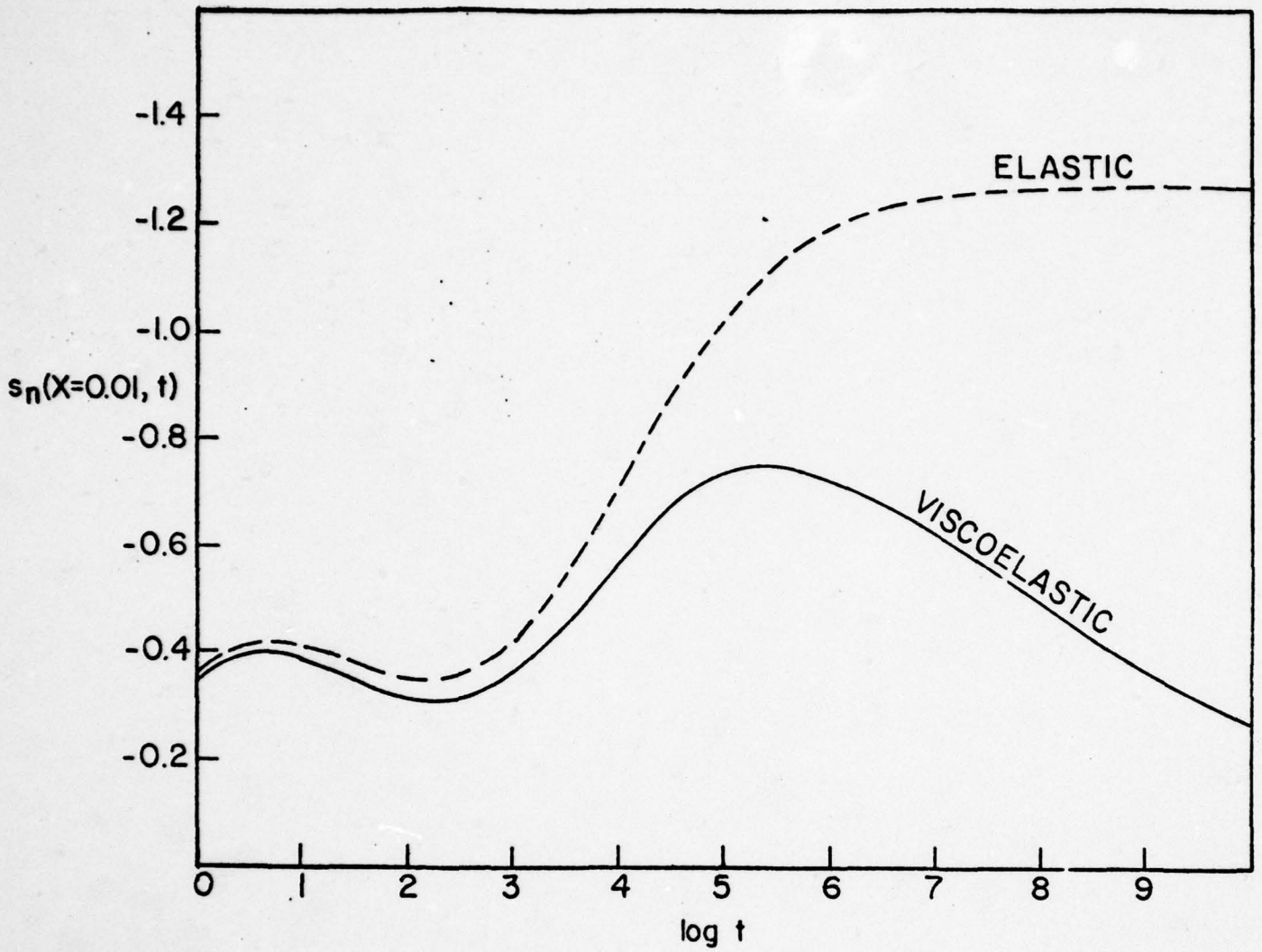
-1.4
-1.2
-1.0
$s_n(X=0.01, t)$
-0.8
-0.6
-0.4
-0.2
ELASTIC
VISCOELASTIC
0
1
2
3
4
5
6
7
8
9
log t

Figure 2.

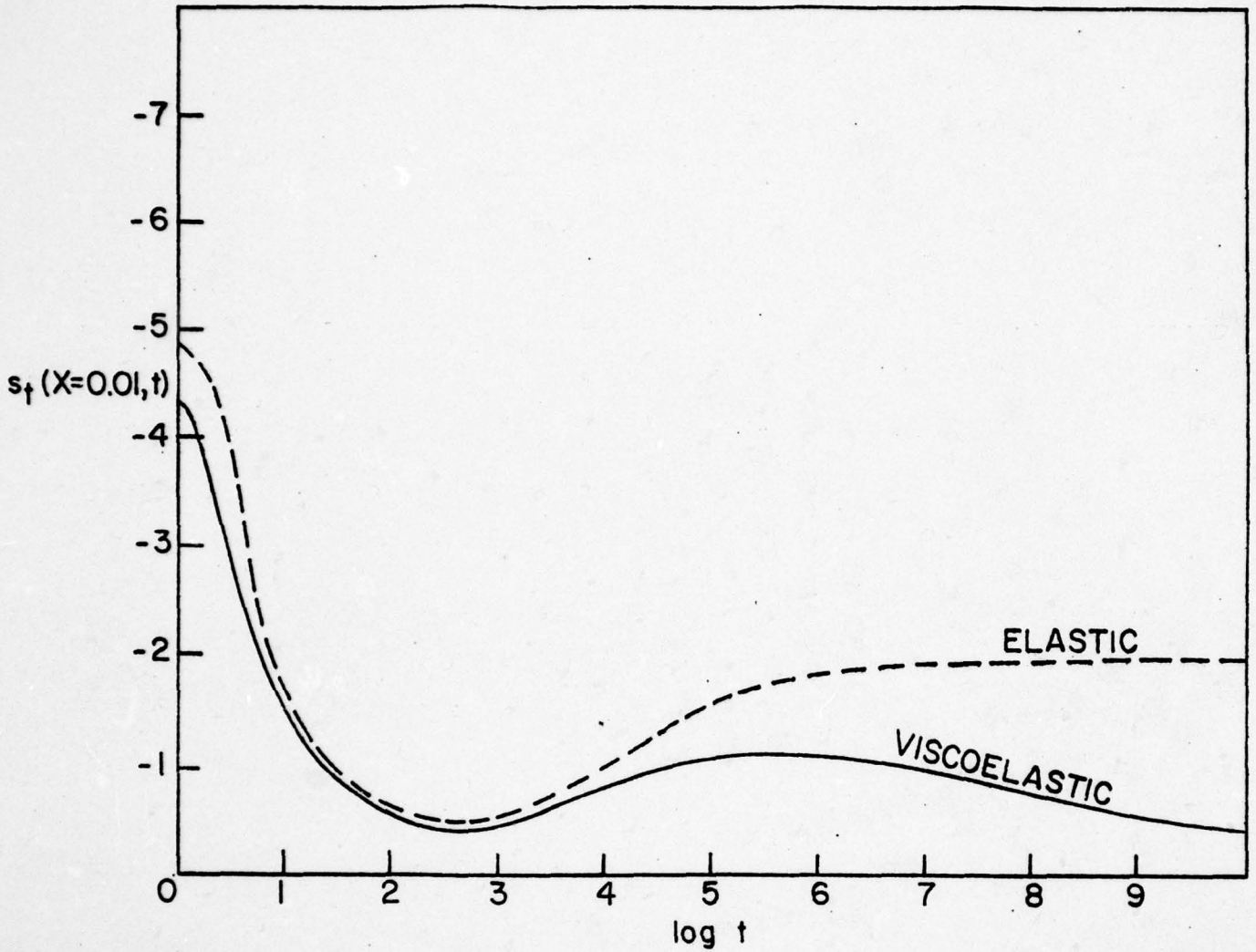

Figure 3.

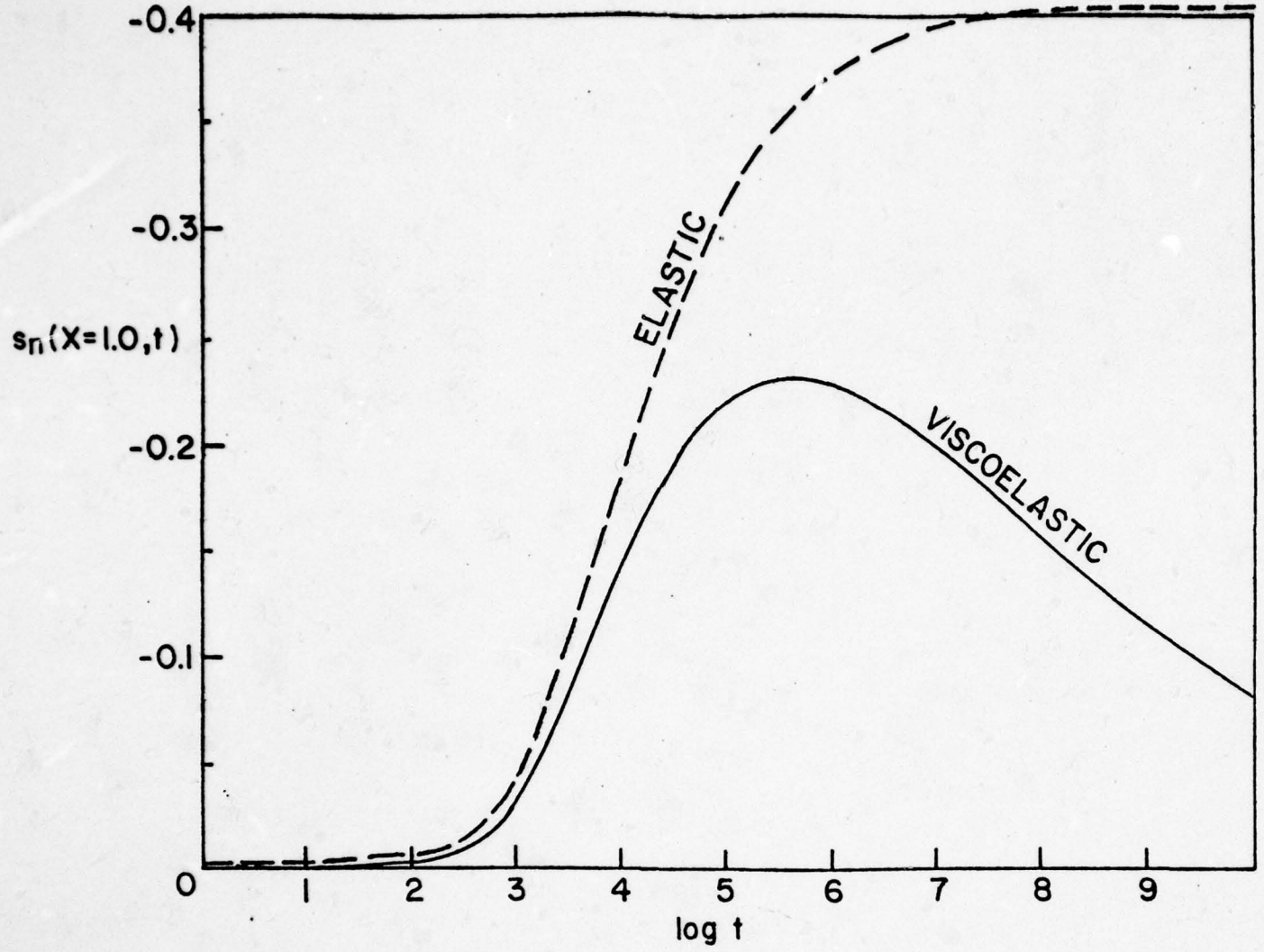

Figure 4.

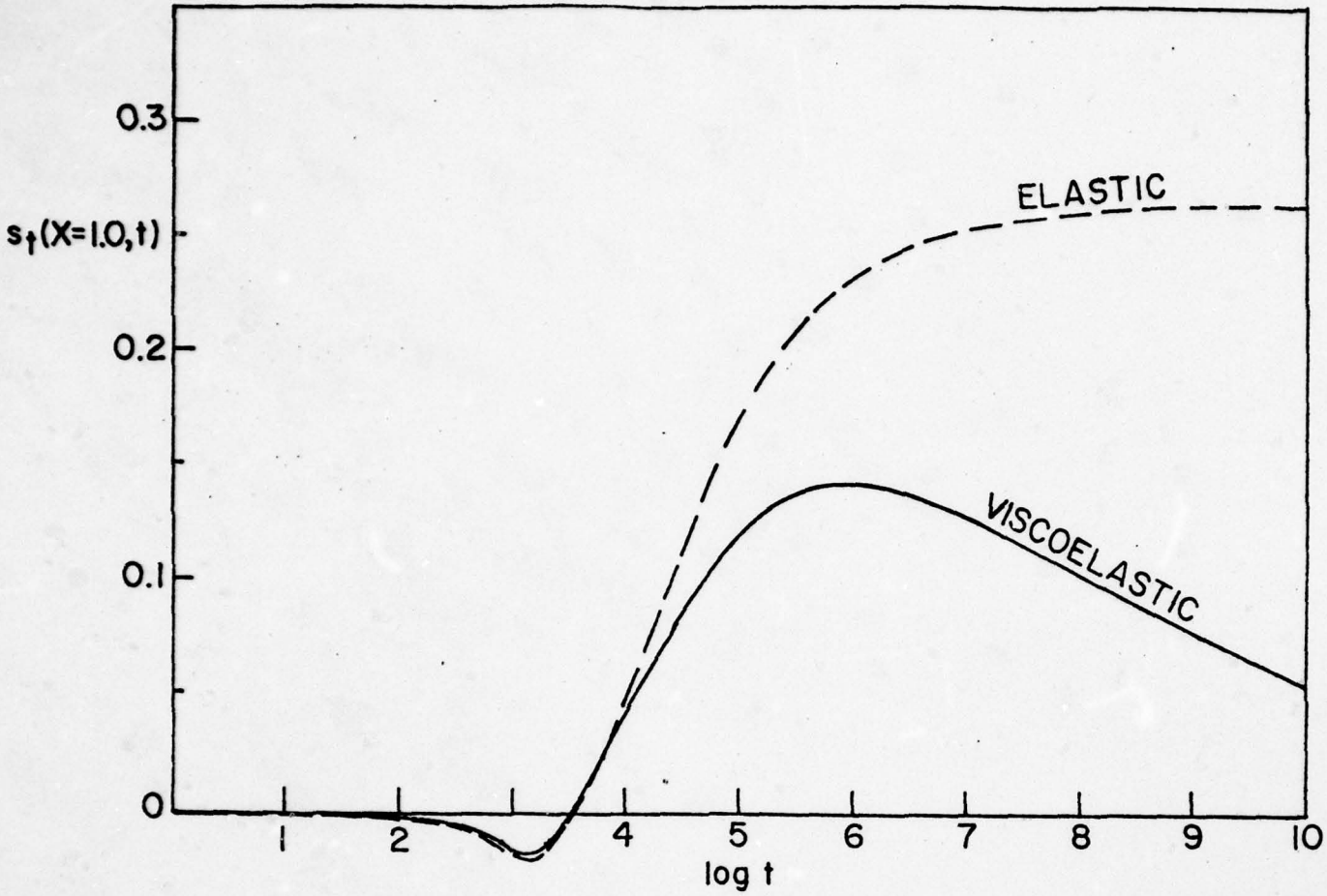

Figure 5.

AD-A066 754 TEXAS A AND M UNIV COLLEGE STATION MECHANICS AND MAT--ETC F/G 11/4
COMPOSITE MATERIALS FOR STRUCTURAL DESIGN.(U)
MAR 79 R SCHAPERY F49620-78-C-0034
UNCLASSIFIED MM-3724-79-2 AFOSR-TR-79-0347 NL

2 OF 2
ADA
066754

END
DATE
FILMED
5-79
DDC

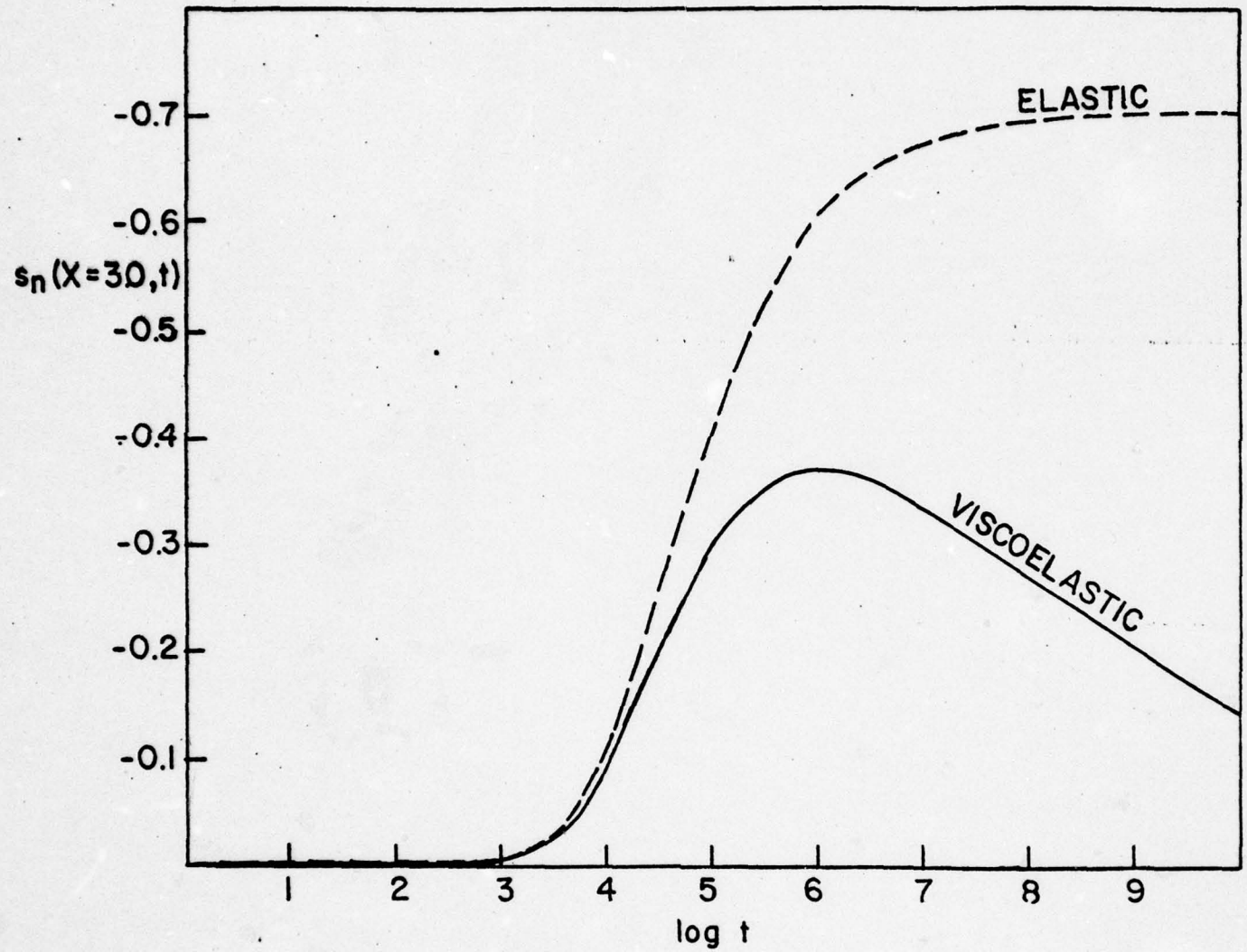
ELASTIC
VISCOELASTIC
-0.7
-0.6
-0.5
-0.4
-0.3
-0.2
-0.1
$s_n(X=30,t)$
1
2
3
4
5
6
7
8
9
log t

Figure 6.

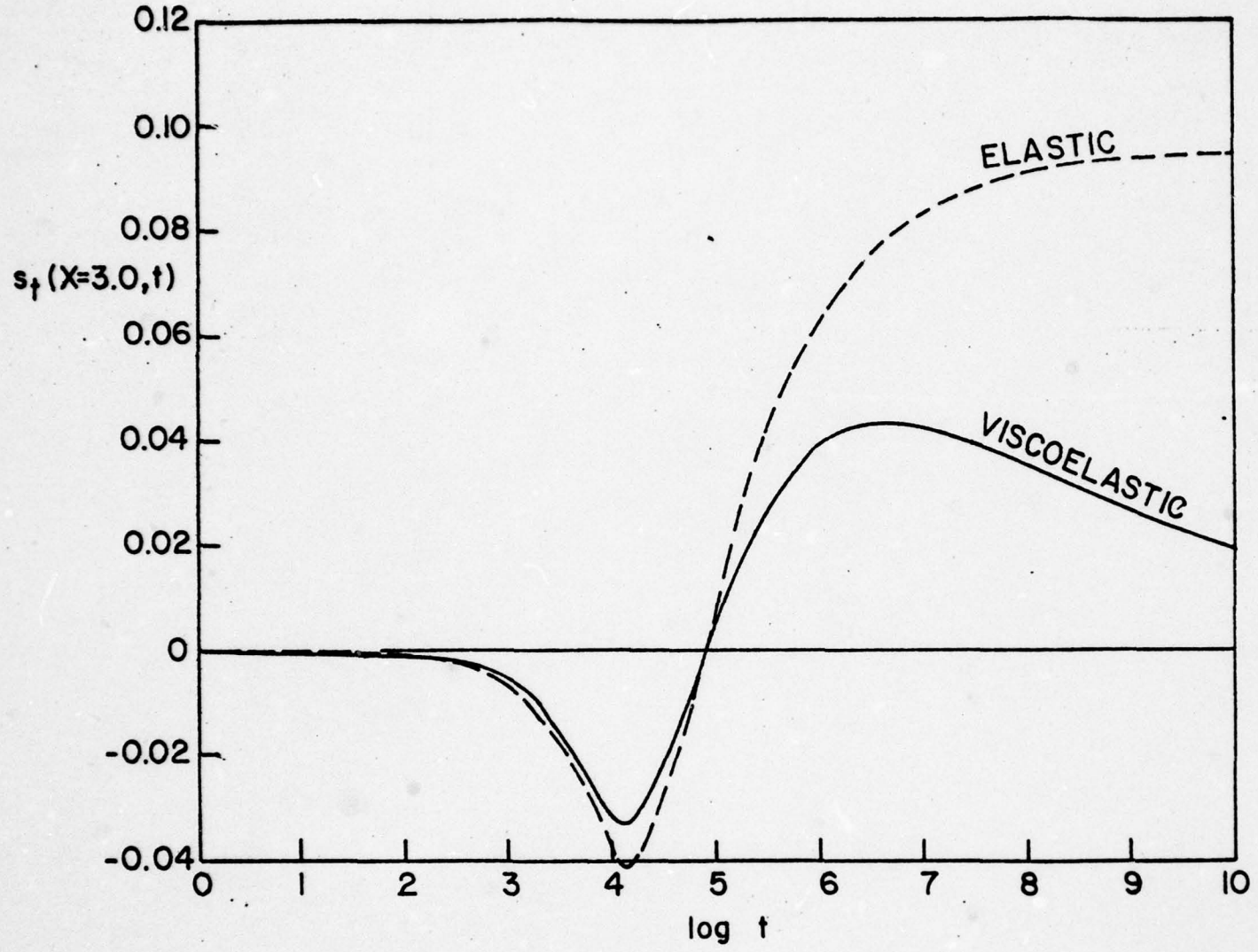
0.12
0.10
0.08
0.06
0.04
0.02
0
-0.02
-0.04
$s_t(X=3.0,t)$
ELASTIC
VISCOELASTIC
0
1
2
3
4
5
6
7
8
9
10
log t

Figure 7.

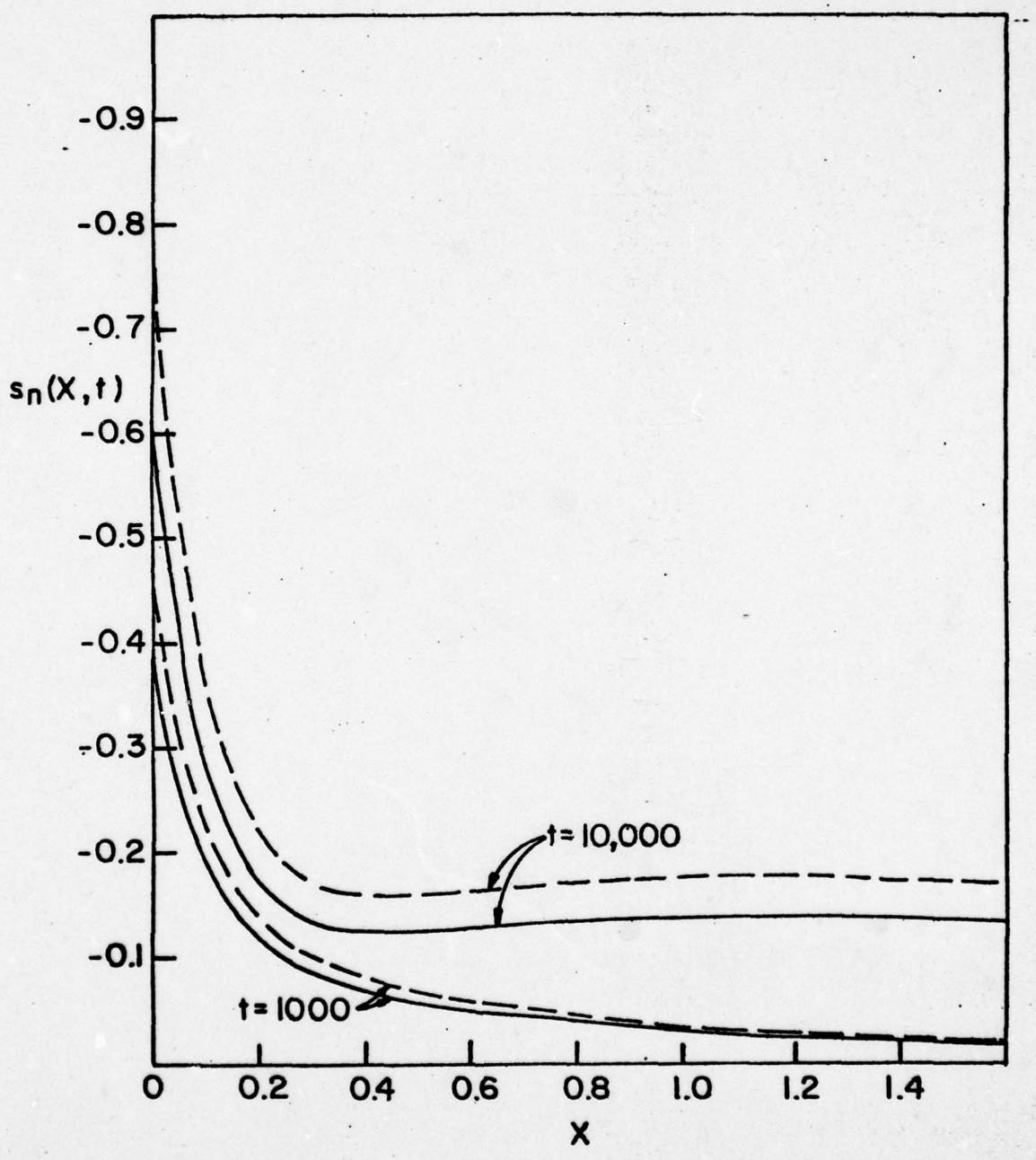

Figure 8.

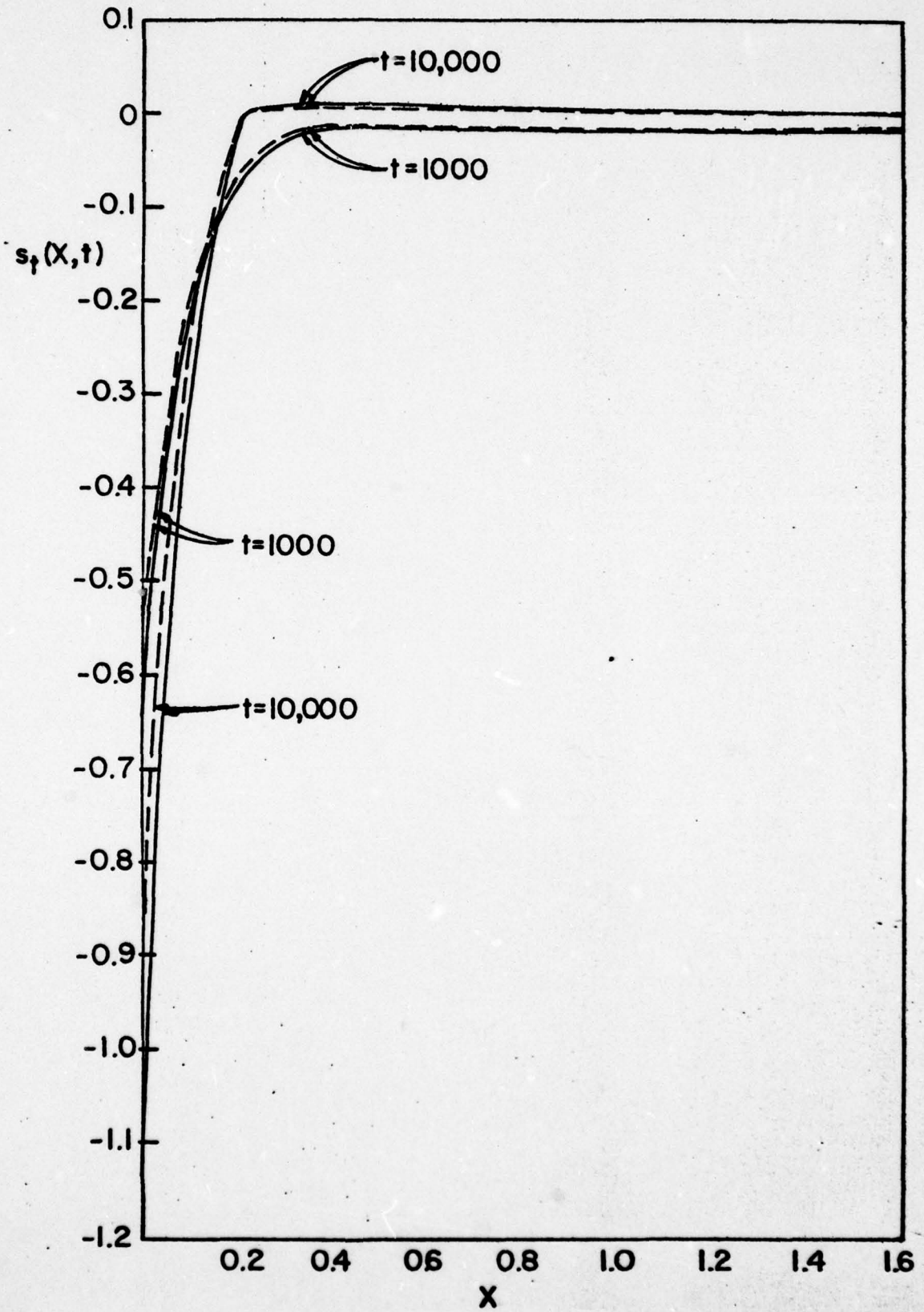
0.1
0
-0.1
-0.2
-0.3
-0.4
-0.5
-0.6
-0.7
-0.8
-0.9
-1.0
-1.1
-1.2
$s_t(X,t)$
t=10,000
t=1000
t=1000
t=10,000
0.2
0.4
0.6
0.8
1.0
1.2
1.4
1.6
X

Figure 9.

SIAM-AMS PROCEEDINGS
Volume 12
1979

ON THE ANALYSIS OF CRACK INITIATION AND GROWTH IN NONHOMOGENEOUS VISCOELASTIC MEDIA

R. A. Schapery[1]

ABSTRACT. Prediction of the rate of crack growth in viscoelastic media, as well as the time at which this growth initiates, is discussed. Emphasis is placed on the particular analytical problems which are associated with composite materials, such as fiber-reinforced plastics, and other nonhomogeneous media. Previous work on the analysis of crack speed and initiation of growth in linear viscoelastic bodies is first reviewed. Some new results are then obtained for initiation of crack growth in linear and nonlinear viscoelastic media. Certain important unsolved problems related to fracture of viscoelastic materials are indicated in the concluding remarks.

1. INTRODUCTION AND SUMMARY. Analysis of the quasi-static fracture of isotropic, homogeneous, linear viscoelastic bodies has received considerable attention, as may be seen in the reviews by Knauss [1, 2]. However, very little work has appeared on the analysis of more general classes of viscoelastic media.

In the former case, there are many applications involving traction boundary conditions in which the stress distribution is independent of viscoelastic properties; for this situation the stresses are the same as in a geometrically identical elastic body which is subjected to the same boundary tractions. This feature greatly simplifies the fracture analysis, and leads to relatively simple equations for predicting crack initiation and growth [3 - 5]. On the other hand, when stresses depend on viscoelastic properties, the fracture analysis is much more involved. This dependence normally exists for nonhomogeneous bodies; nonhomogeneity may be due to moisture or temperature gradients in polymeric materials for example, or to the presence of more than one continuum phase, as in fiber-reinforced plastic. An approximate method for calculating crack growth rate in such materials in their linear range of behavior is developed in [6].

AMS(MOS) subject classifications (1970). Primary 73F15, 73M05; Secondary 73F10, 73F25, 73M20.

[1]Research supported by the Air Force Office of Scientific Research.

The analysis in [6] consists of solving for stress and displacement in the neighborhood of the crack tip and then combining these results with an energy criterion of failure for the material at the crack tip. This work is reviewed in §2 - §4. It will be seen that the model employs a stress distribution which is bounded at the crack tip. In contrast to predictions for linear elastic media, the use of unbounded stresses in viscoelastic media leads to physically unacceptable results for fracture criteria [3, 7].

The initiation of growth is discussed in §5 and §6 for linear and nonlinear viscoelastic media, respectively. An approximate method of analysis is described, which represents an extension of the J-integral criterion to viscoelastic materials.

2. LINEAR STRESS AND DEFORMATION ANALYSIS. In analyzing linear viscoelastic media with growing cracks, the problem will be divided into two parts. First, response to imposed loads, temperatures, etc. is calculated for the case in which all cracks are stationary. The second part consists of predicting the additional response due to crack growth alone. Addition of these two responses yields the complete solution. The specified mechanical input for the second part consists of tractions which are applied to the new surfaces associated with the crack growth. If, in the complete solution, these surfaces are to be traction-free, then the tractions which are specified in the second problem are equal in magnitude, but opposite in sign, to tractions in the first problem acting across suitably defined imaginary surfaces; these surfaces correspond, of course, to the actual instantaneous crack surfaces. In some problems the actual crack faces will not be traction free due to, for example, interfacial rubbing or injection of a fluid under pressure; an appropriate adjustment to the surface tractions specified in the second part must then be made.

Inasmuch as this analysis is concerned with the prediction of crack growth, rather than the total mechanical state of the body, we shall deal with only the second problem. It should be added that the particular manner in which the original problem is decomposed aids in constructing approximate local solutions, as discussed in [6].

General linear, anisotropic viscoelastic relationships connecting the stresses σ_{ij} (i, j = 1, 2, 3) and strains ϵ_{ij} referred to an orthogonal set of Cartesian axes (x_i) may be written in the form

$$\epsilon_{ij} = \int_{0^-}^{t} S_{ijk\ell}(t-\tau)\frac{\partial \sigma_{k\ell}}{\partial \tau}\, d\tau, \tag{1}$$

where $S_{ijk\ell}(t)$ (i,j,k,ℓ = 1, 2, 3) are the linear viscoelastic creep com-

pliances; these mechanical properties form a completely symmetric positive-definite fourth-order tensor [8]. For notational simplicity, explicit dependence on the coordinates x_i is not shown; however, all dependent variables as well as the compliances may vary from point-to-point in the body. Also, the summation convention is used, in that a repeated index is to be summed out over its range.

Crack growth is assumed to start at $t = o$; the lower limit of the integral in Eq. (1) is shown as o^-, rather than o, in order to allow for a timewise jump in the stresses which may occur upon initiation of growth.

It is not necessary to include the expansion or contraction associated with temperature or moisture inasmuch as these effects are taken into account in the problem without crack growth. However, temperature and moisture can be expected to affect the particular values of creep compliances which exist at each point in the body. In order to be able to draw upon certain simplifying features of the Laplace transform, it is assumed that changes in the creep compliances due to timewise variations of temperature, moisture, and other physical and chemical changes are negligible during short periods of crack growth as determined by the crack speed and scale of the failing material at the crack tip [6].

Let us next introduce the Laplace transform (LT),

$$\bar{f} \equiv \int_{o^-}^{\infty} f(t)e^{-st}dt. \tag{2}$$

The quantity $\bar{f}$ is the LT of a time-dependent function f; s is the transform parameter. In some cases it is desirable to use the following notation for the LT,

$$L\{f\} \equiv \bar{f} \tag{3}$$

and to use $L^{-1}\{\bar{f}\}$ for the inverse of LT. Also, the Carson transform,

$$\tilde{f} \equiv s\bar{f} \tag{4}$$

will be employed when notationally convenient.

The constitutive equation (1) is now transformed to obtain

$$\bar{\epsilon}_{ij} = \tilde{S}_{ijk\ell}\bar{\sigma}_{k\ell}. \tag{5}$$

The complete set of transformed field equations consists of these six equations together with the equations of motion

$$\frac{\partial \bar{\sigma}_{ij}}{\partial x_j} = \rho s^2 \bar{u}_i \tag{6}$$

and strain-displacement equations

$$\bar{\varepsilon}_{ij} = \frac{1}{2}\left(\frac{\partial \bar{u}_j}{\partial x_i} + \frac{\partial \bar{u}_i}{\partial x_j}\right), \tag{7}$$

where ρ is the density and u_i are the displacements. The boundary conditions are all homogeneous with exception of those corresponding to the new surfaces which result from crack growth. (We assume that there are no changes in the surfaces of the body other than those due to crack growth; e.g., interaction of crack growth and ablation is excluded.)

Consider next an elastic boundary-value problem. It is supposed that the problem is in all respects identical to that for the viscoelastic body except elastic time-independent compliances $S^e_{ijk\ell}$, say, are used in place of the viscoelastic compliances; the instantaneous crack geometry and the specified tractions acting on the new crack faces are taken to be the same as for the viscoelasticity problem. Furthermore, let each $S^e_{ijk\ell}$ be equal to the corresponding $S_{ijk\ell}$ for one generic real value of the transform parameter s; in general, these elastic compliances will be functions of x_i. Assume now that the elastic boundary-value problem with specified growing cracks is solved. Denote the time-dependent solutions using a superscript e (viz., $\sigma_{ij}{}^e$, $u_i{}^e$, $\varepsilon_{ij}{}^e$). It is important to recognize that even though $S^e_{ijk\ell}$ is a function of s, through its association with $S_{ijk\ell}$, this dependence is suppressed when solving the elasticity problem by using LT theory or other means. Indeed, the time-dependent elastic solutions will depend on s because of this association.

Clearly, the LT of these elastic solutions satisfies the LT of the viscoelastic field equations (5)-(7). If we invert these transformed elastic solutions, and take into account the dependence of $S^e_{ijk\ell}$ on s, the resulting time-dependent solutions will obviously satisfy all of the field equations of viscoelasticity in the time plane.

In some cases (such as those discussed in [3]), this inverse will satisfy all boundary conditions, including those along the growing crack faces, as well as meet the requirement of continuity of material ahead of the crack tips. When this happens, the inverse is the solution to the viscoelasticity problem; uniqueness is assumed, not proved. In general, however, not all conditions will be satisfied by the inverse of the elastic transforms. Pursuing this latter point, we first note that the inverse obviously will satisfy all homogeneous boundary conditions on the original surfaces since the LT vanishes for all s. Also, the requirement of material continuity ahead of

the crack tip is not violated [6]. However, the traction condition on the newly formed crack faces is not necessarily satisfied. Nevertheless, in many cases most of the error in this condition can be eliminated through superposition of an elementary solution; the corrected result, which is derived in [6], then provides the basis for the development of the equation for predicting crack speed.

3. THE CRACK TIP MODEL. The model we employ is for the so-called opening mode of growth, and is shown in Fig. 1; it is analogous to that used by Barenblatt [9] and Dugdale [10] for elastic media. The (x,y,z) coordinate

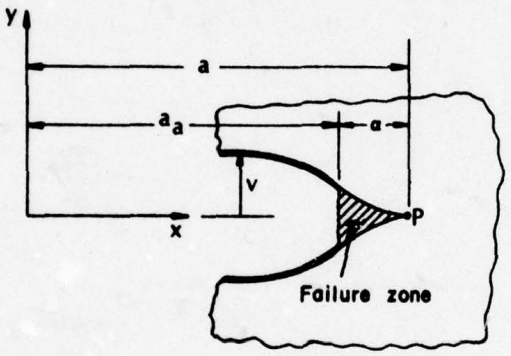

Figure 1. Idealized Crack Tip Neighborhood*

system in Fig. 1 is stationary, with the y-axis located at any convenient position within the continuum; y = 0 defines the local crack surface, and the z-axis is perpendicular to the x-y plane. We assume this surface is locally flat but do not restrict its shape far from the crack tip relative to the scale of the failure zone, α. It is further supposed that the radius of curvature of the crack edge or tip is large relative to this scale. The shape of the crack edge is otherwise unrestricted, so that it may be an "internal", "through", or "surface" crack.

The region between $x = a_a$ and $x = a$ in Fig. 1 is called the "failure zone" in [3]. No constitutive assumption is made for this material. Instead, we simply assume that the disintegrating material exerts a normal load per unit area, σ_f, on the surrounding continuum, where this continuum is taken to be linearly viscoelastic; σ_f is called the "failure" stress distribution. The failure process could therefore be quite arbitrary without invalidating the results of our theory. Indeed, the material in the failure zone need not even satisfy a continuum hypothesis. The layer of damaged material on the crack faces ($x < a_a$) is supposed to be so small that its effects on the motion of

*Reprinted by permission, from R. A. Schapery, "A theory of crack initiation and growth in viscoelastic media. I. Theoretical development", International Journal of Fracture, Vol. II, Feb. 1975, pp. 141–159, copyrighted by Noordhoff International Publishing.

the continuum is negligible.

It should be noted that different names are used by various authors for the thin zone of material which we have called "failure zone". Plastic zone, process zone, and damage zone are commonly used labels. Also, σ_f is often called the "cohesive stress." We prefer to use the word failure in this connection because the material in this zone usually is much thicker than the interatomic spacing, it may contain many cohesive and adhesive microcracks when in a composite material, and of course it is ruptured during the passage of a crack tip [3]. Also, in composites and other materials there may be a much larger zone of damage (e.g., microcracks or plastic deformation) outside of this thin layer; both of these zones are taken into account in the nonlinear theory in §6.

We assume further that the neighborhood of the crack tip P in Fig. 1 is in a state of plane strain. This condition is met provided that (i) the distance α is small compared to the distance β to the nearest geometric feature; (ii) α is small compared to the radius of curvature of the crack edge at P; and (iii) the value of σ_z away from P can be neglected in comparison to σ_y near P (cf. Fig. 2). Just how small α must be depends on the degree of nonhomogeneity [6].

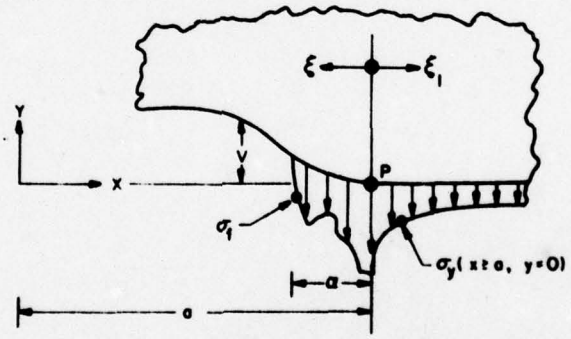

Figure 2. Normal Stress Distribution Along Crack Plane*

The stresses and displacements due to the action of σ_f alone may be taken from [3] if the viscoelastic material in the crack tip neighborhood is homogeneous and isotropic; the superscript f is used to denote σ_f-induced quantities. The normal stress ahead of the crack tip, $\xi_1 > 0$, is the same for elastic and viscoelastic media in this case, and is given by

$$\sigma_y^f = -\frac{1}{\pi\sqrt{\xi_1}} \int_0^a \frac{\sqrt{\xi}\ \sigma_f(\xi)}{\xi + \xi_1}\, d\xi \ , \qquad (8)$$

*Reprinted by permission, from R. A. Schapery, "A theory of crack initiation and growth in viscoelastic media. I. Theoretical development", International Journal of Fracture, Vol. 11, Feb. 1975, pp. 141–159, copyrighted by Noordhoff International Publishing.

where, with reference to Fig. 2,

$$\xi_1 \equiv x - a, \quad \xi \equiv a - x \quad . \tag{9}$$

The viscoelastic normal displacement of the upper crack face relative to the fixed plane $y = 0$ is, for $t \geq t_1$,

$$v^f = -\frac{1}{2\pi} \int_{t_1}^{t} C_v(t - \tau) \frac{\partial}{\partial \tau} \Sigma_f \, d\tau \quad , \tag{10}$$

where

$$\Sigma_f \equiv \int_0^a \sigma_f(\xi') \ln \left| \frac{\sqrt{\xi'} + \sqrt{\xi}}{\sqrt{\xi'} - \sqrt{\xi}} \right| d\xi' \quad , \tag{11}$$

in which C_v is the inverse Laplace transform of the function $\bar{C}_v$ found from

$$\tilde{C}_v = \frac{4(1 - \tilde{\nu}^2)}{\tilde{E}} \tag{12}$$

$\tilde{E}$ and $\tilde{\nu}$ are, respectively, the Carson transformed relaxation modulus and Poisson's ratio obtained from a uniaxial constant strain test. The time t_1 is the time at which the crack tip first reaches the point at x, and ξ is as defined in Eq. (9) with $a = a(t)$ replaced by $a(\tau)$.

The crack tip stress and displacement due to σ_f, Eqs. (8) and (10), may be considered as approximations for a material with temperature and moisture gradients if spatial variations of viscoelastic properties are small in the region affected noticeably by σ_f. Local inertia effects due to σ_f have been neglected; this simplification does not necessarily preclude the use of these results in the presence of large-scale dynamic effects, but it does limit our results to crack speeds which are small compared to characteristic wave speeds for the continuum.

By replacing the creep compliance $C_v(t)$ with another suitably defined function, the results in this section will apply to cracks in orthotropic media and to cracks between different isotropic or orthotropic materials (i.e. adhesive cracks)[11]. However, there are certain conditions which must be met; the local crack surfaces must be parallel to a principal plane of orthotropy and, in the case of adhesive cracks, the two different media must be incompressible.

The stress and displacement distributions due to σ_f, Eqs. (8) and (10), are to be added to those due to the unloading of the crack faces during propagation; these latter solutions are derived by using the procedure

described in §2 for the case $\sigma_f = 0$. It is not necessary to superpose the solution for the body without cracks; the associated crack opening displacement is zero and therefore this solution does not contribute to the energy criterion of failure used in §4.

Now, assume $\sigma_f = 0$ and that the normal stress σ_y^o, say, along the crack plane is independent of viscoelastic properties; in the neighborhood of the crack tip σ_y^o becomes [3],

$$\sigma_y^o = \frac{K_I}{\sqrt{2\pi\xi_1}}, \quad \xi_1 > o \tag{13}$$

where K_I is the stress intensity factor; this result is identical to that for an elastic material. The corresponding displacement is

$$v^o = \frac{1}{\sqrt{2\pi}} \int_{t_1}^{t} C_v(t-\tau) \frac{\partial(K_I\sqrt{\xi})}{\partial\tau} d\tau, \quad t > t_1 \tag{14}$$

The stress obtained by adding Eqs. (8) and (13) is bounded at the crack tip, $\xi_1 = 0$, if

$$K_I = \sqrt{\frac{2}{\pi}} \int_o^a \frac{\sigma_f}{\sqrt{\xi}} d\xi \tag{15}$$

Define

$$f_o = \sigma_f/\sigma_o \quad , \qquad \eta \equiv \xi/a \tag{16}$$

Then, Eq. (15) may be rewritten as

$$a = \frac{\pi}{2}\left[\frac{K_I}{\sigma_o I_o}\right]^2 \tag{17}$$

where σ_o is the failure stress at $\xi \equiv o$ and

$$I_o \equiv \int_o^1 \frac{f_o}{\sqrt{\eta}} d\eta \tag{18}$$

If f_o is a function of only η (i.e., if the shape of the stress distribution σ_f is constant) then I_o is a constant. If in addition σ_o is independent of a, then Eq. (17) provides an explicit result for the length of the failure zone. Use of Eq. (16) in the prediction of a for more general cases is discussed in [5].

Let us now add Eqs. (8) and (13) for stress, Eqs. (10) and (14) for displacement, and eliminate K_I by means of Eq. (15). There results,

$$\sigma_y = \frac{\sqrt{\xi_1}}{\pi} \int_0^a \frac{\sigma_f}{\sqrt{\xi}\ (\xi + \xi_1)}\, d\xi, \quad \xi_1 \geq 0 \tag{19}$$

$$v = \frac{1}{2\pi} \int_{t_1}^{t} C_v(t-\tau) \frac{\partial}{\partial \tau} \sum d\tau\ , \quad t > t_1 \tag{20}$$

where

$$\sum = \sum(x,\tau) \equiv -\sum_f + 2\int_0^a \sigma_f(\xi') \sqrt{\frac{\xi}{\xi'}}\, d\xi'\ . \tag{21}$$

Let us now consider the case in which σ_y is a function of viscoelastic properties. The procedure outlined in §2 leads to an incorrect traction distribution on the crack faces if the given σ_f is used in the bounded elastic solution. However, we may instead use another failure stress distribution σ_f^e, say, in the elastic analysis. This function is selected so as to produce the proper traction condition on the viscoelastic crack faces, which leads to an integral equation for σ_f^e. The solution of this problem is lengthy, and since it is detailed in [6] it will not be given here. This analysis results in a rather simple approximate equation for predicting crack speed, as discussed in the next section.

4. PREDICTION OF CRACK GROWTH RATE. Define Γ such that $2\Gamma dA_f$ is the mechanical energy required to fail an element of material of infinitesimal area dA_f; Γ, which is called the <u>fracture energy</u>, does not include the energy of the element at the starting point for failure, $\xi = 0$. Thus, at some fixed material point, x,

$$\Gamma = \int_0^{v_m} \sigma_f dv \tag{22}$$

where v_m is one-half the crack opening displacement at the point of rupture, $\xi = a$ (cf. Fig. 1). The governing equation for crack growth is derived by substituting into Eq. (22) the displacement v, such as that in Eq. (20) or that in [6, Eq. (39)] for a more general class of problems. In the former situation we assume that crack speed, $\dot{a}$, is essentially constant during the time $a/\dot{a}$, which is the time interval in which the crack tip propagates an amount a; it is further assumed that σ_f and a are essentially timewise constant during the same period. For the latter case, which is studied in [6], this time interval may have to be somewhat larger, possibly as large as $10\ a/\dot{a}$. Additional simplification of the analysis is achieved by accounting

for the fact that the second derivative of the viscoelastic creep compliances and their logarithms with respect to the logarithm of time is typically quite small. There results, finally [6],

$$\Gamma \approx \frac{1}{8} C_v(t_\alpha) \hat{K}^2 , \tag{23}$$

where

$$t_\alpha \equiv \alpha/3\dot{a} . \tag{24}$$

Also,

$$\hat{K} \equiv \left[K_I^e(t_\alpha) K_I^e(3t_\alpha)\right]^{\frac{1}{2}} \tag{25}$$

is the geometric mean of so-called quasi-elastic stress intensity factors; the quantity $K_I^e(\cdot)$ is the stress intensity factor due to crack growth (as defined in §2) in a material which is elastic, except in place of elastic compliances there are viscoelastic creep compliances that are evaluated at the "local" times t_α and $3t_\alpha$. The length of the failure zone is

$$\alpha = \frac{\pi}{2}\left[\frac{K_I^e(3t_\alpha)}{\sigma_o I_o}\right]^2 . \tag{26}$$

When stresses are independent of the viscoelastic creep properties, Eqs. (23) and (26) reduce to those derived in [4]. Thus,

$$\Gamma \approx \frac{1}{8} C_v(t_\alpha) K_I^2 \tag{27}$$

where α is that in Eq. (17).

The quantities Γ and $\sigma_o I_o$ are defined by the behavior of the material in the failure zone, and as such are fracture properties. In general they are functions of crack speed, although they appear to be constant for the polymeric material studied in [5]. Given these properties and the viscoelastic creep compliances, Eqs. (23) - (26) may be solved to predict the instantaneous crack speed. Experimental determination of the fracture properties is discussed in [5].

5. FRACTURE INITIATION IN LINEAR MEDIA. The approach used in [4] to predicting initiation of crack growth consists of applying Eq. (22) to the initial crack tip, which is located at $x = 0$; the initial length of the failure zone is assumed to be zero. The instantaneous displacement v at $x = 0$ and the failure zone length are calculated from Eqs. (20) and (17), respectively. For the case in which σ_f is constant in space and time and

the stress-intensity factor does not decrease in time, we find

$$a = \frac{\pi K_I^2}{8\sigma_o^2} \tag{28}$$

and then obtain an implicit equation for "initiation time", t_i:

$$\Gamma = \frac{1}{8} K_I^2(t_i)\, C_v^{(2)}(t_i), \tag{29}$$

where $C_v^{(2)}$ is a so-called secant compliance,

$$C_v^{(2)}(t) \equiv \frac{1}{K_I^2} \int_{o^-}^{t} C_v(t-\tau) \frac{dK_I^2}{d\tau}\, d\tau . \tag{30}$$

The quantity t_i is the time at which the mechanical work done on the failure zone at $x = 0$ is equal to the fracture energy Γ. Inasmuch as the deformation history of the failure zone in the initiation problem is different from that discussed previously for crack growth rate, the fracture energies in the two cases are not necessarily the same.

These results were derived in [4] for the case in which stresses are independent of viscoelastic properties. However, they also apply to the more general class of problems covered in [6] as long as the conditions stated in §3 are met and the stress intensity factor is interpreted as that due only to growth of a crack by the amount a. For, if the material in the neighborhood of the tip is homogeneous, the stresses due to tractions on the crack faces in the interval $o \le x < a$ are independent of viscoelastic properties; of course, these surface tractions may themselves depend on viscoelastic properties since they are for a globally nonhomogeneous body without cracks.

The secant compliance, Eq. (30), reduces to the creep compliance, $C_v(t)$, when K_I is constant during the interval $o < t \le t_i$. In this case

$$\Gamma = \frac{1}{8} K_I^2(t_i) C_v(t_i) \tag{31}$$

There are many other cases in which Eq. (31) is a good approximation; viz., $C_v^{(2)} \doteq C_v$ if C_v is a sufficiently weak function of time or if the second derivative of C_v and K_I^2 with respect to the logarithm of time is small [8].

Recall that σ_f was assumed to be spacewise and timewise constant in obtaining Eqs. (28) and (30). Whether or not this is a reasonably good assumption depends on the particular material of interest. If, instead of assuming σ_f is timewise constant, we assume a is constant, then it is found Eq. (29) must be replaced by

$$\Gamma = \frac{1}{8} K_I(t_1) \int_{0^-}^{t_1} C_v(t-\tau) \frac{dK_I}{d\tau} d\tau \tag{32}$$

Equation (28) still applies, but σ_o will vary with time in order to satisfy this equation. The assumption of a constant value for a may be a valid approximation in some cases, such as for composite materials in which the size of the damage zone is closely related to the scale of the phases. However, very little is known at this time about the time-dependence of the failure zone size in real materials.

6. FRACTURE INITIATION IN NONLINEAR MEDIA. In this section we shall describe a tentative method for characterizing and predicting the initiation of crack growth in nonlinear viscoelastic materials. The zone of intense damage and rupture is still assumed to be the thin strip of length a in Fig. 1. However, outside of this zone the material may be nonlinear and suffer damage. This approach is motivated, in part, by the similarity of the linear viscoelastic result for fracture initiation (cf. Eq. 29) and that for an elastic material (C_v = constant), as well as the success of the J-integral criterion for elastic-plastic and nonlinear elastic media [e.g. 12-14].

In order to illustrate the method, consider the viscoelastic test specimen in Fig. 3 which contains an initial crack of length a. The applied force is given as $F = Rt^n$, where R and n are positive constants; we suppose that several different specimens are tested using different values of R and a, but with the same value of n. Figure 4 shows displacement-time curves for a viscoelastic material prior to crack propagation. From these results the

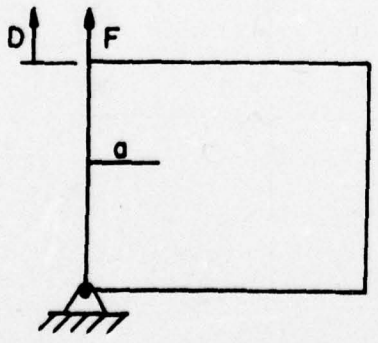

Figure 3. Plate Specimen for Fracture Test

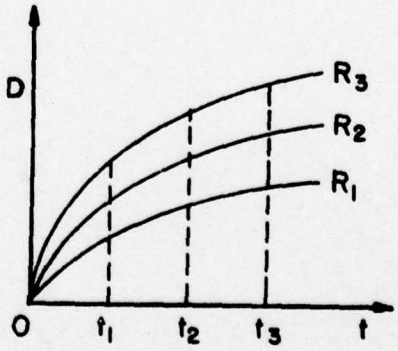

Figure 4. Corner Displacement Response for One Initial Crack Length

isochronal force-displacement curves in Fig. 5 can be constructed.

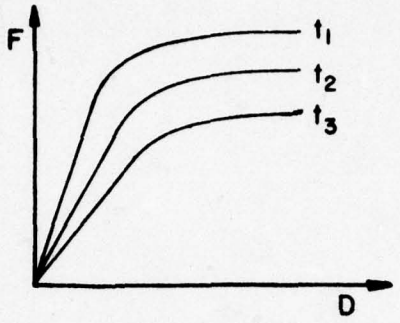

Figure 5. Force Displacement Curves Constructed from Figure 4.

If the material were elastic or elastic-plastic there would be no dependence on time, and it would be possible to use such data from specimens with different initial crack lengths to establish a fracture initiation criterion in terms of the J-integral. We shall show that there are some nonlinear viscoelastic materials for which the isochronal data in Fig. 5 may be employed in the manner described in [14] for time-independent materials.

It is sufficient to show that there exists a so-called stress-working density $W = W(\epsilon_{ij}, x_i, t)$ with the property that

$$\sigma_{ij} = \frac{\partial W}{\partial \epsilon_{ij}} . \tag{33}$$

If W is independent of x_i the J-integral will be path-independent for two-dimensional deformations [12], but this independence is not needed for the fracture criterion. Let us start with the following stress-strain equations for an isotropic material,

$$\epsilon'_{ij} = \frac{1}{2} \int_0^t J(\psi - \psi') \frac{\partial(\sigma'_{ij} g)}{\partial \tau} d\tau , \tag{34}$$

$$\vartheta = \frac{B}{3} \theta , \tag{35}$$

where ψ is "reduced time",

$$\psi = \psi(t) \equiv \int_0^t dt'/a_D , \quad \psi' \equiv \psi(\tau) , \tag{36}$$

and ϵ'_{ij} and σ'_{ij} are the deviatoric strains and stresses,

$$\epsilon'_{ij} \equiv \epsilon_{ij} - \frac{1}{3} \delta_{ij} \vartheta , \quad \sigma'_{ij} \equiv \sigma_{ij} - \frac{1}{3} \delta_{ij} \theta . \tag{37}$$

Also, δ_{ij} is the Kronecker delta and

$$\vartheta \equiv \varepsilon_{ii} , \quad \theta \equiv \sigma_{ii} \tag{38}$$

are the first strain and stress invariants, respectively. $J(\psi)$ is the linear viscoelastic creep compliance under shear stress and B is the compliance under hydrostatic loading. Nonlinearity is due to the stress-dependence of the material functions g and a_D. In view of the data on plastics in [15] and the microcracking model for composites in [16], it is assumed that g and a_D are functions of the so-called effective stress

$$\sigma_e \equiv (1.5\,\sigma'_{ij}\,\sigma'_{ij})^{1/2} \tag{39}$$

and the Lebesgue norm of effective stress,

$$\|\sigma_e\| \equiv \left[\int_0^t \sigma_e^{\,q}\, dt'\right]^{1/q} . \tag{40}$$

These constitutive equations are special versions of more general results derived from nonequilibrium thermodynamics; by means of $\|\sigma_e\|$ they incorporate microcracking effects [16]. The equations are quite realistic in that they predict behavior which is observed for various viscoelastic materials. Other, more general relations could be employed to generalize the J-integral criterion, but we shall limit our discussion to the above ones.

As in establishing the deformation theory of plasticity, proportional stressing is assumed,

$$\sigma_{ij} = h\, s_{ij} , \tag{41}$$

where s_{ij} is independent of time. Also, let us assume that $h = ct^m$, where $m = m(x_i)$ is a positive exponent and $c = c(x_i)$.

It is now possible, with some amount of work, to show that a stress-working density exists. Therefore, at any fixed time prior to fracture initiation [12]

$$2\int_0^a \sigma_f \frac{\partial v}{\partial \xi}\, d\xi = -\frac{1}{H}\frac{\partial A}{\partial a} , \tag{42}$$

where H is specimen thickness, and $A = A(D,a,t)$ is the area under any one curve in Fig. 6. The left-hand side of Eq. (42) is the J-integral. Thus, by observing when fracture initiates, the experimental procedure illustrated above may be used to determine critical J-values, J_c; for viscoelastic

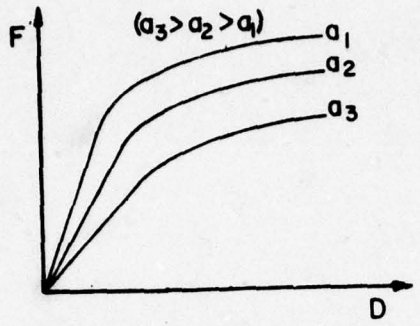

Figure 6. Force-Displacement Curves for Various Initial Crack Lengths at One Time

materials they will depend on the loading exponent n and on the time.

It is important to observe that if $\sigma_f = \sigma_f(v)$,

$$J = 2 \int_0^a \sigma_f \, dv \quad , \tag{43}$$

which is equal to 2Γ. Thus, for this case J is equal to the mechanical work input to an element of material in the failure zone (per unit area) at the instant of rupture. When $a_D = g = 1$, Eq. (34) reduces to that for a linear viscoelastic material, and it can be shown that fracture initiation Eq. (32) is recovered from Eq. (42) if Poisson's ratio is one-half. However, when one accounts for the small curvature property possessed by viscoelastic creep compliances, as noted in §5, it is found that this restriction on Poisson's ratio can be removed without introducing serious error in many cases. Also, recall from the discussion in §5 that Eqs. (29) and (32) often yield approximately the same fracture initiation time.

7. CONCLUDING REMARKS. The intent of the discussion on nonlinear behavior was to suggest a procedure for applying the J-integral to fracture initiation in viscoelastic materials, and to provide a theoretical motivation for this extension. However, much experimental and theoretical work is needed before one can have confidence in the technique. Prediction of crack speed in nonlinear viscoelastic materials is a relatively untouched area, except for materials in which viscoelastic effects are limited to the neighborhood of the crack tip [17].

The linear viscoelastic analysis described herein is limited to slow crack growth and to materials for which the neighborhood of the crack tip is homogeneous. A few studies exist in which these restrictions are not imposed, but they are for very special cases. For example, it was noted that some

explicit results exist for slow crack propagation between two different incompressible materials.

REFERENCES

1. W. G. Knauss, "The Mechanics of Polymer Fracture," Applied Mechanics Reviews, 26, 1973, pp. 1-17.

2. W. G. Knauss, "Fracture of Solids Possessing Deformation Rate Sensitive Material Properties, A.S.M.E. - AMD No. 19, 1976, pp. 69-97.

3. R. A. Schapery, "A Theory of Crack Initiation and Growth in Viscoelastic Media. I. Theoretical Development." Int. Journal of Fracture, Vol. 11, Feb. 1975, pp. 141-159.

4. R. A. Schapery, "A Theory of Crack Initiation and Growth in Viscoelastic Media, II. Approximate Methods of Analysis." Int. Journal of Fracture, Vol. 11, No. 3, Jun. 1975, pp. 369-388.

5. R. A. Schapery, "A Theory of Crack Initiation and Growth in Viscoelastic Media, III. Analysis of Continuous Growth." Int. Journal of Fracture, Vol. 11, No. 4, Aug. 1975, pp. 549-562.

6. R. A. Schapery, "A Method for Predicting Crack Growth in Nonhomogeneous Viscoelastic Media." Int. Journal of Fracture, in press.

7. R. J. Nuismer, "On the Governing Equation for Quasi-Static Crack Growth in Linearly Viscoelastic Materials," Journal of Applied Mechanics, Vol. 41, Sept. 1970, pp. 631-634.

8. R. A. Schapery, "Viscoelastic Behavior and Analysis of Composite Materials." Mechanics of Composite Materials, Vol. 2, G. P. Sendeckyj, ed., Academic Press, New York, 1974, pp. 85-168.

9. G. I. Barenblatt, "The Mathematical Theory of Equilibrium Cracks in Brittle Fracture," Advances in Applied Mechanics, Vol. 7, Academic Press, 1962, pp. 55-129.

10. D. S. Dugdale, "Yielding of Steel Sheets Containing Slits." Journal of Mechanics and Physics of Solids, 8, 1960, pp. 100-104.

11. G. S. Brockway, and R. A. Schapery, "Some Viscoelastic Crack Growth Relations for Orthotropic and Prestrained Media," Engineering Fracture Mechanics, 1978 in press.

12. J. R. Rice, "Mathematical Analysis in the Mechanics of Fracture." Fracture: An Advanced Treatise, ed. H. Liebowitz, Vol. 2, Academic Press, 1968, pp. 191-311.

13. J. R. Rice, "Elastic-Plastic Fracture Mechanics." A.S.M.E.-AMD, No. 19, 1976, pp. 23-53.

14. S. T. Rolfe, and J. M. Barsom, Fracture and Fatigue Control in Structures. Prentice-Hall, Englewood Cliffs, N. J., 1977.

15. R. A. Schapery, "On the Characterization of Nonlinear Viscoelastic Materials." Polymer Engineering and Science, Vol. 9, No. 4, 1969, pp.295-310.

16. R. A. Schapery, "A Non-linear Constitutive Theory for Particulate Composites Based on Viscoelastic Fracture Mechanics." Proceedings of JANNAF Structures & Mechanical Behavior Working Group, 12th. Meeting, Jan. 1974, CPIA Publication No. 253.

17. E. H. Andrews, Fracture in Polymers. Oliver & Boyd, London, 1968.

TEXAS A&M UNIVERSITY. College Station, Texas. 77843

AN INCREMENTAL FORM OF THE SINGLE-INTEGRAL NONLINEAR VISCOELASTIC THEORY FOR ELASTIC-PLASTIC-CREEP FINITE ELEMENT ANALYSIS *

Duane R. Sanders and Walter E. Haisler

A single-integral nonlinear viscoelastic theory is cast into a generalized incremental form for use in predicting creep response of materials. The incremental creep constitutive model is tailored for use in an incremental finite element program wherein the equations of motion are integrated numerically step-by-step. Recursive relations for material memory parameters are developed which allow the retention of all past history prior to the current time step and require integration over the current time step only. The creep model parameters required in the theory are obtainable from a standard creep and recovery test. The incorporation of the model within an incremental elastic-plastic finite element formulation is outlined.

*To be presented at the 3rd ASME National PVP Congress, San Francisco, California, June 25-29, 1979.

INTRODUCTION

In a majority of the finite element programs in use today for analyzing metal components, the traditional approach of separating the total strain into elastic, plastic, and creep components is used [1,2,3]. The most widely accepted means of predicting the creep strain in this context is the phenomenological creep theory [4,5]. As an alternative to this approach, a single integral nonlinear viscoelastic theory derived by Schapery from thermodynamic considerations in reference [6] is presented. It has a form similar to the Boltzman integral used in linear viscoelasticity, but the physical time is replaced by a so called reduced time; several other material functions enter into the theory. This representation of the creep strain component should provide within the same constitutive theory the capability of analyzing both polymeric and metallic materials.

Two constitutive theories similar in appearance to the single integral theory of Schapery's are given by Rashid [7] and Valanis [8]. Rashid uses a modified superposition principle with the compliance, which is a function of stress and time, transformed such that it is a function of a single parameter called reduced time. Valanis's theory [8] is derived from thermodynamic considerations with the resulting single integral equation appearing in terms of the strain history instead of the stress history as in reference [6]. This theory is very similar to Schapery's theory [9]wherein he employed strain as the independent variable instead of stress. The functional difference in references [7] and [9] being their respective definitions of reduced time. The other material functions entering into reference [6,9] are not present in Rashid's or Valanis's theory.

Application of the single integral theory has been made by Valanis [10,11] for the viscoplastic response of several metals. It has also been shown to give accurate results for several polymeric composites in creep, creep-recovery and

multistep input tests on uniaxial specimens [12,13].

A potential advantage of the single integral is that it easily handles multistep input histories including stress reversal and creep-recovery. This is not true of the phenomenological theory of creep for metals based on strain hardening which must resort to special procedures to handle the stress reversal situation as outlined in [14]. These procedures have in some cases resulted in rather poor results as indicated in reference [14]. Futher, the phenomenological theory has no predictive capability for creep-recovery input stress history. Thus, the single integral constitutive theory may offer additonal predictive capabilities over the phenomenological theory of creep.

To put the single integral theory in a form suitable for use with a incremenatal finite element program wherein the equations of motion are integrated numerically step-by-step, the time derivative of the single integral equation is taken. In this form, the creep strain increment can be determined for the current time interval based on the creep strain rate at the beginning of the step. Computationally, the relationships derived for the rate form of the single integral equation are particularly appealing since recursive relationships are developed which allow for the retention of all past history prior to the current time step and require integration over the current time step only.

The incorporation of the model within an incremental elastic-plastic finite element formulation is outlined. The time-independent incremental plasticity relations with a Von Mises yield criterion and a kinematic hardening rule are employed to describe the plastic component of strain.

A graphical procedure for determining the material functions from either creep data or creep equations is presented. It is shown that this procedure is only applicable to materials whose elastic strain on

unloading is equal to that on loading.

Numerical comparison of the single integral theory to that of phenmenological theory of creep are given for creep, creep recovery, multistep and reverse loading histories for a type 304 stainless steel. The numerical results were obtained using the computer program NONVIS which implements the integration procedure developed below for the single integral creep equation.

It is suggested that the rate from of the single-integral equations appearing in [7,8,9] could be integrated by employing a procedure similar to that given in this paper for the single integral constitutive theory of references [6], provided the kernel function is a combination of constants, linear , and exponential terms as will be outlined below.

RATE FORM OF THE SINGLE INTEGRAL EQUATION

The single integral nonlinear viscoelastic constitutive equation derived in reference [6] for an initially isotropic material is written for isothermal conditons, incompressible creep strains, and infinitesimal strains as,

$$\epsilon_{ab} = J(0)\,\sigma_{ab} + \frac{\partial \hat{\sigma}_{cd}}{\partial \sigma_{ab}} \int_{-\infty}^{\psi'} \Delta J(\psi - \psi') \frac{dG_{cd}}{d\psi'} d\psi' \tag{1}$$

$$\psi = \int_0^t \frac{a_G}{a_D}\, dt \quad , \tag{2a}$$

$$G_{cd} = \frac{\hat{\sigma}_{cd}}{a_G} \quad , \tag{2b}$$

$$\Delta J(\psi) = \sum_r A^{(r)} \left(1 - e^{-\psi/\tau_r}\right) + \sum_{r'} B^{(r')} \psi \quad , \tag{2c}$$

and $A^{(r)}$, $B^{(r')}$, and τ_r are constants. The functions a_G, a_D and $\hat{\sigma}_{cd}$ are material properties and are in general function of the three stress invariants. ϵ_{ab} are the engineering strain components and σ_{cd} are the components of the Cauchy stress

tensor. The function $\Delta J(\psi)$ is the transient component of the so called linear viscoelastic shear creep compliance. The first term in equation (1) represents the instantaneous elastic response of the material.

To cast equation (2) into a form suitable for use in a incremental finite element analysis the time derivative of equation (1) is taken, and equation (2a) is used to obtain,

$$\dot{\epsilon}_{ab} = J(0)\,\dot{\sigma}_{ab} + \frac{\partial\left(\frac{\partial \hat{\sigma}_{cd}}{\partial \sigma_{ab}}\right)}{\partial t} \int_{-0}^{t} \Delta J(\psi-\psi') \frac{dG_{cd}}{dt'}\, dt' + \frac{a_D}{a_G}\left(\frac{\partial \hat{\sigma}_{cd}}{\partial \sigma_{ab}}\right)\int_{-0}^{t} \frac{d(\Delta J(\psi-\psi'))}{d\psi} \frac{dG_{cd}}{dt'}\, dt' \quad . \tag{3}$$

Equation (3) is rewritten as,

$$\dot{\epsilon}_{ab} = J(0)\,\dot{\sigma}_{ab} + \frac{\partial\left(\frac{\partial \hat{\sigma}_{cd}}{\partial \sigma_{ab}}\right)}{\partial t} X_{cd} + \frac{a_D}{a_G}\left(\frac{\partial \hat{\sigma}_{cd}}{\partial \sigma_{ab}}\right) Y_{cd} \quad , \tag{4}$$

where,

$$X_{cd} = \int_{-0}^{t} \Delta J(\psi-\psi') \frac{dG_{cd}}{dt'}\, dt' \quad , \tag{5}$$

$$Y_{cd} = \int_{-0}^{t} \Delta J'(\psi-\psi') \frac{dG_{cd}}{dt'}\, dt' \quad , \tag{6}$$

and

$$\Delta J'(\psi-\psi') = \frac{d\,\Delta J(\psi-\psi')}{d\psi} \quad . \tag{7}$$

A time marching procedure for evaluating X_{cd} and Y_{cd} is formulated below.

Evaluation of X_{cd} and Y_{cd}

The evaluation of the two integrals X_{cd} and Y_{cd} given by equations (5) and (6) are put in a form suitable for use in an incremental finite element analysis. Once the value of the integrals are known, the creep strain rate is evaluated from the sum of the second and third terms of equation (4) as:

$$\dot{\epsilon}^c_{ab} = \frac{\partial\left(\frac{\partial \hat{\sigma}_{cd}}{\partial \sigma_{ab}}\right)}{\partial t} X_{cd} + \frac{a_D}{a_G}\left(\frac{\partial \hat{\sigma}_{cd}}{\partial \sigma_{ab}}\right) Y_{cd} \quad . \tag{8}$$

Two important features in the evaluation X_{cd} and Y_{cd} are the determination of two recursive formula's whose values are known from the previous time step and the evaluation of the two integrals which require integration only over the current time step. The formulation presented is similar to the integration technique employed by Zak and Hermann in reference [15,16] for a thermorheological simple material due to a variable temperature field.

Subdivide the time from 0 to t_n into N subintervals such that $t_0 = 0, t_1 = t_0 + \Delta t_1, \ldots, t_N = t_{N-1} + \Delta t = t$. For $\sigma_{cd}(\underline{x}, t_N)$ and $\epsilon_{cd}(\underline{x}, t_N)$ write σ_{cd_N} and ϵ_{cd_N} and assume that $\sigma_{cd_N}(0, t_N) = 0$ and $\epsilon_{cd_N}(0, t_N) = 0$. Then X_{cd} and Y_{cd} can be written as

$$X_{cd_N} = \int_0^{t_N} \Delta J\left(\psi_N - \psi'\right) \frac{dG_{cd}}{dt'}\, dt' \tag{9}$$

and

$$Y_{cd_N} = \int_0^{t_N} \Delta J'\left(\psi_N - \psi'\right) \frac{dG_{cd}}{dt'}\, dt' \quad . \tag{10}$$

Evaluation of X_{cd_N}

Using equation (2c) in equation (9), one obtains

$$X_{cd_N} = \int_0^{t_N} \sum_r A^{(r)} \frac{dG_{cd}}{dt'} dt' - \int_0^{t_N} \sum_r A^{(r)} e^{-(\psi_N - \psi')/\tau_r} \frac{dG_{cd}}{dt'} dt' + \int_0^{t_N} \sum_{r'} B^{(r')} (\psi_N - \psi') \frac{dG_{cd}}{dt'} dt' \quad . \tag{11}$$

By evaluating the first integral in equation (11), expanding the second and third as the sum of two integrals and approximating the time rate of change of G_{cd} as

$$\frac{dG_{cd}}{dt} = \frac{G_{cd_N} - G_{cd_{N-1}}}{\Delta t_N} \tag{12}$$

within the time interval, $t_{N-1} < t < t_N$, equation (11) can be written as

$$X_{cd_N} = \sum_r A^{(r)} G_{cd_N} - \left[\int_0^{t_{N-1}} \sum_r A^{(r)} e^{-(\psi_N - \psi')/\tau_r} \frac{dG_{cd}}{dt'} dt' + \left(\frac{G_{cd_N} - G_{cd_{N-1}}}{\Delta t_N} \right) \int_{t_{N-1}}^{t_N} \sum_r A^{(r)} e^{-(\psi_N - \psi')/\tau_r} \frac{dG_{cd}}{dt'} dt' \right] + \left[\int_0^{t_{N-1}} \sum_{r'} B^{(r')} (\psi_N - \psi') \frac{dG_{cd}}{dt'} dt' + \frac{G_{cd_N} - G_{cd_{N-1}}}{\Delta t_N} \int_{t_{N-1}}^{t_N} \sum_{r'} B^{(r')} (\psi_N - \psi') dt' \right] . \tag{13}$$

Define the following quanities,

$$\mu 1_N = \sum_r A^{(r)} J1_N^{(r)} \quad , \tag{14}$$

$$\mu 2_N = \sum_{r'} B^{(r')} J2_N^{(r')} \quad , \tag{15}$$

$$\mu_N = \mu 1_N + \mu 2_N \quad , \tag{16}$$

where,

$$J1_N^{(r)} = \frac{1}{\Delta t_N} \int_{t_{N-1}}^{t_N} e^{-(\psi_N - \psi')/\tau_r} dt' \tag{17}$$

and

$$J2_N^{(r')} = \frac{1}{\Delta t_N} \int_{t_{N-1}}^{t_N} (\psi_N - \psi')\, dt' . \tag{18}$$

Now, rewrite equation (13) using equation (16), as,

$$X_{cd_N} = \sum_r A^{(r)} G_{cd_N} - G_{cd_N}(\mu_N) + L_{cd_N} \tag{19}$$

Where,

$$L_{cd_N} = -G_{cd_{N-1}}(\mu_N) + \psi 1_{cd_N} + \psi 2_N , \tag{20}$$

and

$$\psi 1_{cd_N} = \sum_r A^{(r)} C1_{cd_N}^{(r)} , \tag{21}$$

$$\psi 2_{cd_N} = \sum_{r'} B^{(r')} C2_{cd_N}^{(r')} , \tag{22}$$

$$C1_{cd_N}^{(r)} = \int_0^{t_{N-1}} e^{-(\psi_N - \psi')/\tau_r} \frac{dG_{cd}}{dt'}\, dt' , \tag{23}$$

$$C2_{cd_N}^{(r')} = \int_0^{t_{N-1}} (\psi_N - \psi') \frac{dG_{cd}}{dt'}\, dt' . \tag{24}$$

Recursive relationships for equations (23) and (24) are developed in Appendix I and are given below as:

$$C1_{cd_N}^{(r)} = e^{-\frac{1}{\tau_r}\Delta\psi_N} \left\{ C1_{cd_{N-1}}^{(r)} + \left(G_{cd_{N-1}} + G_{cd_{N-2}}\right) J1_{N-1}^{(r)} \right\} \tag{I.6}$$

and

$$C2_{cd_N}^{(r')} = \Delta\psi_N\, G_{cd_{N-1}} + C2_{cd_{N-1}}^{(r')} + \left(G_{cd_{N-1}} + G_{cd_{N-2}}\right) J2_{N-1}^{(r')} \tag{I.7}$$

where $C1^{(r)}_{cd_{N-1}}$, $C2^{(r')}_{cd_{N-1}}$, $J1^{(r)}_{N-1}$ and $J2^{(r')}_{N-1}$ are known from the previous time step. Thus, equation (19) can be evaluated by integrating $J1^{(r)}_{cd_N}$ and $J2^{(r')}_{cd_{N-1}}$ equations (17) and (18) respectively, over the current time step only. All history effects are contained in L_{cd_N}, equation (20). In Appendix I, Equations (17) and (18) are set up for numerical integration using Gaussian Quadrature. The resulting equation for equation (17) is:

$$J1^{(r)}_N = \frac{\tau_r}{\Delta t_N}\left(1 - e^{-\Delta\psi_N/\tau_r}\right) + J^{*(r)}_N \qquad (I.15)$$

where,

$$J^{*(r)}_N = \frac{1}{2}\int_{-1}^{1}\left[e^{-(\psi_N-\psi')/\tau_r} - e^{-(1-\tau)\frac{\Delta\psi_N}{2}/\tau_r}\right]d\tau \qquad (I.16)$$

and

$$\Delta\psi_N = \psi_N - \psi_{N-1} .$$

The resulting equation for equation (18) is:

$$J2^{(r)}_N = \psi_N - J2^{*(r)}_N \qquad (I.20)$$

where,

$$J2^{*(r)}_N = \frac{1}{4}\int_{-1}^{1}\frac{a_G}{a_D}\left(\tau\,\Delta t_N + t_N + t_{N-1}\right)d\tau \qquad (I.19)$$

Evaluation of the reduced time integral equation (2a) is also presented in Appendix I.

Evaluation of Y_{cd_N}

Following a procedure similar to that used in evaluating X_{cd_n} above, the intergration of Y_{cd_N} is performed. Y_{cd_N} is given by equation (10) as,

$$Y_{cd_N} = \int_0^{t_N} \Delta J'(\psi_N - \psi') \frac{dG_{cd}}{dt'} dt' \tag{10}$$

where,

$$\Delta J'(\psi_N - \psi') = \sum_r \frac{A^{(r)}}{\tau_r} e^{-\psi/\tau_r} + \sum_{r'} B^{(r')} \tag{25}$$

Expanding equation (10) as the sum of two integrals, using equation (25), and approximating the time rate of change of G_{cd} given by equation (12), equation (10) is rewritten as,

$$Y_{cd_N} = \int_0^{t_{N-1}} \left[\sum_r \frac{A^{(r)}}{\tau_r} e^{-(\psi_N - \psi')/\tau_r} + \sum_{r'} B^{(r')} \right] \frac{dG_{cd}}{dt'} dt'$$

$$+ \frac{dG_{cd_N} - dG_{cd_{N-1}}}{\Delta t_N} \int_{t_{N-1}}^{t_N} \left[\sum_r \frac{A^{(r)}}{\tau_r} e^{-(\psi_N - \psi')/\tau_r} + \sum_{r'} B^{(r')} \right] dt' \tag{26}$$

Defining the following quanities,

$$\eta_N = \sum_{r'} B^{(r')} + \sum_r \frac{A^{(r)}}{\tau_r} J1_N^{(r)} , \tag{27}$$

$$K_{cd_N} = - G_{cd_{N-1}} \eta_N + \gamma_{cd_N} , \tag{28}$$

and

$$\gamma_{cd_N} = \sum_r \frac{A^{(r)}}{\tau_r} F_{cd_N}^{(r)} + \sum_{r'} B^{(r')} G_{cd_{N-1}} , \tag{29}$$

where

$$J1_N^{(r)} = \frac{1}{\Delta t_N} \int_{t_{N-1}}^{t_N} e^{-(\psi_N - \psi')/\tau_r} \, dt'$$

$$F_{cd_N}^{(r)} = \int_0^{t_{N-1}} e^{-(\psi_N - \psi')/\tau_r} \frac{dG_{cd}}{dt'} \, dt' \quad . \tag{30}$$

Note that $J1_N^{(r)}$ is the same quantity that appears in the evaluation of X_{cd_N}. Using equation (27) and (28), equation (26) is rewritten as,

$$Y_{cd_N} = G_{cd_N} \eta_N + K_{cd_N} \tag{31}$$

A recursive relationship for equation (31) is developed in Appendix I and is given below as:

$$F_{cd_N}^{(r)} = e^{-\frac{1}{\tau_r} \Delta\psi_N} \left\{ F_{cd_{N-1}}^{(r)} + \left(G_{cd_{N-1}} - G_{cd_{N-2}} \right) J1_{N-1}^{(r)} \right\}$$

where $F_{cd_{N-1}}^{(r)}$ and $J1_{N-1}^{(r)}$ are known from the previous time step. Thus Yc_{d_n}, equation (31), can be evaluated by intergrating $J1_N^{(r)}$, equation (17) over the present time step only. All history effects are represented by K_{cd_N}, equation (28). In Appendix I, equation (17) is set up for numerical integration using Gaussian Quadrature (the results were given above by equations (I.15) and (I.16).

INCREMENTAL EQUATIONS OF EQUILIBRIUM

In this section, an incremental finite element formulation for the isothermal, elastic-plastic-creep-large strain problem is developed. The formulation is suitable for use with any creep constitutive theory which will predict the incremental creep strain component based on the creep strain rate the beginning of the step. Although the creep and plasticity relations are for small strains, the formulation is developed for large strain. One may begin with the equations of equilibrium written in terms of the second Piola-Kirchoff stress:

$$\frac{\partial}{\partial a_j}\left[S_{jk}\left(\delta_{ik} + \frac{\partial u_i}{\partial a_k}\right)\right] + \rho_o F_{oi} = 0 \tag{32}$$

where a_j and u_i are Lagrangian coordinates and displacements, respectively, S_{jk} is the 2nd Piola-Kirchhoff stress tensor, ρ_0 is undeformed density and F_{oi} is the body force per unit undeformed volume per unit mass. Applying the virtual work principle at time t + Δt yields

$$\int_{V_o} S_{ij}^{t+\Delta t}\, \delta E_{ij}^{t+\Delta t}\, dV = \delta R^{t+\Delta t} \tag{33}$$

where

$$\delta R^{t+\Delta t} = \int_S T_i^{t+\Delta t}\, \delta u_i^{t+\Delta t}\, dS + \int_{V_o} \rho_o F_{oi}^{t+\Delta t}\, \delta u_i^{t+\Delta t}\, dV \tag{34}$$

and $\delta E_{ij}^{t+\Delta t}$ is the variation of the Green-Lagrange strains at time t+Δt and $T_i^{t+\Delta t}$ are surface tractions at time t+Δt applied to the deformed surface S. Equation (2) may be put into incremental form by writing

$$S_{ij}^{t+\Delta t} = S_{ij}^{t} + \Delta S_{ij}$$
$$E_{ij}^{t+\Delta t} = E_{ij}^{t} + \Delta E_{ij} \tag{35}$$

where S_{ij}^{t} and E_{ij}^{t} are stresses and strains at time t and ΔS_{ij} and ΔE_{ij} are increments of stress and strain, respectively. The strain increment may be decomposed into components which are linear and nonlinear in the displacement increments

$$\Delta E_{ij} = \Delta E_{ij}^{L} + \Delta E_{ij}^{NL} \tag{36}$$

Where

$$\Delta E_{ij}^{L} = \frac{1}{2}\left(\frac{\partial \Delta u_i}{\partial a_j} + \frac{\partial \Delta u_j}{\partial a_i} + \frac{\partial \Delta u_k}{\partial a_i}\frac{\partial u_k^{t}}{\partial a_j} + \frac{\partial u_k^{t}}{\partial a_i}\frac{\partial \Delta u_k}{\partial a_j}\right)$$
$$\Delta E_{ij}^{NL} = \frac{1}{2}\left(\frac{\partial \Delta u_k}{\partial a_i}\frac{\partial \Delta u_k}{\partial a_j}\right) \tag{37}$$

Substituting equations (35) and (36) into (33) yields

$$\int_{V_0} S_{ij}^{t}\,\delta\Delta E_{ij}^{L}\,dV + \int_{V_0} S_{ij}^{t}\,\delta\Delta E_{ij}^{NL}\,dV + \int_{V_0}\Delta S_{ij}\,\delta(\Delta E_{ij}^{L} + \Delta E_{ij}^{NL})\,dV = \delta R^{t+\Delta t} \tag{38}$$

The stress increment may be decomposed into two components, one which is dependent upon total strain and one which is independent of strain (i.e., creep, thermal, etc.):

$$\Delta S_{ij} = D_{ijkl}\,\Delta E_{kl} + \Delta P_{ij} \tag{39}$$

where D_{ijkl} is the usual effective tangent modulus and ΔP_{ij} is a stress increment due to strain independent phenomena (as is usually assumed in creep). Substituting equation (39) into equation (38), making use of equation (36), and neglecting terms which would be nonlinear in displacement increments, yields the following:

$$\int_{V_0} \Delta E^{L}_{kl}\, D_{ijkl}\, \delta(\Delta E^{L}_{ij})\, dV + \int_{V_0} (S^{t}_{ij} + \Delta P_{ij})\, \delta(\Delta E^{NL}_{ij})\, dV$$

$$= -\int_{V_0} (S_{ij} + \Delta P_{ij})\, \delta(\Delta E^{L}_{ij})\, dV + \delta R^{t+\Delta t} \tag{40}$$

The term ΔP_{ij} may be interpreted as the change in stress required to account for the creep and thermal strains. Equation (40) takes on the following form when put into matrix form

$$[M]\{\ddot{q}^{t+\Delta t}\} + ([K^{t}_{L}] + [K^{t}_{NL}])\{\Delta q\} = \{R^{t+\Delta t}\} - \{F^{t}\} \tag{41}$$

where [M] is the mass matrix, $[K^{t}_{L}]$ and $[K^{t}_{NL}]$ are "linear" and "nonlinear" stiffness matrices, $\{R^{t+\Delta t}\}$ is a vector of forces due to externally applied loads, $\{F^{t}\}$ is a vector of forces due to internal stress, and $\{\Delta q\}$ is the increment of the nodal displacements. Complete details of the derivation of the quantities in equation (41), without creep, may be found in reference [17].

We now present a summary of the determination of D_{ijkl} and ΔP_{ij} for kinematic hardening for the isothermal case, we assume a yield function can be expressed by

$$F = f - K^2 = 0 \tag{42}$$

For kinematic hardening, write

$$f = \tfrac{1}{2}(S'_{ij} - \alpha'_{ij})(S'_{ij} - \alpha'_{ij}) \tag{43}$$

and S_{ij}' and α_{ij}' are deviataric components of the 2nd Piola-Kirchoff stress and yield surface center, respectively and K is a constant.

The associated flow rule is then given by

$$d\varepsilon_{ij} = \lambda \frac{\partial F}{\partial S_{ij}} \tag{44}$$

where λ is a scalar to be determined. Using the Ziegler modification of the Pr ger kinematic workhardening rule, it is assumed that the projection of the increment of stress onto the normal to the yield surface in a scalar multiple of the dot product of the plastic strain and yield surface normal

$$dS_{ij} \frac{\partial F}{\partial S_{ij}} = c\, dE^{P}_{ij} \frac{\partial F}{\partial S_{ij}} \tag{45}$$

where C is a scalar (hardening modulus) to be determined from a uni-axial stress-strain curve. It can be shown that equation (45) is equivalent to the consistency condition for kinematic hardening and isothermal conditions. For small strains, the decomposition of strain is assumed:

$$dS_{ij} = E_{ijmn} \left(dE_{mn} - dE^{P}_{mn} - dE^{c}_{mn} \right) \tag{46}$$

where E_{ijmn} is the elastic constitutive tensor and dE^{c}_{mn} are the incremental creep strain components. The incremental creep strain components are determined from equation (8) and a time increment over which it is assumed the creep strain components are constant. Substituting equation (44) into equation (45) and (46) and solving the resulting equation for λ,

$$\lambda = \frac{E_{ijmn} \left(dE_{mn} - dE^{c}_{mn} \right) \frac{\partial F}{\partial S_{ij}}}{E_{ijmn} \frac{\partial F}{\partial S_{mn}} \frac{\partial F}{\partial S_{ij}} + C \frac{\partial F}{\partial S_{ij}} \frac{\partial F}{\partial S_{ij}}} \tag{47}$$

Substituting equation (47) into equation (44) and the results into equation (46) and comparing the results with equation (39) one can show that the instantaneous modulus tensor is given by

$$D_{ijmn} = E_{ijmn} - \frac{E_{ijvw}\frac{\partial F}{\partial S_{vw}}\frac{\partial F}{\partial S_{tu}}E_{tumn}}{E_{pqrs}\frac{\partial F}{\partial S_{pq}}\frac{\partial F}{\partial S_{rs}} + c\frac{\partial F}{\partial S_{pq}}\frac{\partial F}{\partial S_{pq}}} \tag{48}$$

and the change of stress due to creep strains is given by

$$dP_{ij} = - D_{ijmn}\, d\,E^{c}_{mn} \tag{49}$$

Equation (46) can now be written as,

$$dS_{ij} = D_{ijkl}\left(dE_{mn} - dE^{c}_{mn}\right) \tag{50}$$

DETERMINATION OF MATERIAL FUNCTIONS FROM EXPERIMENTAL DATA

In this section, equation (1) is specialized to the case of uniaxial loading; and to materials whose elastic response on loading and unloading in a creep and recovery test are the same. The required material functions can then be evaluated by a graphical procedure from the results of creep tests. For a general description of the methods for obtaining the material functions from experimental data, see Lou and Schapery [13].

Consider a uniaxial bar which is in a uniform uniaxial state of stress at a uniform temperature considering only one stress σ, and one strain ε . we let $\varepsilon = \varepsilon_{11}$ and $\sigma = \sigma_{11}$. When equation (1) is specialized to this uniaxial loading, the creep term is given by

$$\varepsilon^{c} = g_1(\sigma) \int_0^t \Delta D\,(\psi - \psi')\,\frac{d\,g_2(\sigma)}{d\tau}\,d\tau \tag{51}$$

and the three independent material functions are given by

$$g_1(\sigma) = \frac{d\hat{\sigma}_{11}}{d\sigma_{11}} \quad , \tag{52}$$

$$g_2(\sigma) = G_{11}(\sigma) = \frac{\hat{\sigma}_{11}}{\sigma a_\sigma} \quad , \tag{53}$$

$$a_\sigma(\sigma) = \frac{a_D(\sigma)}{a_G(\sigma)} \quad , \tag{54}$$

and

$$\Delta D(\psi) = \sum_r A^{(r)} (1 - e^{-\psi/\tau_r}) + \sum_{r'} B^{(r')} \psi \quad . \tag{55}$$

It is shown in reference [12] that $g_1(\sigma) = 1$, implies that the amount of elastic straining on unloading is the same as on loading and that $\hat{\sigma}_{ab} = \sigma_{ab}$. Using $g_1(\sigma) = 1$ and $\hat{\sigma}_{ab} = \sigma_{ab}$, equation (51) is now given by,

$$\varepsilon^c = \int_{-\infty}^{t} \Delta D(\psi - \psi') \frac{dg_2(\sigma)}{d\tau} d\tau \tag{56}$$

where

$$g_2(\sigma) = \frac{\sigma}{a_G} \tag{57}$$

and

$$a_\sigma(\sigma) = \frac{a_G(\sigma)}{a_D(\sigma)} \tag{58}$$

When equation (56) is subjected to a creep test the resulting equation can be used to evaluate the material functions g_2 and a_σ. Consider equation (56) subject to the stress history:

$$\sigma(t) = H(t)\, \sigma \quad . \tag{59}$$

Substituting equation (59) into equation (56) gives

$$\varepsilon^c = g_2\, \Delta D \left(\frac{t}{a_\sigma}\right) \sigma \; ; \tag{60}$$

and the creep compliance is given by

$$\Delta D(t) = \frac{\varepsilon}{\sigma} = g_2 \, \Delta D\left(\frac{t}{a_\sigma}\right) \quad . \tag{61}$$

Taking the log of both sides of equation (61) gives,

$$\log \Delta D(t) = \log g_2 + \log \Delta D\left(\frac{t}{a_\sigma}\right) \quad . \tag{62}$$

The simple form of equation (62) is such that a simple graphical procedure can be employed to evaluate the material functions. This is easily demonstrated by plotting ΔD and t on double - logarithmic paper, then curves at different stress levels can be superimposed by translating them along the ΔD and t axes. If the curves are shifted to a reference stress, σ_r , the amount of horizontal shift (t) and vertical shift (ΔD) equals $\log g_2 = \log \frac{g_2(\sigma)}{g_2(\sigma_r)}$ and $\log a_\sigma = \log \frac{a_\sigma(\sigma_r)}{a_\sigma(r)}$, respectively. These shifts are graphically demonstrated in figure (1).

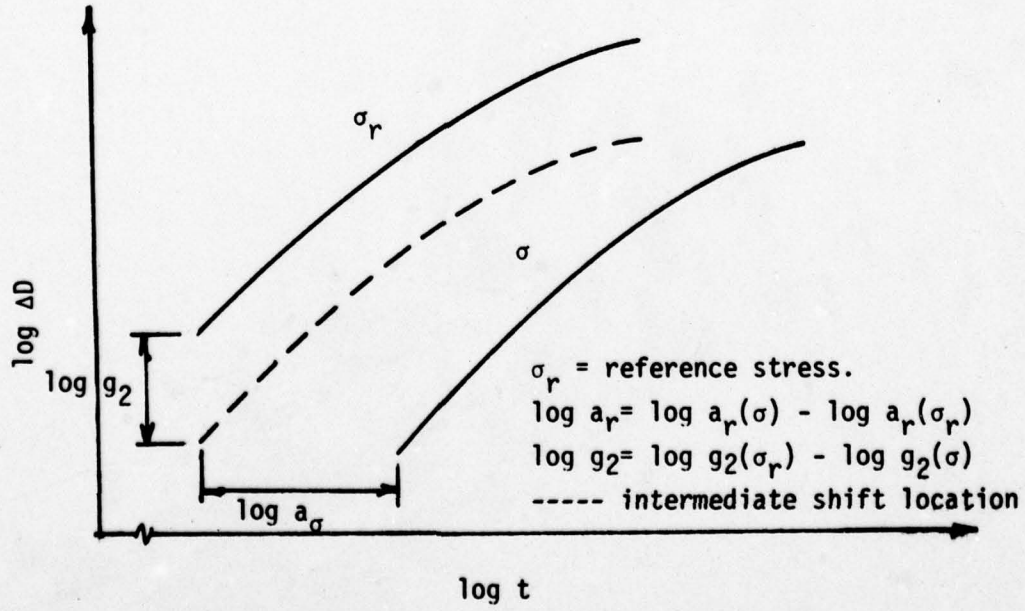

Figure 1. Horizontal and Vertical Shifts

The direction at the shifts are as follows:

$$\frac{g_2(\sigma)}{g_2(\sigma_r)} < 1 \quad , \quad \text{shift is up} \, ,$$
$$\frac{g_2(\sigma)}{g_2(\sigma_r)} > 1 \quad , \quad \text{shift is down,} \tag{63}$$

and

$$\frac{a_\sigma(\sigma_r)}{a_\sigma(\sigma)} < 1 \quad , \quad \text{shift is to left,}$$
$$\frac{a_\sigma(\sigma_r)}{a_\sigma(\sigma)} > 1 \quad , \quad \text{shift is to right.}$$

SOME NUMERICAL RESULTS

This section presents some numerical results obtained for a type 304 stainless steel with the computer program NONVIS which implements the procedures developed above for integrating equation (1) for the following stress histories: creep (figure 2), multi-step (figure 3), creep-recovery (figure 4), and stress reversal (figure 5). The results obtained are compared with those of the phenomenological creep theory based on strain hardening using total creep strain [18].

An effective creep equation of the form:

$$\bar{\varepsilon}^c = A\left(1 - e^{-rt}\right) + Kt \tag{64}$$

was used to determine the material functions in lieu of the actual experimental data. Two different heats of type 304 stainless steel are considered. The creep strain parameters for heat no. 9T2796 at 1100°F are:

$$A(\bar{\sigma}) = 5.436 \times 10^{-5} \quad \bar{\sigma}^{1.843}$$
$$r(\bar{\sigma}) = 5.929 \times 10^{-5} \quad \exp(0.2029\,\bar{\sigma}) \tag{65}$$
$$K(\bar{\sigma}) = 6.73 \times 10^{-9} \left[\sinh(0.1479\,\bar{\sigma})\right]^{3.0}$$

with $\bar{\sigma}$ (effective stress) in ksz, and t in hours. The creep strain parameters for hear No. 8043813 at 1200°F are:

$$A(\bar{\sigma}) = 2.33 \times 10^{-6} \quad \bar{\sigma}^{3.083}$$
$$r(\bar{\sigma}) = 1.354 \times 10^{-3} \quad \exp(0.129\,\bar{\sigma}) \tag{66}$$

and

$$K(\bar{\sigma}) = 7.91 \times 10^{-11} \left[\sinh(0.1932\,\bar{\sigma})\right]^{4.0}.$$

The vertical shift is defined by the function $A(\bar{\sigma})$ and the horizontal shift by the function $r(\bar{\sigma})$. This can be seen by equating the transient term given in equation (60) (for r = 1, r' = 0) and (64) from which it is determined that

$$A = g_2\,\sigma \tag{67a}$$
$$\psi = t/a_\sigma \tag{67b}$$
$$A^{(1)} = 1.0 \tag{67c}$$

and

$$\tau_r = 1.0 \quad . \tag{67d}$$

Rearranging equation (67a) gives

$$A/\sigma = g_2 \,, \tag{68}$$

and from equation (2a) and (67b)

$$r = 1/a_\sigma \tag{69}$$

Therefore, the actual shifting of the creep compliance wasn't necessary to determine the material functions $g_2(\sigma)$ and $\frac{1}{a_\sigma(\sigma)}$. It is easy to check the function g_2 and $\frac{1}{a_\sigma}$ given above by using the graphical procedure.

If the steady state creep term in equation (65), term linear in ψ, is subjected to the creep stress history, equation (59), it gives,

$$\varepsilon_s = B^{(1)} \frac{g_2 \sigma}{a_\sigma} . \tag{70}$$

Using equations (68) and (69), equation (70) becomes

$$\varepsilon_s = B^{(1)} A r t . \tag{71}$$

Equation (64) above gives for the steady state creep term

$$\varepsilon_s = k t . \tag{72}$$

However, from equations (71), (72), and (65c) it is seen that equations (71) and (72) are not equal. Thus it is concluded that the reduced time cannot be related through the reduced time use for transient creep.

In the application to the type 304 stainless steels, the steady state term will be given by the second term of equation (64), $\varepsilon_s = kt$.

Figure 2 presents creep strain vs. time for a uniaxial stainless steel (heat No. 9T2796) specimen for a creep test. The results of both the nonlinear viscoelastic and the phenomenological creep theory are nearly identical as is expected. Only the nonlinear viscoelastic theory is presented.

Figure 3 presents the creep strain response of a type 304 stainless steel (heat No. 8043813) subjected to a creep and recovery tests for a

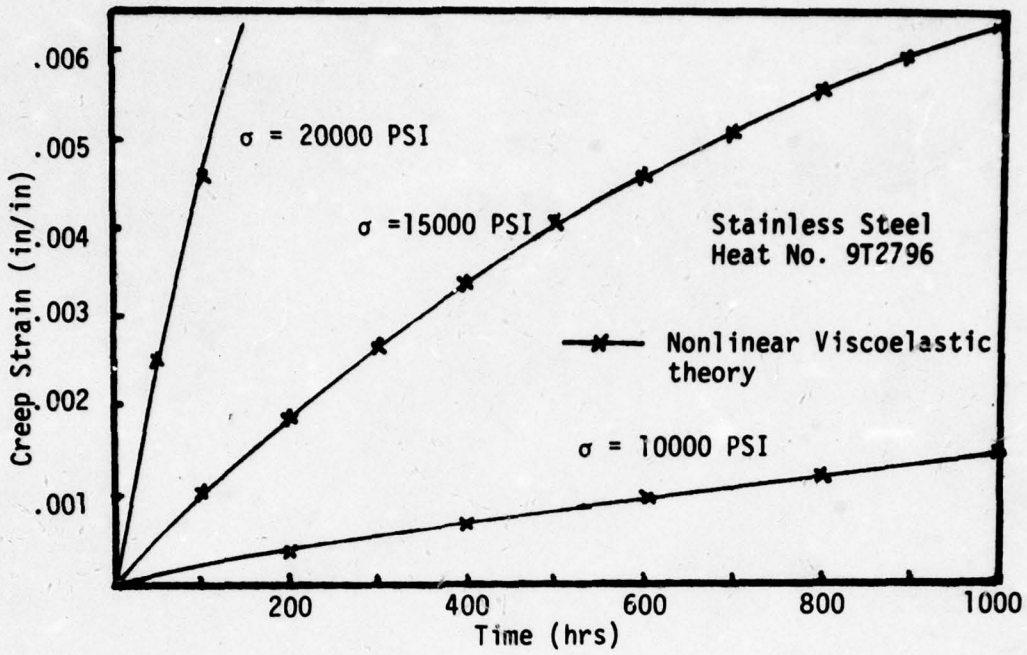

Figure 2. Creep of A Uniaxial Specimen

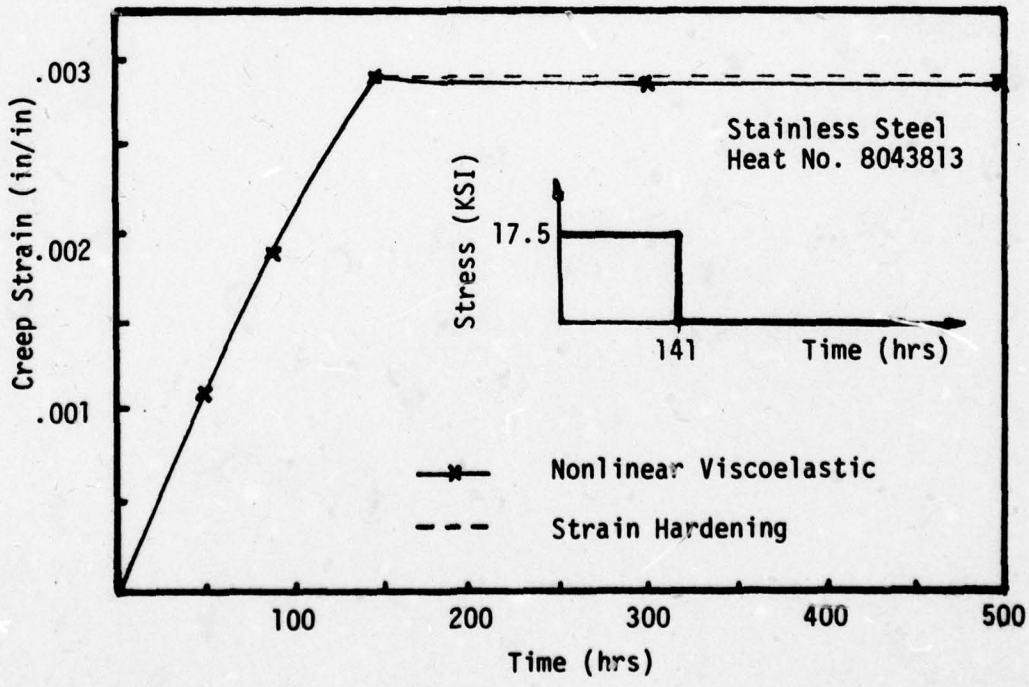

Figure 3. Creep-Recovery

uniaxial specimen. The results indicate very little recovery; of course, the phenomenological theory predict no recovery. However, it should be noted that the nonlinear viscoelastic theory would predict complete recovery if the creep-recovery curve were extended to larger values of time.

Figure 4 presents the creep strain response of a type 304 stainless steel (heat No. 8043813) uniaxial speciman subjected to montonically increasing load. The results are in reasonable agreement with the experimental results and are very close to the results base on strain hardening.

Figure 5 presents the creep strain response of a uniaxial specimen subjected to a reversed cyclic loading history. On the first reversal the nonlinear viscoelastic theory over predicts the creep response as given by the experimental data. This is due in part to the lack of significant recovery for Type 304 stainless steel. To study the behavior consider the stress history up to the time of the second stress reversal,

$$\sigma(t) = \sigma\, H(t) - 2\sigma\, H(t-t_1) \quad , \quad 0 < t < t_2 \tag{73}$$

Substituting equation (73) into equation (56) gives

$$\epsilon^c = D(\psi)\, g_2(\sigma) - 2 g_2(\sigma_1)\, D(\psi - \psi_1) \, . \tag{74}$$

Thus it is seen that the second term gives $2g_2(\sigma_1)$ times the compliance. Thus twice the value of $g_2(\sigma_1)$ is multiplying the compliance than was on initial loading. This seems to be okay for materials with an active recovery, i.e., polymers. However, for metals the recovery is only slight and the second term over predicts its contribution to the recovery. Futher the first term is related to the concept of a fading memory, which is questionable for the stress reversal situation. Note the curve plotted for the first stress reversal with no recovery or memory of past history. This curve was obtained by initializing equation (20) to zero, which represents the memory of the material to prior

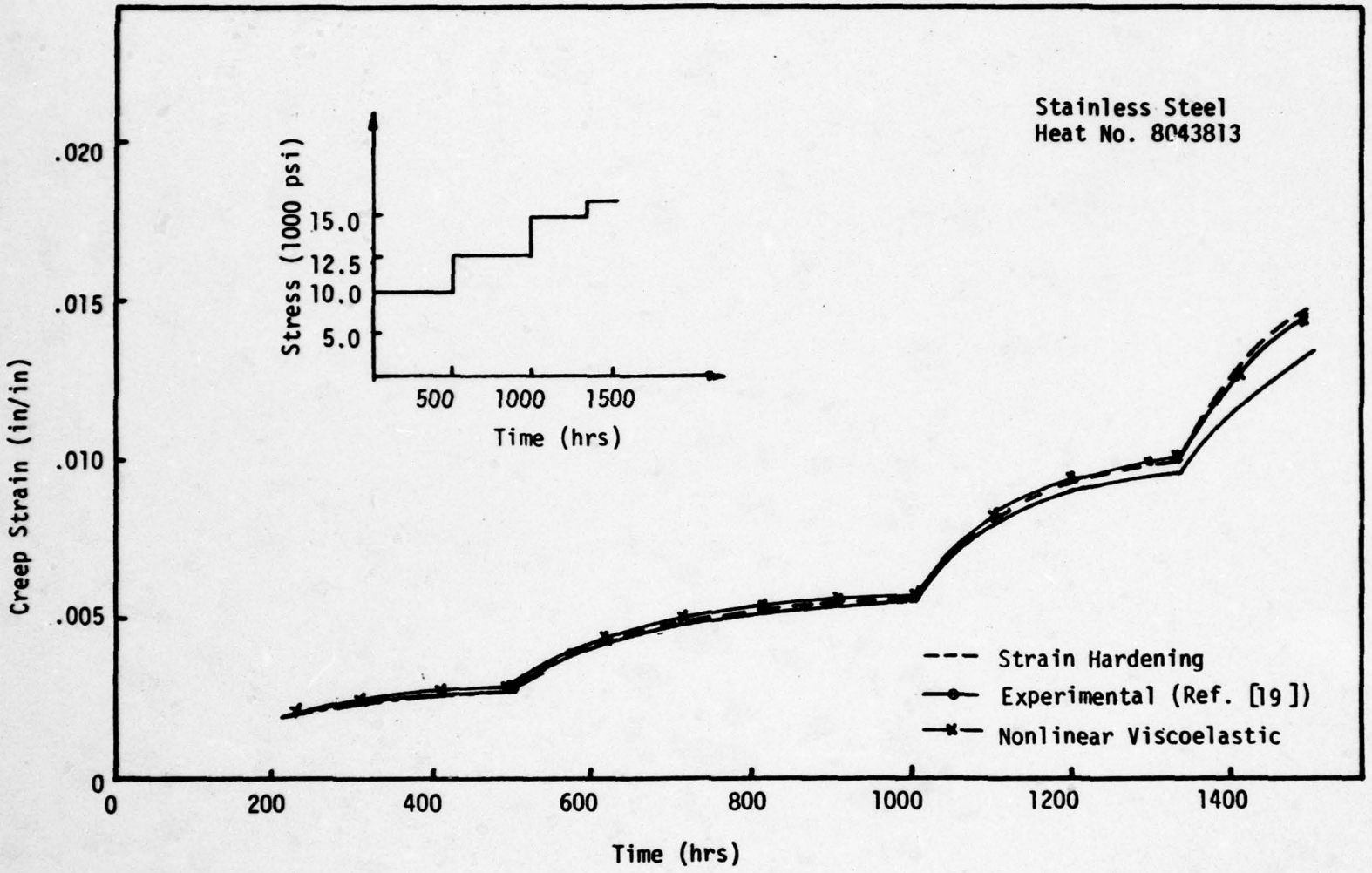

Fig. 4 Creep Strain Response of Uniaxial Specimen Subjected to Monotonically Increasing Load

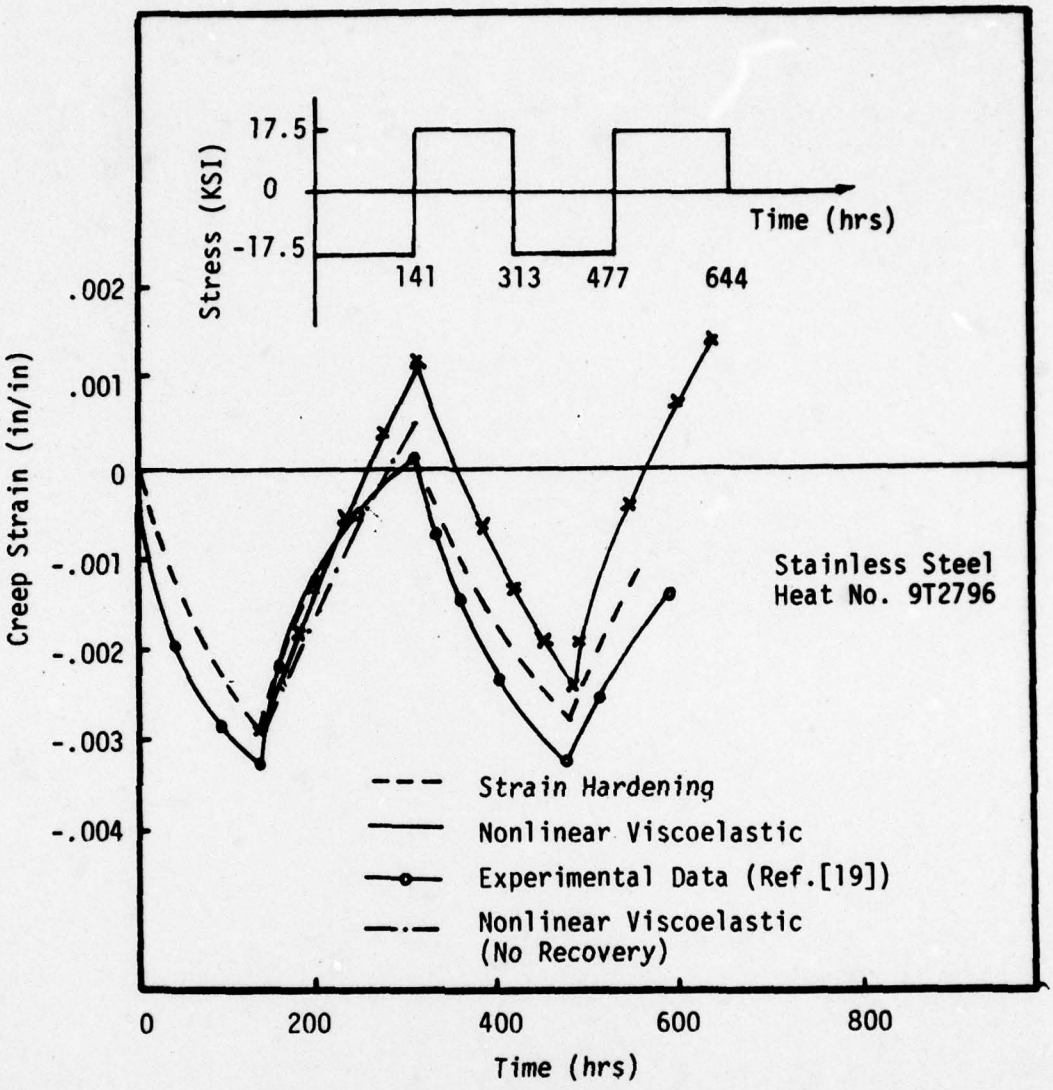

Figure 5. Creep Strain Response of Uniaxial Specimen Subjected to Cyclic Load.

histories, and setting $G_{11}{}_{N-2}$ =0 when a stress reversal occurs. This gives the same response as an initial loading with the strain accumulated at the time of the reversal serving as a new origin.

CLOSURE

The purpose of this paper was first to present an efficient method of integrating Schapery's single integral equation for use in a incremental finite element program wherein the equations of motion are integrated step-by-step. And secondly to present some preliminary results for metals using this theory.

It is believed that the method presented for integrating the single integral equation is efficient based on the fact that the integrations required are for the current time step only and does not require integration over the entire past history to determine the current creep rate. From the experience gained with NONVIS, the programming aspect of implementing the theory is straight forward and can easily be incorporated into existing finite element programs.

The results of this paper are not presented to draw final conclusions regarding whether Schapery's nonlinear viscoelastic theory are the phenomenological theory based on strain hardening is superior. Obviously, the application of the phenomenological theory for metals has developed over many years and the application of nonlinear viscoelastic theory is just beginning its development for metals. However, from the results presented here, it is seen that in all except the case of stress reversal the nonlinear viscoelastic theory gives results as acceptable as those based on strain hardening theory and in fair agreement with experimental data. For the stress reversal case two problems arise. The nonlinear viscoelastic theory predicts a complete recovery of the (as in linear viscoelasticity) strain accumulated at the first and subsequent reversals. Secondly, the theory has a fading memory of past stress history. However, as was noted these effects can be neglected for the stress reversal case by initializing to zero the parameters that contain the memory of past histories when a stress reversal occurs and setting the value of $G_{11_{N-2}}=0$.

Although the results obtained have been for the response of a stainless steel most of the results reported to date have been for a polymer or polymer composite. As noted in the introduction, reference [12,13] show the theory in good agreement for a polymer composite for the following stress histories: creep, creep-recovery, and multistep inputs. Therefore, it is believed that the use of the integration technique for the single integral equation in conjunction with a incremental finite element analysis has immediate application.

Current work with the single integral equation of Schapery's involves: (1) providing a better predictive capability for the stress reversal and other stress histories for metals, (2) determining the creep compliance and material function for several composite materials and (3) incorporating the above integration procedure into a finite element program for testing on two dimensional problems.

ACKNOWLEDGEMENT

This research was supported jointly by the Office of Naval Research under contract N00014-76-0150 and the Air Force Office of Scientific Research under contract F49620-78-C-0034. Appreciation is expressed to Dr. Richard A. Schapery for the many helpful suggestions made during this study.

REFERENCES

[1] Bathe, K.J., "Static and Dynamic Geometric and Material Nonlinear Analysis Using ADINA," MIT Report No. 82448-2, May 1976.

[2] DeSalvo, G.J. and Swanson, JA., "ANSYS Engineering Analysis System User's Manual," Swanson Analysis System, Inc., Elizabeth, Penn., March, 1975.

[3] Sartory, W.K., "PLACRE User's Manual," ORNL/ TM-5626, February 1977.

[4] Nickell, R.E., "Thermal Stress and Creep," Structural Mechanics Computer Programs, University of Virginia Press, 1974, pp. 103-122.

[5] Boresi, A.P. and Sidebottom, O.M., "Creep of Metals under Multiaxial States of Stress," Nuclear Engineering and Design, 15.1972, pp. 415-456.

[6] Schapery, R.A., "Further Development of a Thermodynamic Constitutive Theory: Stress Formulation," Purdue University, Report No. 69-2, February, 1969.

[7] Rashid, Y.R., "Part I, Theory Report for CREEP-PLAST Computer Program: Analysis of Two-Dimensional Problems under Simultaneous Creep and Plasticity," GEAP 10546, AEC Research and Development Report, January, 1972.

[8] Valanis, K.C., "A Theory of Viscoplasticity Without a Yield Surface: Part I. General Theory," Archives of Mechanics, Vol. 23, 1971, pp. 517-533.

[9] Schapery, R.A. "A Theory of Nonlinear Thermoviscoelasticity Based on Irreversible Thermodynamics," Proc. 5th U.S. Nat. Cong. Appl. Mech., ASME, 1966, pp. 511-530.

[10] Valanis, K.C. and Wu, H.C., "Endochronic Representation of Cyclic Creep and Relaxation of Metals," Journal of Applied Mechanics, Vol. 42, 1975, pp. 67-73.

[11] Valanis, K.C., "Effect of Prior Deformation on Cyclic Response of Metals," Journal of Applied Mechanics, Vol. 41, 1974, pp. 441-447.

[12] Schapery, R.A. "On the Characterization of Nonlinear Viscoelastic Materials," J. Polymer Eng. Sci., Vol. 9,1969, pp. 295.

[13] Lou, Y.C. and Schapery, R.A., "Viscoelastic Characterization of a Nonlinear Fiber reinforced Plastic," J. Composite Material, Vol. 5, 1971.

[14] Guidelines and Procedures for Design of Nuclear System Components at Elevated Temperatures (Supplement to ASME Code Case), Vol. I, FD7 F9-5T. Division of Reactor Research and Development, AEC (1974).

[15] Schapery, R.A., Personal Communication (Appendix to Aerojet General Technical report).

[16] Schapery, R.A., Personal Communication.

[17] Hunsaker, B., "The Application of Combined Kinematic-Isotropic and the Mechanical Sublayer Model to Small Strain Inelastic Structural Analysis by the Finite Element Method," Ph.D. Dissertation, Texas A&M University, 1976.

[18] Haisler, W.H., and Sanders, D.R., "Elastic-Plastic-Creep-Large Strain Analysis at Elevated Temperatures by the Finite Element Mehtod", Symposium on Future trends in Computerized Structural Analysis and Synthesis, 1978.

APPENDIX I

Recursive Relationships for $C1^{(r)}_{cd_N}$ and $C2^{(r')}_{cd_N}$

After expanding equation (23) as the sum of two integral, it can be rewritting as

$$C1^{(r)}_{cd_N} = e^{-(\psi_N - \psi_{N-1})/\tau_r} \left\{ \int_0^{t_{N-2}} e^{-(\psi_{N-1} - \psi')/\tau_r} \frac{dG_{cd}}{dt'} dt' + \int_{t_{N-2}}^{t_{N-1}} e^{-(\psi_{N-1} - \psi')/\tau_r} \frac{dG_{cd}}{dt'} dt' \right. \tag{I.1}$$

To evaluate equation (I.1) note that if in equation (23) N is replaced by N-1, equation (23) can be written as,

$$C1^{(r)}_{cd_{N-1}} = \int_0^{t_{N-2}} e^{-(\psi_{N-1} - \psi')/\tau_r} \frac{dG_p}{dt'} dt' \tag{I.2}$$

which is the value of $C1^{(r)}_{cd}$ from the previous time step.

Define $\Delta\psi_N$ as,

$$\Delta\psi_N = \psi_N - \psi_{N-1} \tag{I.3}$$

and approximate the time rate of change of G_{cd} as

$$\frac{dG_{cd}}{dt} = \frac{G_{cd_{N-1}} - G_{cd_{N-2}}}{\Delta t_{N-1}} \tag{I.4}$$

on the time interval $t_{N-2} < t < t_{N-1}$. Using equation (I.2), (I.3) and (I.4) in equation (I.1), gives,

$$C1^{(r)}_{cd_{N-1}} = e^{-\Delta\psi_N/\tau_r} \left\{ C1^{(r)}_{cd_{N-1}} + \frac{G_{p_{N-1}} - G_{p_{N-2}}}{\Delta t_{N-1}} \int_{t_{N-2}}^{t_{N-1}} e^{-(\psi_N - \psi')/\tau_r} dt' \right. . \tag{I.5}$$

In the integral given by equation (17), replace N by N-1 to get,

$$J1^{(N)}_{N-1} = \frac{1}{\Delta t_{N-1}} \int_{t_{N-2}}^{t_{N-1}} e^{-(\psi_{N-2} - \psi')/\tau_r} dt' \quad . \tag{I.6}$$

Which is $J1^{(r)}$ from the previous step. Thus, equation (I.5) can be written as,

$$C1^{(r)}_{cd_N} = e^{-\Delta\psi_N/\tau_r}\left\{ C1^{(r)}_{cd_{N-1}} + \left(G_{cd_{N-1}} + G_{cd_{N-2}}\right) J1r_{N-1}\right\} \qquad (I.7)$$

Note that the values of $C1^{(r)}_{cd_{N-1}}$, $J1^{(r)}_{N-1}$, $G_{cd_{N-1}}$ and $G_{cd_{N-2}}$ are known values from previous steps.

Similarly, equation (24) can be manipulated and rewritten as,

$$C2^{(r')}_{cd_N} = \Delta\psi_N\, G_{cd_{N-1}} + C2^{(r')}_{cd_{N-1}} + \left(G_{cd_{N-1}} - G_{cd_{N-2}}\right) J2_{r'_{N-1}} \qquad (I.8)$$

Where $C2^{(r')}_{cd_{N-1}}$ and $J2^{(r')}_{N-1}$ are values of equation (24) and (18) from the previous step.

Recursive Relationship for $F^{(r)}_{cd_N}$

After expanding equation (30) as the sum of two integrals, it can be written as,

$$F^{(r)}_{cd_N} = \int_0^{t_{N-2}} e^{-(\psi_N - \psi_{N-1} + \psi_{N-1} + \psi')/\tau_r}\ \frac{dG_{cd}}{dt'}\, dt'$$

$$+ \int_{t_{N-2}}^{t_{N-1}} e^{-(\psi_N - \psi_{N-1} + \psi_{N-1} - \psi')/\tau_r}\ \frac{dG_{cd}}{dt'}\, dt' \qquad (I.9)$$

To evaluate equation (I.9) note that if in equation (30) N is replaced by N-1, equattion (30) can be rewritten as,

$$F^{(r)}_{cd_{N-1}} = \int_0^{t_{N-2}} e^{-(\psi_{N-1} - \psi')/\tau_r}\ \frac{dG_{cd}}{dt'}\, dt' \qquad (I.10)$$

which is the value of $F^{(r)}_{cd}$ from the previous step. Using equations (I.9). (I.10) and (I.4), equation (30) can be written as,

$$F^{(r)}_{cd_N} = e^{-\Delta\psi_N/\tau_r}\left\{ F^{(r)}_{cd_{N-1}} + \frac{G_{cd_{N-1}} - G_{cd_{N-2}}}{\Delta t_{N-1}} \int_{t_{N-2}}^{t_{N-1}} e^{-(\psi_{N-1} - \psi')/\tau_r}\, dt' \right. \qquad (I.11)$$

The integral term in equation (I.14) can be written as $J1^{(r)}_{N-1}$ using equation (I.6) thus

$$F^{(r)}_{cd_N} = e^{-\Delta\psi_N/\tau_r}\left\{ F^{(r)}_{cd_{N-1}} + \left(G_{cd_{N-1}} - G_{cd_{N-2}}\right) J1^{(r)}_{N-1} \right\} . \qquad (I.12)$$

Evaluation of the quanities $J1_N^{(r)}$ and $J2_N^{(r')}$

Expanding $J1_N^{(r)}$, equation (17) as

$$J1_{r_N} = \frac{1}{\Delta t_N}\left\{ \int_{t_{N-1}}^{t_N} e^{-(\psi_N-\psi')/\tau_r}\, dt' + \int_{t_{N-1}}^{t_N} e^{-\frac{a}{\tau_r}(t_n-t')}\, dt' - \int_{t_{N-1}}^{t_N} e^{-\frac{a}{\tau_r}(t_N-t'}\, dt' \right\}$$

or

$$J1_{r_N} = \frac{1}{\Delta t_N}\left\{ \int_{t_{N-1}}^{t_N} e^{-\frac{a}{\tau_r}(t_N-t')}\, dt' + \int_{t_{N-1}}^{t_N} \left[e^{-(\psi_N-\psi')/\tau_r} - e^{-\frac{a}{\tau_r}(t_N-t')} \right] dt' \right\} \qquad \text{(I.13)}$$

Let the change in reduced time during the interval Δt_N be related to Δt_N through the parameter, a

$$\psi_N - \psi_{N-1} = a\,(t_N - t_{N-1}) \quad \text{or} \quad a = \frac{\Delta\psi_N}{\Delta t_N} \qquad \text{(I.14)}$$

Define the quantity $J1^*_{r_N}$ as

$$J1_N^{*(r)} = \frac{1}{\Delta t_N} \int_{t_{N-1}}^{t_N} \left[e^{-(\psi_N-\psi')/\tau_r} - e^{-\frac{a}{\tau_r}(t_N-t')} \right] dt' \qquad \text{(I.15)}$$

Thus,

$$J1_N^{(r)} = \frac{1}{\Delta t_N}\frac{\tau_r}{a}\left[e^{-\frac{a}{\tau_r}(t_N-t)} \right]_{t_{N-1}}^{t_N} + J1^*_{r_N} \qquad \text{(I.16)}$$

$$= \frac{\tau_r}{\Delta\psi_N}\left(1 - e^{-\Delta\psi_N/\tau_r}\right) + J1^*_{r_N}$$

Make the following change of variable in $J1_N^{*(r)}$

$$\tau = \frac{t-\tau_N}{\Delta t_N} + \frac{t-t_{N-1}}{\Delta t_N}$$

at lower limit

$$\tau = -1$$

at upper limit

$$\tau = +1$$

and

$$d\tau = \frac{2\,dt}{\Delta t_N} \quad \text{OR} \quad dt = \frac{\Delta t_N}{2}\, d\tau$$

$$\tau = \frac{2t - t_N - t_{N-1}}{\Delta t_N}$$

$$t = \frac{\tau\,\Delta t_N + t_N + t_{N-1}}{2}$$

Hence

$$J1_N^{*(r)} = \frac{1}{2} \int_{-1}^{+1} \left[e^{-(\psi_N - \psi)/\tau_r} - e^{-\frac{c}{\tau_r}\left(t_N - \frac{\tau \Delta t_N - t_N - t_{N-1}}{2} \right)} \right] d\tau$$

or

$$J1_N^{*(r)} = \frac{1}{2} \int_{-1}^{+1} \left[e^{-(\psi_N - \psi)/\tau_r} - e^{-\frac{1}{\tau_r}\frac{\Delta \psi_N}{2}(1-\tau)} \right] d\tau \qquad \text{(I.17)}$$

where

$$\Delta \psi_N = \psi_N - \psi_{N-1}$$

Equation (I.17) is set up so Gaussian Quadrature can be used for numerical evaluation.

Expanding $J2_N^{(r')}$, equation (18) as

$$J2_N^{(r')} = \frac{1}{\Delta t_N} \int_{t_{N-1}}^{t_N} (\psi_N - \psi')\, dt' \qquad \text{(I.18)}$$

$$= \psi_N - \frac{1}{\Delta t_N} \int_{t_{N-1}}^{t_N} \psi'\, dt' \quad .$$

using

$$\psi' = \frac{a_G}{a_D} t'$$

in equation (I.18)

$$J2^{(r)} = \psi_N - \frac{1}{\Delta t_N} \int_{t_{N-1}}^{t_N} \frac{a_G}{a_D} t' dt' \tag{I.19}$$

Define,

$$J2_N^{*(r)} = \frac{1}{\Delta t_N} \int_{t_{N-1}}^{t_N} \frac{a_G}{a_D} t' dt' \tag{I.20}$$

and write equations (I.19) as

$$J2_N^{(r)} = \psi_N - J2_N^{*(r)} \tag{I.21}$$

Using the same change of variable as above,

$$\tau = \frac{t - t_N}{\Delta t_N} + \frac{t - t_{N-1}}{\Delta t_N}$$

at the upper limit $\tau = +1$

at the lower limit $\tau = -1$

Thus,

$$J2_N^{*(r)} = \frac{1}{4} \int_{-1}^{+1} \frac{a_G}{a_D} (\tau \Delta t_N + t_N + t_{N-1}) d\tau \tag{I.22}$$

Equation (I.22) is set up so Gaussian Quadrature can be used for numerical intergration.

Evaluation of ψ

$$\psi = \int_0^t \frac{a_G}{a_D} dt' \tag{2a}$$

For the interval $t_{N-1} \leq t \leq t_N$, we have

$$\psi = \int_0^{t_{N-1}} \frac{a_G}{a_D} dt' + \int_{t_{N-1}}^{t_N} \frac{a_G}{a_D} dt'$$

or
$$\psi = \psi_{N-1} + \int_{t_{N-1}}^{t_N} \frac{a_G}{a_D}\, dt' \quad . \tag{I.23}$$

at a given point in space approximate the stress as a linear function of time with the interval Δt_N:

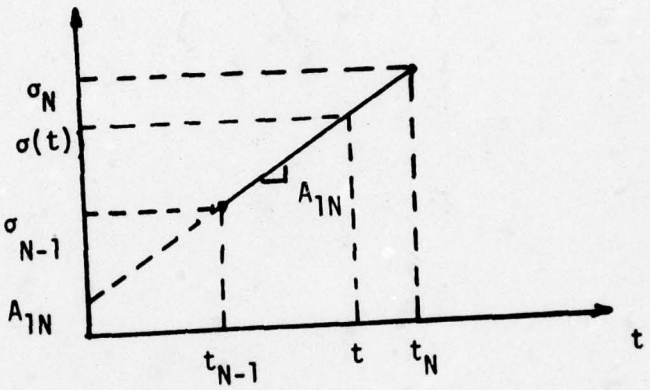

Thus,
$$\sigma(t) = A_{1_N} + A_{2_N} t \quad , \qquad t_{N-1} \le t \le t_N$$

where
$$A_{1N} = \frac{\sigma_{N-1}\, t_N - \sigma_N\, t_{N-1}}{\Delta t_N} \quad \text{and} \quad A_{2_N} = \frac{\Delta \sigma_N}{\Delta t_N}$$

Now change the variable of integration to σ, and obtain
$$\psi = \psi_{N-1} + \int_{\sigma_{n-1}}^{\sigma_N} \frac{a_G(\sigma')}{a_D(\sigma')} \frac{d\sigma'}{A_{2_N}} \tag{I.29}$$